Zeitschrift: IABSE reports = Rapports AIPC = IVBH Berichte
Band: 37 (1982)

Rubrik: Theme 2: Steel base material, welded joints

THEME 2

Steel Base Material, Welded Joints

Matériau de base en acier, assemblages soudés

Grundmaterial aus Stahl, geschweisste Verbindungen

Leere Seite
Blank page
Page vide

Fatigue Strength of Flame Cut Plates

Résistance à la fatigue des tôles oxycoupées

Ermüdungsfestigkeit von mittels Sauerstoffbrenner geschnittener Bleche

E. PIRAPREZ
Ingénieur
C.R.I.F.
Liège, Belgium

SUMMARY
When steel plate is flame cut the resulting edges exhibit different mechanical characteristics to those of the basic product. These changes are particularly significant in the case of AE 355 steel. Many fatigue tests have shown that grinding does not improve behaviour beyond that of the untreated edge. However, shot peening of the flame cut edge raises the allowable fatigue stress by 30 to 35 MPa which is better than that obtained by preheating before cutting. Thus, with regards to fatigue strength, shot peened, flame cut elements fall into the highest class of welded connections.

RESUME
Lorsque la mise à dimension des tôles se fait par oxycoupage, les bords de ces tôles présentent des caractéristiques mécaniques modifiées par rapport à celles du produit de base, particulièrement dans le cas de l'acier de qualité AE 355. Un grand nombre d'essais de traction dynamique ont montré que des éprouvettes meulées n'ont pas un comportement meilleur que celui des éprouvettes oxycoupées n'ayant subi aucun traitement. Par contre, le grenaillage de la face oxycoupée permet de relever leur résistance à la fatigue de 30 à 35 MPa; valeur qui est supérieure à celle obtenue en préchauffant la tôle avant le coupage. On obtient ainsi des valeurs qui sont comparables à celles des meilleures classes d'assemblages soudés.

ZUSAMMENFASSUNG
Beim Zuschneiden von Blechen mittels Sauerstoffbrenner verändern sich an den Rändern die mechanischen Eigenschaften gegenüber denjenigen des Basisproduktes. Dies trifft insbesondere für den Stahl der Qualität AE 355 zu. Zahlreiche dynamische Zugversuche haben gezeigt, dass Prüfkörper mit nachgeschliffenen Schnittstellen kein besseres Ermüdungsverhalten aufweisen als unbehandelte. Im Gegensatz dazu erhöht das „shot-peening" den Ermüdungswiderstand um 30 bis 35 MPa. Dieser Wert ist besser als derjenige, der mittels Vorerwärmung vor dem Schneiden erreicht werden kann. Man erhält so Ermüdungsfestigkeiten, die mit den besten Klassen von Schweissverbindungen verglichen werden können.

1. INTRODUCTION

Whenever the size dressing of steel plates is carried out by thermal cut, the edges present modified mechanical characteristics as compared with the basis product. These modifications are particularly perceptible in the case of AE 355.

These modifications are due to the particular thermal treatment endured by the cut edge which results in the creation of tempering structures with variable carbon contents. Additionaly, the non-homogeneous thermal distribution during the oxygen-cut operation entails the creation of residual stresses, the influence of which cannot be neglected as far as the fatigue strength or the stability are concerned.

Up to now, in Belgium, the treatment of such faces is quite expensive as most authorities required the grinding of the all oxygen-cut face on a deapth of 1 mm in order to remove all the matter which was structurally modified during the cutting. Therefore, a research was undertaken in order to investigate the influence of such modifications on the statical and dynamic behaviour of AE 355 steel plates and to try to discover some means of improving their mechanical characteristics.

2. CHARACTERISTICS OF OXYGEN-CUT EDGES

The priming of the cutting operation requires a heat quantity sufficient to bring a small portion of the piece to be cut to a high temperature, around 1350° C [1].

During the cooling, the cut edges undergo metallurgical transformations which induce hardening structures.

Generally that heat affected zone presents one of the two structures shown at fig. 1, depending on whether the cutting operation was performed with preheating or not [2].

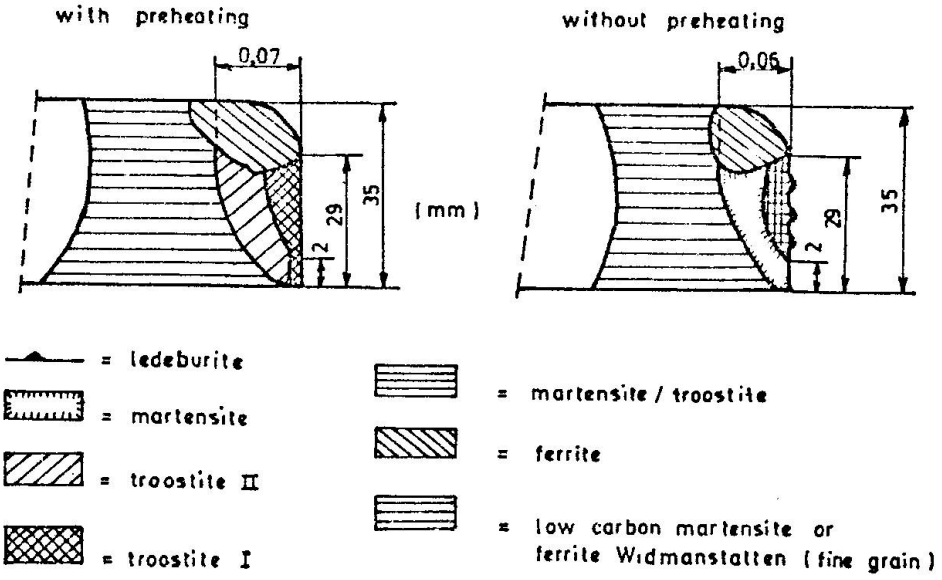

Figure 1. Structure of the heat affected zone after oxygen-cutting.

In addition to these metallurgical modifications several phenomena may be observed :

a) The carbon concentration is increased along the cut edge in a very thin layer about 0,1 mm deep.
As the hardness is a direct function of the carbon contents, one observes very high hardnesses in this thin layer and therefore along the cut edge. This increase of the carbon contents does not come from the cutting flame nor from the diffusion of carbon towards the cut edges, but from the material which was melt during the cutting. However, and this has not yet been explained, it is only beneath a depth of 1,5 mm (and not 0,1 mm) that the hardness begins to decrease to reach the value for the basic material about 3 mm from the surface (fig. 2).

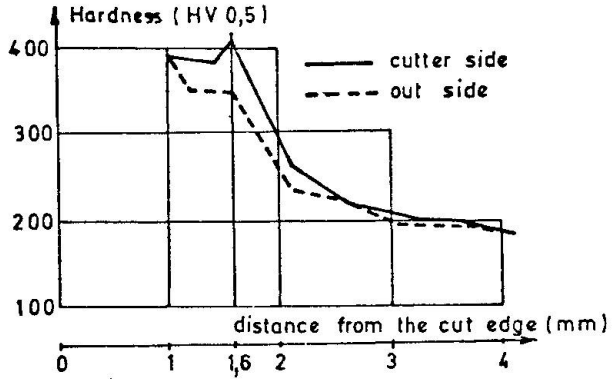

Figure 2. Measurement of the hardness near the cut edge.

b) The heat distribution due to the oxygen-cutting produces a field of residual stresses in the cut pieces. The distribution of these stresses along the edge has not yet been defined neither in sign nor in value. The tests made up to now are not significant as some authors speak of compression stresses [2,11] while others speak of traction stresses [6,10,11] .

c) The cut surface presents grooves oriented in the direction of the cutting flame. In most cases these grooves happen to be perpendicular to the stress fields when the plate is put into service, which is very unfavorable as far as the fatigue resistance is concerned. Moreover the fatigue resistance may still be further hampered by additional imperfections. In addition such grooves also affect the resistance to brittle fracture which depends mostly on the depth and the sharpness of the grooves.

Generally, the defects are caused by a bad setting of the cutting torch or by a stop in the cutting operation. Some of these defects are always present particularly at the initial point of the cut. As a result of the thermal effect of the oxygen-cutting and of the geometrical characteristics of the cut edge, the following mechanical characteristics are modified :

a) The resistance to brittle fracture, related to the ductility of the material which is itself influenced by deformation of the hardening structures and by the increase of the carbon contents of the cut edge.
b) The fatigue resistance, influenced by the residual stresses, the presence of grooves and the metallurgical structures.
c) The bearing capacity, influenced by the residual stresses near the cut edge.

The nature of the resulting metallurgical structures depends on the heat treatment applied to the edge to be cut. This treatment is a function of the heat quantity introduced and of the cooling speed. These two main parameters depend on various factors :

- the practical conditions of the cutting operation,
- the thickness of the plate,
- the nature of the cutting gas,
- the type of nozzle used,
- the cutting speed,
- the oxygen pressure.

3. TESTING PROGRAM

In order to determine the importance of the previously described effects on the actual behaviour of oxygen-cut pieces in practical situations, the following tests have been undertaken :

- measurements of surface conditions,
- folding tests of residual stresses,
- traction tests,
- dynamical tests.

The tests were performed on specimen coming from various pieces of steel before and after the cutting operation.

4. SPECIFICATIONS OF THE SPECIMENS

A great many factors influence the quality of an oxygen-cut surface. In the frame of this research, it is obviously not possible to consider the whole set of parameters nor to realize all their possible combinations.

All parameters which are usually fixed by the cutting equipment manufacturer or for which the setting is easy and not prone to error have been fixed for the whole test program.

For the other parameters, the following values corresponding to general practice have been used :

- steel grade : AE 355 steel sheets with a carbon ratio around 0,18 %.The specimens were always cut in the direction of rolling.
- thickness of the sheets : most tests were made using two thicknesses : 20 and 35 mm. Complementary tests were made using 12 and 44 mm.
- initial steel temperature : two temperatures were considered : room temperature (20°C) and preheating to 100°C. The preheating was achieved with a flame torch in front of the cutter.
- post cutting treatment : several treatments were studied :
  - no treatment,
  - light grinding (whitened surfaces),
  - grinding up to the elimination of grooves (0,7 to 1 mm),
  - shot peening.

In the particular case of shot peening, the following parameters were used :

- shot material : steel shot of 1 mm diameter,
- shot peening duration : 1.5 minute,
- the shot peening machine had 6 turbines of 500 mm diameter rotating at a speed of 3.000 rev/min,
- distance between piece and turbine : 1 m.

In order to detect a possible influence of the nature of the shot material on the test results, some specimens were shot peened using cupper shot while others were treated in very unfavorable conditions for the final surface state :

- shot material : brand new corindon
- granulometry : 1190 to 1410 µm; type 16-80
- pressure : 60 to 70 MP_a.

5. TEST RESULTS

5.1. Surface Conditions

Surface condition measurements have been made on samples representing all the situations described above. Fig. 3 shows the resulting diagrams of some of these measurements. The general conclusion is that the overall aspect of the surface is not modified by the various treatments and that the grooves have still the same deapth.

The diagrams however do not show any evidence of a possible reducing of the sharpness at the grooves bottom , although this has been mentioned by several authors.

5.2. Residual Stresses

On the oxygen cut faces shot peening reduces the residual stresses (in traction) by about 100 MP_a (see Fig. 4).

On the other hand, the steel temperature before cutting has no significant influence on the value of these stresses.

5.3. Statical Tests

5.3.1. Folding tests

Several specimens have been folded around a mandrel having a diameter of 10 times the thickness of the steel sheet.

To achieve the most several situation, many specimens were folded in their plane with one cut edge in traction.

No cracking was ever observed after 90° folding even after a verification using a penetrating liquid.

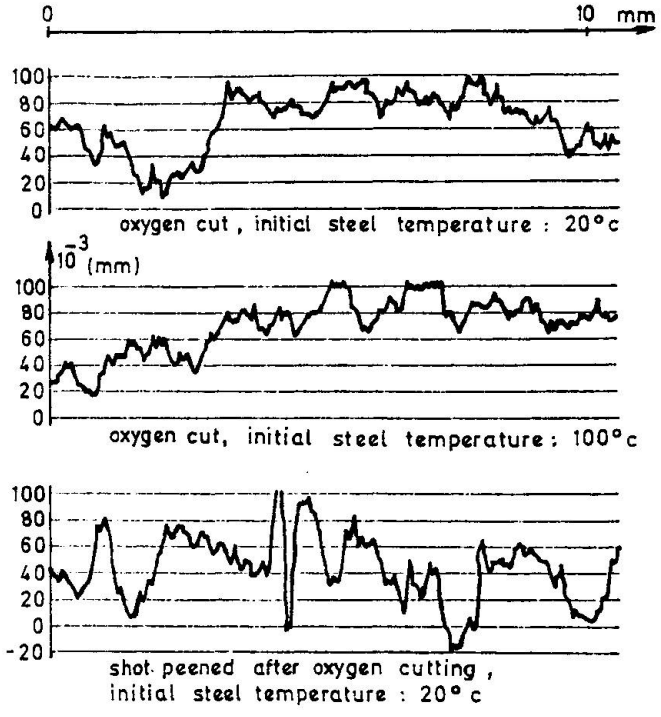

Figure 3. Measurements of surface conditions.

5.3.2. Traction tests

A typical stress-strain diagram for an oxygen-cut specimen is represented at Fig. 5 in comparison with the stress-strain diagram for the base metal.

It may be seen that the conventional 0,2 % elastic limit of the oxygen cut steel is equal or slightly higher than that of the base steel.

On the other hand, the apparent elastic limit cannot be pinpointed : during the loading of the specimen, the section yields progressively due to the traction residual stresses. It is however not possible to derive the level and distribution of the traction stresses on the only basis of these tests.

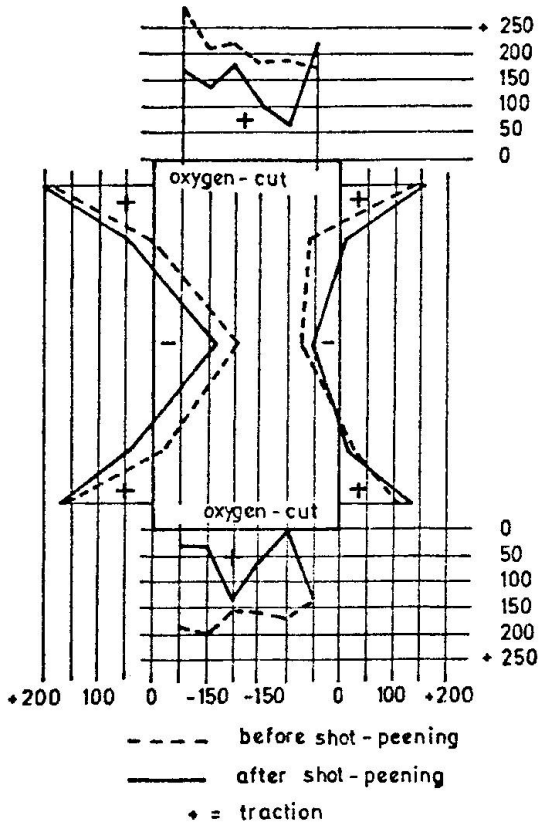

Figure 4. Residual stresses (MP_a).

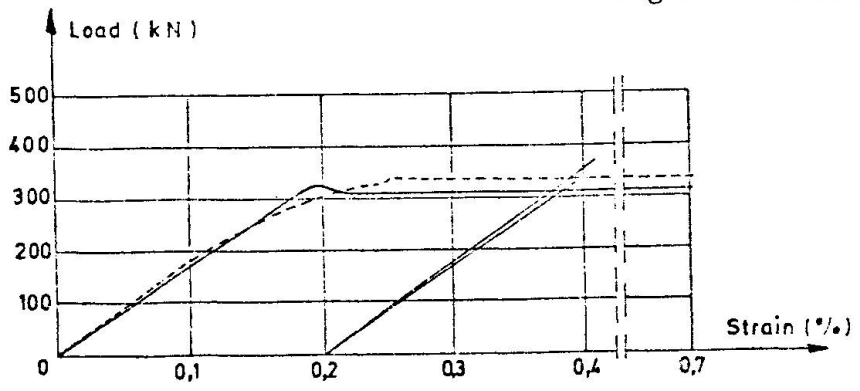

Figure 5. Diagram stress-strain.

5.4. Dynamic Tests

In reason of the severity of the grooves on the oxygen-cut edges and of the residual stress level measured on such edges, we have processed the dynamic test results using the method in application in the case of fatigue-loaded unrelaxed welded joints, for which the conditions are similar.

In this method, the fatigue cycles are only characterized by the stress range $\Delta\sigma = \sigma_{max} - \sigma_{min}$ without consideration for the stress ratio $R_s = \frac{\sigma_{min}}{\sigma_{max}}$.

Fig. 6 and 7 show some of the resulting WOHLER curves. Fig. 6 shows the effect of preheating on the fatigue resistance while Fig. 7 shows the effet of shot peening. In addition, Fig. 7 also shows the ultimate values for the 4 specimens shot-peened using corindon. If one considers that the two weakest results correspond to ruptures in sections where cutting defects had been ground and not in shot-peened regions,one may conclude that corindon gives as good results as other types of shot.

The tests have also shown that grinding the cut pieces only raises the characteristic value of the stress range from 132 to 150 MP_a and that all the corresponding endurance limits are valid whatever the thickness of the steel.

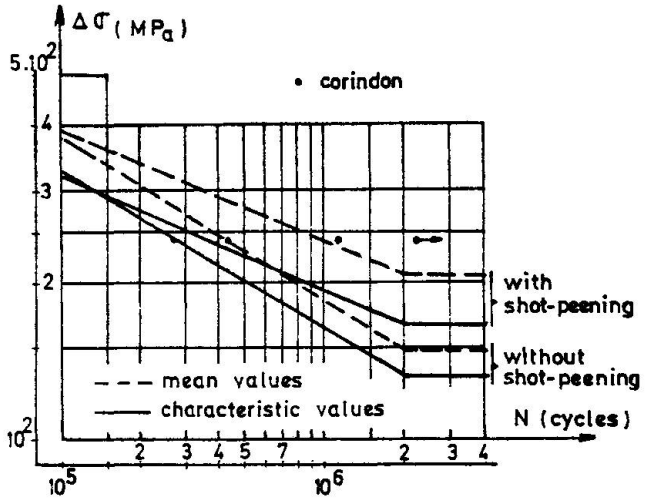

Figure 6. Fatigue tests results with and without shot-peening.

6. CONCLUSIONS

The shot-peening after oxygen cutting increases the fatigue resistance by 30 to 35 MP_a and the preheating by about 25 MP_a. Both effects may be cumulated.

The following table gives the 90 % characteristic values of the stress range for life duration longer than 2.10^6 cycles obtained for the various combinations of preheating and shot peening.

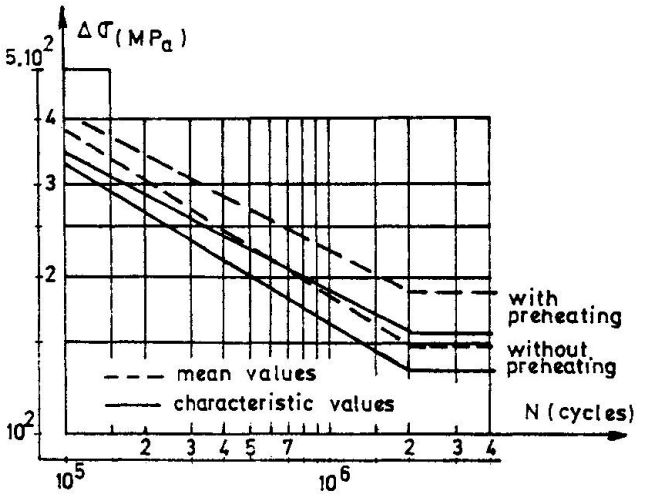

Figure 7. Fatigue tests results with and without preheating.

Characteristics values (90 %) of the stress range

Peening / Preheating	Without	With
Without	132	164
With	158	201

If these values are compared with those given for welded joints in function of their fatigue resistance, one can see that shot-peening, preheating and,better, combination of these treatments lead to oxygen-cut pieces with a resistance equivalent to that of the best joints. Now, constructions without any welding are very scarce. We are therefore of the opinion that in most cases the use of oxygen-cut steel sheets does not require any particular treatment, as most often the sheets are cleaned by shot-peening after shaping, before being prepainted.

On the other hand, if the construction must offer a high fatigue resistance, oxygen-cut edges must be milled out as simple grinding is not efficient enough.

REFERENCES

1 R. BAUS, W. CHAPEAU : Application du soudage aux constructions. Sciences et Lettres, Liège.
2 Netherlands Institute of Welding-Working Group 1913 : The Properties of Flame Cut Edges. Final Report, May 1973.
3 A. LEROY, M. EVRARD, G. D'HERBEMONT : La pratique du soudage oxyacétylénique et des techniques connexes. Publications de la soudure autogène, 1963.
4 SELLIER : Cours de soudage et de découpage au chalumeau.
5 Institut International de la Soudure : Projet de classification des surfaces obtenues par coupage thermique-soudage et tehcniques connexes. Vol. 25, mai-juin 1971.
6 JURGEN RUGE und Alfred KRAHL : Etude de la capacité au formage à froid des zones thermiquement influencées des tôles oxycoupées. Schweissen und Schneiden, n° 19, 1967.
7 A. ARCOUTEIL et J. MONNET : Conditions de mise en oeuvre des tôles en aciers résistant à la corrosion.
8 F. GOLDBERG : Origine de l'accroissement de la teneur en carbone à la surface des coupes dans l'oxycoupage des aciers. Soudage et techniques connexes, vol. 26, n° 12, 1972.
9. GOLDBERG, FREDRIKSSON, NOREN-BRANDEL : Coupage aux gaz des aciers de construction à basses températures. Le soudage dans le monde, vol. 11, 1973.
10 B.W. YOUNG and J.B. DWIGHT : Residual stresses due to longitudinal welds and flame cutting. University of Cambridge, Department of Engineering.
11 Von KURLAGUNDA N. RAO, JURGEN RUGE und HEINZ SCHIMMOLLER : Détermination des contraintes résiduelles dues à l'oxycoupage des tôles. Forschung n° 36, 1970.
12 Recommandations de l'I.B.S. (Institut Belge de Soudure)-Commission 15 B : Le calcul à la fatigue des assemblages soudés des constructions métalliques en acier.
13 H. THOMAS and F. GOLDBERG : Quality Recommendations for Thermal Cut Surfaces in Steel Structures subjected to Fatigue Loading. Document IIS n° XIII-902-78.
14 NBN 11702. Essai de pliage (2ème édition), 1961.
15 A. PLUMIER : Relation entre les paramètres de soudage d'une colonne et sa charge de flambement. Thèse de doctorat, Université de Liège, 1979.

Ermüdungsrisse in Schweisskonstruktionen

Fatigue Cracks in Welded Steel Structures

Fissures dues à la fatigue dans les constructions métalliques soudées

J.A. NOWIKOW
Kandidat der techn. Wissenschaften
Moskauer Bauingenieur-Institut
Moskau, UdSSR

ZUSAMMENFASSUNG
Die Dauerhaftigkeit geschweisster Metallkonstruktionen wird in erster Linie durch das Auftreten von Ermüdungsrissen vermindert. Es wurde festgestellt, dass die Beständigkeit gegen Ermüdungsrisse in den verschiedenen Zonen von Schweissverbindungen nicht identisch ist. Die wesentlichen Einflussgrössen sind der Wärmeenergiewert des Schweissbogens, die Art der Eigenspannungen infolge Schweissens sowie die mechanischen Eigenschaften des Materials.

SUMMARY
One of the principal causes of strength reduction in welded steel structures is the occurrence of fatigue cracking. It has been shown that the resistance, with respect to fatigue cracking, varies according to different zones of welded joints. This is dependent on the amount of thermal energy introduced during welding and fixed by both the resulting level of residual stresses, and the mechanical properties of the material.

RESUME
Une des principales causes de diminution de la durabilité des constructions métalliques soudées réside dans l'apparition de fissures dues à la fatigue. On a constaté que la résistance vis-à-vis de fissures dues à la fatigue varie selon les différentes zones des assemblages soudés. Elle dépend de l'énergie thermique dégagée lors du soudage et est fixée par la valeur des contraintes résiduelles et par les propriétés mécaniques des matériaux.

1. EINLEITUNG

In der Praxis finden geschweisste Metallkonstruktionen eine vielseitige Verwendung : in Konstruktionen von Industrie- und Gesellschaftsbauten, in Brückenkränen, an Baggern und an anderen Ingenieurbauten.

Eine grosse Gefahr für das normale Funktionieren dieser Konstruktionen stellen Ermüdungsrisse dar, deren Entstehen durch technologische Defekte gefördert werden. Ungenügender Einbrand, Schlackeeinschlüsse sowie andere Defekte und deren Entwicklung haben einen grossen Einfluss auf die Lebensdauer dieser Konstruktionen.

Ungeachtet der Wichtigkeit der Erfoschung der Wachstumsbedingungen von Ermüdungsrissen gibt es wenig experimentelle Untersuchungen auf diesem Gebiet und ihre Resultate sind in der Mehrzahl widersprechend.

Maddox [1] meint nach der Untersuchungen des Risswachstums im Material der Schweissnaht und in der Zone der thermischen Einwirkung, dass die Entwicklungsgeschwindigkeit der Ermüdungsrisse in der Hauptsache von den Festigkeitseigenschaften abhängt.

Walton und Ellison [2] verbinden im Gegensatz zu Maddox den Prozess der Verbreitung der Risse mit dem Einfluss von Eigenspannungen, die vom Schweissen herrühren.

2. EXPERIMENT

Das Hauptziel der vorliegenden Untersuchungen besteht in der Erforschung des Einflusses der Festigkeitseigenschaften des Materials und der Grösse der Schweisseigenspannungen auf die Ermüdungsfestigkeit von Schweissverbindungen in Metallkonstruktionen.

Forschungsobjekte waren Schweissverbindungen aus niedriggekohltem und niedriglegiertem Stahl. Die Wärmezufuhr wurde beim Schweissen von Platten (600 x 145 x 12 mm) durch Varierung der Stromstärke verändert.

Zyklische Prüfungen der Platten wurden unter annähernd pulsierenden Bedingungen bei verschiedener Belastung durchgeführt.

Das Wachstum der Risse wurde visuell, mit Hilfe eines Mikroskops der Auflösung 2,5 x, festgestellt.

Die Resultate der Prüfungen wurden in Graphiken der Abhängigkeit der Gesamtlänge der Risse 2 a, welche sich von zwei Seiten der Platte ausbreiteten, und von der Prüfungsdauer N dargestellt. Mit Hilfe dieser Figuren wurden sodann die mittleren und Augenblicksgeschwindigkeiten des Risswachstums auf Zerstörungsdiagrammen in Abhängigkeit von der Differenz des Spannungsintensitätskoeffizienten ΔK dargestellt, welche nach der Formel von Garny [3] berechnet wurden.

3. BESPRECHUNG

Die Versuchsresultate zeigten, dass in allen Fällen die Risse ungefähr in der gleichen Zeit entstanden. Die Periode der Rissentstehung N_3 überschritt nicht 15 % der gesamten Lebensdauer.

Die Entwicklung der sichtbaren Risse verlief nicht gleichmässig. Bei den Platten, die bei geringerer Wärmezufuhr hergestellt wurden, war die gefährlichste Stelle für die Entstehung von Ermüdungsrissen die Zone der thermischen Einwirkung

Bild 1

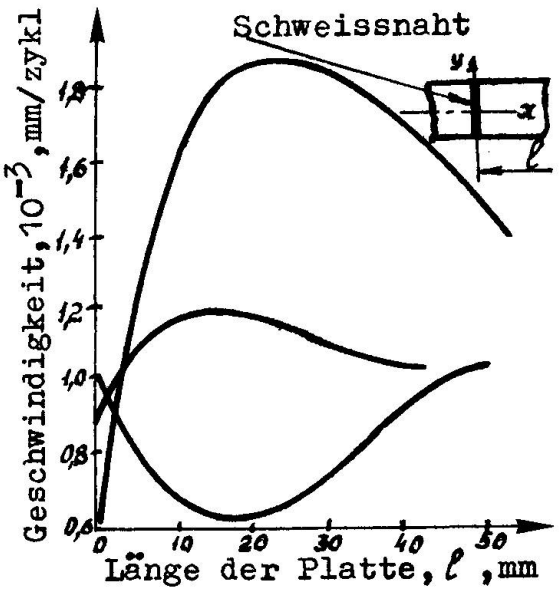

(Bild 1). Das angeschmolzene Metall der Schweissnaht dagegen wies erhöhte Beständigkeit gegenüber Ermüdungsrissen auf.

Die Erhöhung der Stromstärke beim Schweissen führt zu einer Abnahme der mittleren Geschwindigkeit des Risswachstums in der Zone der thermischen Einwirkung und zur Vergrösserung der Geschwindigkeit der Rissentwicklung in der Mitte der Naht. Man kann sagen, dass die Zerstörung von geschweissten Metallkonstruktionen, welche bei grosser Wärmezufuhr hergestellt wurden, höchstwahrscheinlich an der Naht oder im Hauptmetall erfolgt.

Der Vergleich der mittleren Wachstumsgeschwindigkeiten (Bild 1), der Festigkeitseigenschaften (Bild 2) und der Schweisseigenspannungen (Bild 3) zeigte, dass in den Platten, die bei geringerer Wärmezufuhr hergestellt wurden, die Senkung der mittleren Rissausbreitungsgeschwindigkeit im Metall der Naht durch erhöhte Materialeigenschaften in diesen Punkten bedingt wird. Die Schweissspannungen erreichten in der Zone der Schweissnaht ihren grössten Wert. Mit der Entfernung von der Symmetrieachse nehmen die Festigkeitseigenschaften etwas ab, in der gleichen Zeit behalten die Schweissspannungen ihren hohen Wert. Das führt zu einer Zunahme der Rissausbreitungsgeschwindigkeiten in der Zone der thermischen Einwirkung in unmittelbarer Nähe der Naht.

Die Vergrösserung der Schweissstromstärke führt zu einer Verminderung der Fliessgrenze des angeschmolzenen Metalls der Naht. Im Zusammenhang damit wachsen die mittleren Rissgeschwindigkeiten im Material der Schweissnaht ungeachtet dessen, dass die Schweisseigenspannungen beim Schweissen mit höherer Energie des Lichtbogens abnehmen.

In der Zone der thermischen Einwirkung wird das Schweissen bei hohen Stromstärken von einer gleichmässigen Verteilung der Restspannungen und einer Verbesserung der mechnischen Eigenschaften begleitet. Das führt zur Verringerung der Rissgeschwindigkeiten in der Zone der thermischen Einwirkung, was eine Verlängerung der Lebensdauer der Platten bei Entwicklung der Risse in unmittelbarer Nähe der Naht gewährleistet.

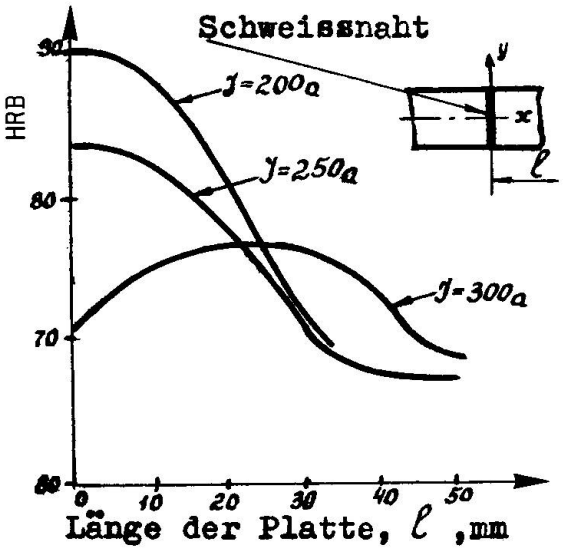

Bild 2

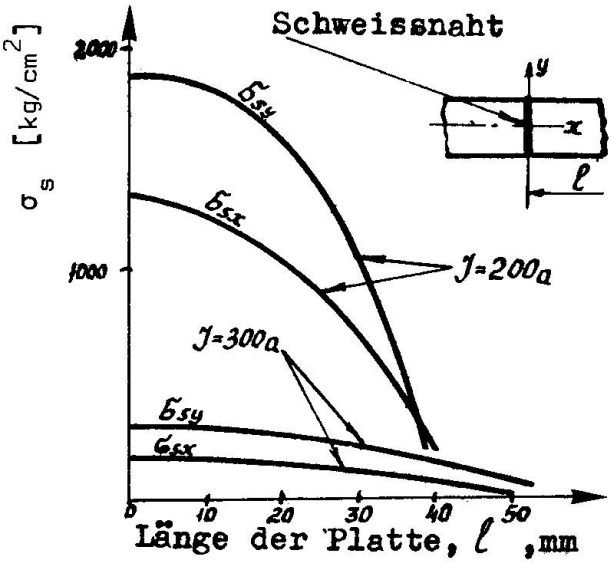

Bild 3

Auf diese Art und Weise kann man durch Veränderung der Schweissstromstärke (Wärmezufuhr) die schwächste Stelle in Schweissverbindungen in bezug auf Rissbildung verschieben. Durch das Benutzen der Graphiken der Abhängigkeit der mittleren Ausbreitungsgeschwindigkeiten von Ermüdungsrissen, welche für verschiedene Stellen der Schweissverbindung konstruiert wurden, kann man die optimalen Schweissverhältnisse ermitteln, welche die gleiche Festigkeit der geschweissten Elemente in Schweissverbindungen auf Rissbildung gewährleisten (Bild 4).

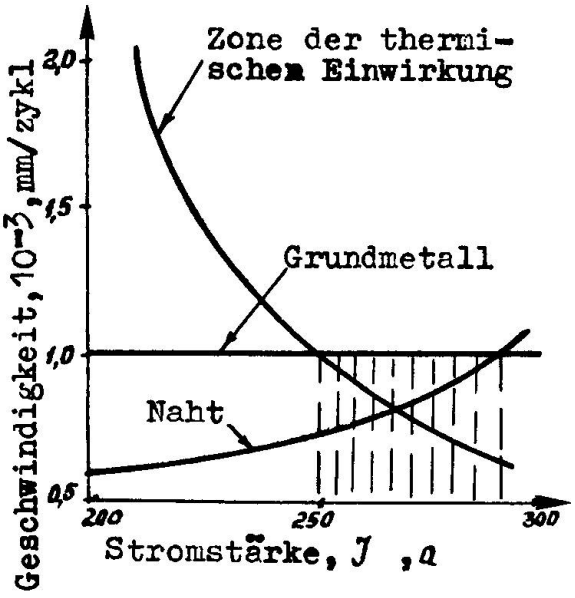

Bild 4

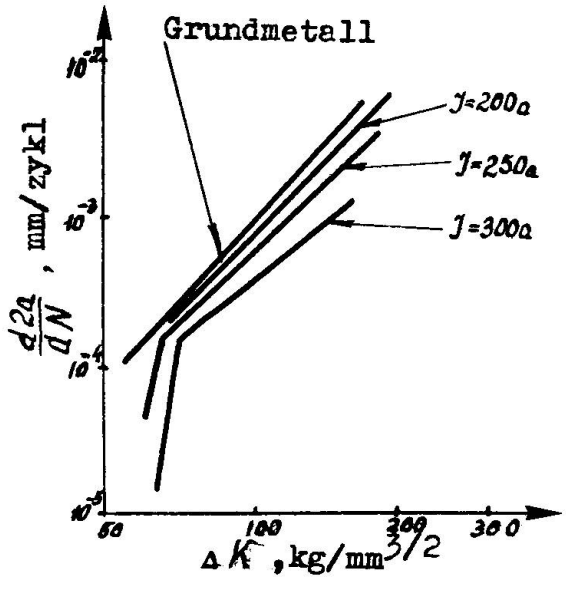

Bild 5

Die Untersuchung der Zerstörungsdiagramme d2a/dN - ΔK (Bild 5) zeigte, dass man den Prozess der Ausbreitung von Ermüdungsrissen in drei Etappen einteilen kann : in eine langsame, eine beschleunigte und eine intensive.

Die Phase der langsamen Rissausbreitung ist durch einen steileren Neigungswinkel der Graphik d2a/dN - ΔK gekennzeichnet und ihre Ausdehnung hängt von der Fliessgrenze des Materials und vom Niveau der äusseren Belastung unter Berücksichtigung der Schweissspannungen ab [4]. Je grösser der Wert von σ_f und je weniger die Summe der Spannungen σ und σ_S, um so grösser ist die Ausdehnung der Anfangsetappe.

In den zwei anderen Etappen (der beschleunigten und der intensiven) kann man die Entwicklung der Risse durch das Gesetz von Paris : $d2a/dN = C(\Delta K)^n$ beschreiben. Der Neigungswinkel der Graphik d2a/dN - ΔK auf den Zerstörungsdiagrammen für diese Phasen, der zahlenmässig durch den Koeffizienten n ausgedrückt wird, verändert sich etwas für die Zone der thermischen Einwirkung mit der Vergrösserung der Wärmezufuhr. Es wurde festgestellt [4], dass sich der Wert von n verringert. Dies hängt mit dem Wachstum der Fliessgrenze des Materials zusammen. Für das angeschmolzene Metall der Naht wird die umgekehrte Abhängigkeit beobachtet.

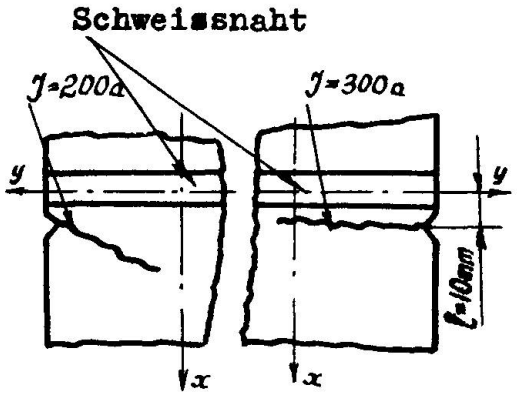

Bild 6

Die Erforschung der Trajektorien der Risse in den Platten, die bei verschiedenen Schweissverhältnissen hergestellt wurden, bestätigte, dass das Wachstum der Ermüdungsrisse auf die Schweisseigenspannungen einwirkt (Bild 6). Es wurde festgestellt, dass die Bewegungsrichtungen der Risse ungefähr senkrecht zu den Hauptzugspannungen standen. Holl und Kichara gelangten für spröde Zerstörungen zu einer analogen Schlussfolgerung [5]. Die grösste Abweichung der Trajektorien betrug ungefähr 10 mm und wurde in den Platten beobachtet, welche mit grosser Wärmezufuhr (grosse Schweisseigenspannungen) hergestellt wurden.

In den Platten, die bei hohen Stromstärken geschweisst wurden, entwickelten sich die Ermüdungsrisse praktisch ohne von der geradlinigen Richtung abzuweichen. Das kann man durch den wesentlich geringeren Einfluss der Schweissspannungen auf das Risswachstum erklären.

4. SCHLUSSFOLGERUNGEN

1. In Schweissverbindungen aus niedriggekohltem und niedriglegiertem Stahl kann man das Risswachstum in drei Etappen einteilen : in eine langsame, eine beschleunigte und eine intensive, welche durch den Neigungswinkel im Zerstörungsdiagramm charakterisiert sind.

   Die Dauer der Phase des langsamen Wachstums hängt vom Verhältnis der statischen Festigkeit des Metalls und der Belastung ab. Je grösser dieses Verhältnis, desto länger ist die Dauer dieser Phase. Bei kleinen Verhältnissen kann die Phase des langsamen Wachstums fehlen.

   Während der beschleunigten und der intensiven Etappe des Risswachstums wird die Geschwindigkeit in der Hauptsache von der Differenz des Spannungsintensitätskoeffizienten kontrolliert. In diesen Abschnitten kann die Rissausbreitung durch das Gesetz von Paris beschrieben werden.

   Die Parameter n und C werden von den mechanischen Eigenschaften des Stahls bestimmt. C ist auch von der Grösse der Spannung abhängig.

2. Die Rissbeständigkeit der verschiedenen Zonen der Schweissverbindung ist nicht gleich und hängt von den mechanischen Eigenschaften des Materials und von der Verteilung der Schweisseigenspannung ab. Auf die Beständigkeit gegenüber Ermüdungsrissen hat die Wärmzufuhr beim Schweissen einen wesentlichen Einfluss. Durch das Verändern der Schweissverhältnisse kann man eine gleichfeste Verbindung bei allgemeiner Erhöhung der Lebensdauer erreichen.

3. Die Kinetik und die Trajektorie des Risswachstums in Schweissverbindungen hängt von der Grösse und Verteilung der Schweisseigenspannungen ab. Zugspannungen vergrössern und Druckspannungen verringern die Risswachstumsgeschwindigkeit. Risse entstehen vorwiegend senkrecht zur Hauptzugspannung.

BEZEICHNUNGEN

2a	: Gesamtlänge der Risse
N	: Anzahl Lastwechsel
d2a/dN	: Augenblicksgeschwindigkeit der Risse
ΔK	: Differenz des Spannungsintensitätskoeffizienten
n, C	: Parameter des Gesetzes von Paris

LITERATUR

[1] MADDOX, S. : Fatigue Crack Propagation in Weld Metal and HAZ, Metal Construction and British Welding Journal, 1970.

[2] WALTON, D., ELLISON, E. : Entstehung und Verbreitung von Ermüdungsrisse, International Metal, Rec, 1972.

[3] GARNY, T. : Der Einfluss der mittleren Spannung und der Fliessgrenze auf die Verbreitung von Rissen im Stahl, Metal Construction and British Welding Journal, 1969.

[4] NOWIKOW, Ju.A., SOTEEW, W.S. : Der Einfluss vorhergehender Deformation auf die Entwicklung von Ermüdungsrissen in der Umgebung der Naht einer Schweissverbindung, Swarothnoe proiswodstwo, 1976.

[5] HOLL, G., KICHARA, C. : Spröde Zerstörungen geschweisster Konstruktionen, Maschinostroenie, 1974.

Fissuration par fatigue d'assemblages soudés en acier HLE

Ermüdungsrissbildung in Schweissverbindungen hochfester Stähle

Fatigue Crack Growth in Welded Joints in HSLA Steels

H.-P. LIEURADE
Institut de recherche de la sidérurgie française
Saint-Germain-en Laye, France

C. MAILLARD-SALIN
Institut de recherche de la sidérurgie française
Saint-Germain-en Laye, France

M. TRUCHON
Institut de recherche de la sidérurgie française
Saint-Germain-en Laye, France

RESUME
Les aciers à haute limite d'élasticité (HLE) sont de plus en plus utilisés dans le cas des structures métalliques soumises à des sollicitations cycliques. Pour concevoir ces structures en toute sécurité, il est nécessaire de connaître le comportement en fatigue de tels aciers. C'est pourquoi cette étude concerne des aciers de limites d'élasticité comprises entre 280 et 520 MPa. Pour ces nuances, les vitesses de fissuration du métal de base et de la zone affectée par la chaleur ont été comparées. L'influence de la limite d'élasticité et de l'épaisseur de la tôle ainsi que du niveau des contraintes résiduelles a été prise en compte.

ZUSAMMENFASSUNG
Die Verwendung von hochfesten Stählen für Konstruktionen, die wechselnder Beanspruchung ausgesetzt sind, ist in stetem Anwachsen. Zur sicheren Erstellung derartiger Bauten ist die Kenntnis des Ermüdungsverhaltens dieser Stähle nötig. Die vorliegende Untersuchung befasst sich mit Stählen, deren Streckgrenzen zwischen 280 und 520 MPa liegen. Die Rissausbreitungsgeschwindigkeit im Grundmetall wird mit derjenigen in der Wärmeinflusszone verglichen, und zwar unter Berücksichtigung der Streckgrenze, der Blechdicke und des Eigenspannungsniveaus.

SUMMARY
The steadily increasing use of high strength low alloy steels in cyclically loaded structures requires a knowledge of their fatigue behaviour for safe design. This paper deals with steels whose yield stresses range from 280 to 520 N/mm^2. Fatigue crack growth rates are compared in the base metal and heat affected zone with the influence of yield strength, plate thickness and residual stress level also being considered.

I - INTRODUCTION

En construction métallique une meilleure connaissance de la résistance des aciers, d'une part, des contraintes en service, d'autre part, a permis aux constructeurs de diminuer considérablement les coefficients de sécurité employés au cours des calculs. Le poids propre d'une structure peut représenter alors une source de sollicitations non négligeable. Pour alléger les structures, l'emploi d'aciers à haute limite d'élasticité (HLE), permettant de réduire les épaisseurs à mettre en oeuvre, est de plus en plus souvent envisagé par les constructeurs métalliques.

Pour une structure métallique soudée la détermination des caractéristiques de fatigue peut être faite :
- soit par le tracé expérimental de courbes de Wöhler ou courbe σ-N, où σ est l'amplitude de contrainte imposée et N la durée de vie correspondante.
- soit par le calcul de la durée de vie en fissuration de la structure, sans tenir compte de la durée d'amorçage. Des études récentes [1 à 3] montrent en effet qu'à partir de défauts de soudage : soufflures, manques de pénétration, inclusions de laitier, etc .. , le stade d'amorçage d'une fissure de fatigue peut être négligeable. La durée de vie en propagation d'un joint donné correspond alors au nombre de cycles nécessaires pour faire propager une fissure de fatigue de défauts initiaux de taille connue jusqu'à la rupture du joint.

La présente étude a pour but de fournir des données quantitatives concernant la cinétique de propagation des fissures de fatigue dans le métal de base (MB) et dans la zone affectée par la chaleur (ZAC), pour des aciers ayant des limites d'élasticité échelonnées.

2 - CONDITIONS EXPERIMENTALES

2.1. Nuances d'aciers

Cette étude concerne quatre aciers de construction métallique :
- trois aciers de qualité courante : E24-4, E355 et A70-2 (normes AFNOR 35-501, 36-201), les éprouvettes étant prélevées dans des tôles laminées à 12 mm d'épaisseur.
- un acier pour lequel les propriétés de striction dans le sens de l'épaisseur, perpendiculairement à la surface sont garanties : E36-4 Z35 (norme AFNOR 36-202), les éprouvettes étant prélevées dans des tôles laminées à 20 et 40 mm d'épaisseur.

La composition chimique des aciers étudiés est précisée dans le tableau 1.

Tableau 1.

Acier	C	Mn	Si	P	S	Ni	Cr	V	Al	N_2	Cu	Mo	Nb
E24	0,10	0,74	0,19	0,015	0,019								
E36-Z	0,145	1,40	0,292	0,006	0,003	0,42	0,075		0,019	0,012		0,031	
E355	0,15	1,35	0,30	0,016	0,019								0,022
A70	0,20	1,41	0,38	0,092	0,012	0,10	0,03	0,15	0,04	0,014	0,18	0,01	

Les quatre nuances ont été étudiées à l'état normalisé.

Les caractéristiques de traction monotones et cycliques (R'_e, n') mesurées en long, sont rassemblées dans le tableau 2.

Tableau 2.

Acier	Re (MPa)	Rm (MPa)	A (%)	Z (%)	R'_e (MPa)	n'
E 24	280	400	42,5	78,5		
E 36-Z	375	545	34,2	77	350	0,21
E 355	395	540	35,5	74,5	325	0,16
A 70	515	660	24	54		

2.2. Eprouvettes d'essais

Les éprouvettes utilisées pour déterminer les vitesses de fissuration sont du type ASTM CT.

- Joints soudés en croix

Les joints sont constitués d'une tôle sur laquelle deux ailettes ont été rapportées (figure 1).

Pour les aciers E24 et E355, un soudage automatique sous flux (ASTM-AWS 62 EL12) a été réalisé.

Pour les aciers de nuance A70, un soudage manuel a été utilisé avec des électrodes à enrobage basique (ASTM-A 316 1969).

- Joints soudés bout-à-bout

Dans le cas de la nuance E36-Z35, une préparation en V dissymétrique a été utilisée (figure 2). Le soudage manuel à l'arc a été réalisé avec des électrodes au C-Mn (ASTM-AWS E 7018).

- Prélèvement

Aussi bien dans le cas du métal de base que dans celui des joints soudés (figures 1 et 2), les éprouvettes ont été prélevées en sens long : la fissure se propage dans toute l'épaisseur de la tôle, perpendiculairement au sens de laminage.

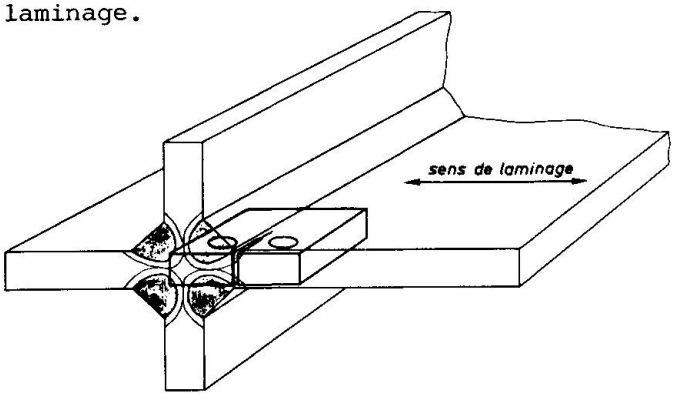

Figure 1 Prélèvement des éprouvettes dans les joints soudés en croix

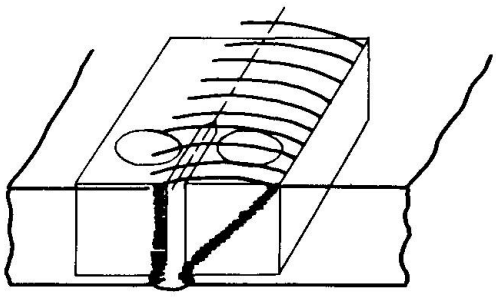

Figure 2 Prélèvement des éprouvettes dans les joints soudés bout à bout

2.3. procédure d'essai

- Tous les essais ont été effectués à l'air ambiant, à une température voisine de 20°C. Les éprouvettes ont été sollicitées en traction ondulée (rapport de charge R_S égal à 0,1 ou 0,7). La fréquence du cycle de chargement était comprise entre 5 et 110 Hz.
- La mesure de la longueur de la fissure a été faite en surface, soit par méthode optique soit à l'aide de divers dispositifs automatiques de suivi de fissure.
- A partir des données enregistrées (a,N), le calcul de la vitesse de fissuration da/dN en fonction de l'amplitude, ΔK, du facteur d'intensité de contrainte a été effectué automatiquement par ordinateur.

3 - RESULTATS DES ESSAIS

Les figures 3 à 6 comparent les résultats obtenus dans le métal de base et la ZAC, pour les 4 nuances étudiées.

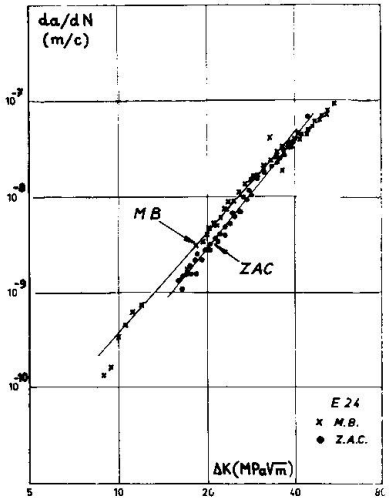

Figure 3 Evolution de da/dN = f (ΔK)
Acier E24

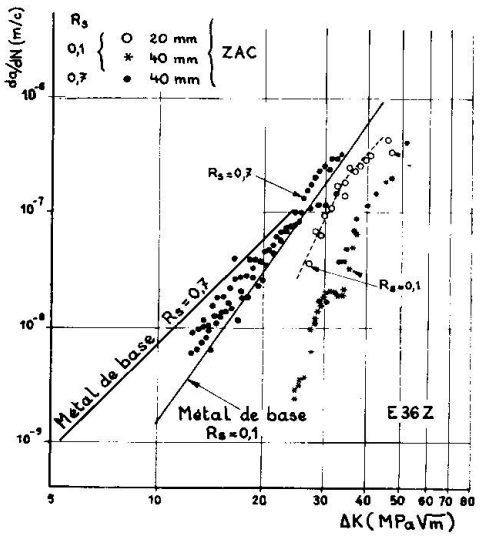

Figure 4 Evolution de da/dN = f (ΔK)
Acier E36-Z

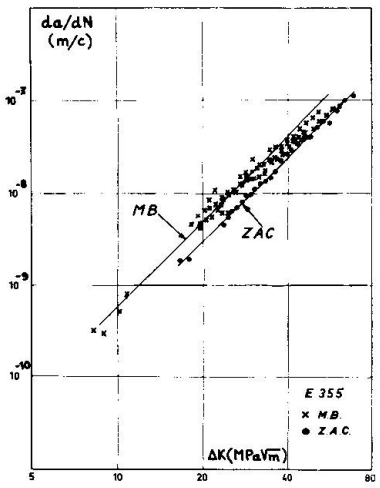

Figure 5 Evolution de da/dN = F (ΔK)
Acier E355

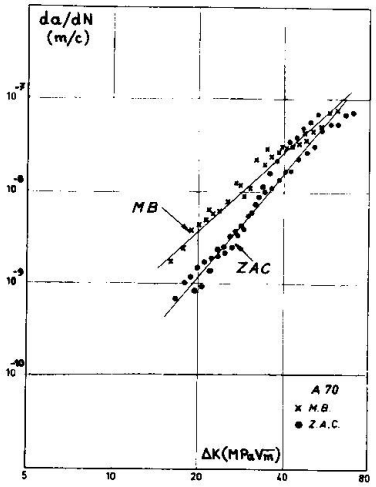

Figure 6 Evolution de da/dN = f (ΔK)
Acier A70

Dans chaque cas, les coefficients C et m de la loi de vitesse de fissuration suivante ont été calculés :

$$da/dN = C\ (\Delta K)^m$$

Ces coefficients sont reportés dans le tableau 3.

Tableau 3

Acier	E 24		E 36-Z					E 355		A70	
	MB	ZAC	MB		ZAC			MB	ZAC	MB	ZAC
Epaisseur	10	10	20/40		20	40		10	10	10	10
R_s	0,1	0,1	0,1	0,7	0,1	0,1	0,7	0,1	0,1	0,1	0,1
m	3,5	3,8	4,5	3,1	(7)	(9,3)	3,8	2,9	3,3	2,8	4,1
C (10^{13})	12	3,4	0,41	60	(0,05)	(3.10^{-5})	46	9,3	14	86	0,39

4 - DISCUSSION DES RESULTATS

4.1. Corrélation entre m et C

Plusieurs auteurs [1, 2] ont montré que les coefficients de la loi de fissuration ne sont généralement pas indépendants. Une relation linéaire entre m et log C a été trouvée. Récemment GURNEY [3] a donné une application de cette relation au cas des aciers de construction métallique, incluant aussi des résultats obtenus dans le cas du métal fondu (MF) et de la ZAC. La corrélation qu'il obtient entre m et C lui permet d'écrire que la largeur du faisceau des droites log da/dN - log ΔK est minimale au point de coordonnées :

$$da/dN = 1{,}32 \cdot 10^{-7} \text{ m/cycle} \quad \Delta K = 28{,}3 \text{ MPa } \sqrt{m}$$

Sur le diagramme m-logC de la figure 7 nous avons reporté :
- les résultats compilés par GURNEY,
- des résultats obtenus à l'IRSID sur des aciers de construction [4],
- les résultats de la présente étude, obtenus aussi bien dans le métal de base que dans la ZAC, pour des épaisseurs de tôle égales à 10 mm.

L'ensemble des résultats vérifie bien la relation proposée par GURNEY ; cette relation permet de limiter la discussion à l'étude de l'évolution d'un seul coefficient de la loi de vitesse de fissuration. C'est pourquoi par la suite nous caractériserons le comportement en fissuration par l'exposant m.
On peut noter cependant que cette relation n'est pas vérifiée pour les épaisseur 20 et 40 mm (acier E 36-Z).

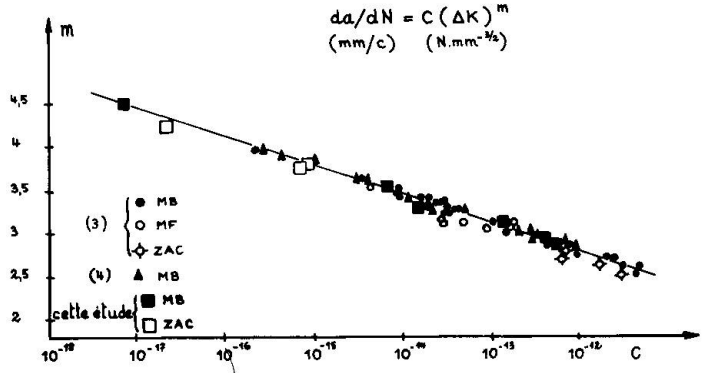

Figure 7 Relation entre m et log C

4.2. Variation de la loi de fissuration en fonction de la limite d'élasticité

Nous avons reporté sur le diagramme m - R_e de la figure 8 de nombreux résultats obtenus sur des aciers de construction métallique [3] et mécanique [5], ainsi que ceux obtenus sur les aciers étudiés dans ce travail.

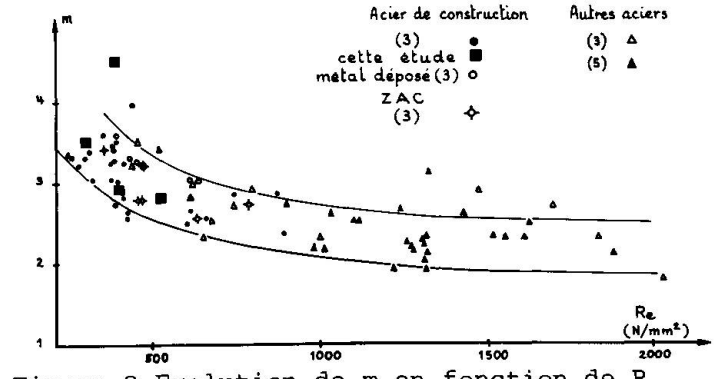

Figure 8 Evolution de m en fonction de R_e

L'ensemble des résultats présente en moyenne une diminution de l'exposant m quand R_e augmente. La bande de dispersion des résultats est relativement large : pour une valeur R_e donnée, m est connu à environ $\pm$ 15 %. En ce qui concerne les 3 aciers de qualité courante étudiés, m passe de 3,5 à 2,8 quand R_e augmente de 280 à 515 MPa.

L'acier E36-Z a un comportement sensiblement différent ; le niveau de m (4,5) est élevé compte tenu de sa limite d'élasticité. La considération de la limite d'élasticité cyclique, R'_e, ne permet pas d'expliquer les différences de comportement entre les aciers E355 et E36-Z. Par ailleurs, BAUS et coll [6] ont montré que la vitesse de fissuration dépendait des capacités d'écrouissage

cyclique du matériau et qu'il existait une relation entre m et n' (coefficient d'écrouissage cyclique). La relation moyenne proposée, m = 20 n', indique que pour des matériaux présentant une rupture ductile, la vitesse diminue (m croît) lorsque le coefficient d'écrouissage cyclique augmente.
Dans le cas des aciers E36-Z et E355, les valeurs de m estimées à l'aide de n' (respectivement 4,2 et 3,2) sont proches des valeurs expérimentales (respectivement 4,5 et 2,9). La valeur élevée de n' (0,21), qui conduit à un très bon comportement en fissuration, semble reliée à l'analyse chimique de l'acier E36-Z, en particulier aux bas niveaux en S et P et peut être à la présence de Ni (tableau 1).

4.3. Effet de divers paramètres sur la loi de fissuration dans la ZAC

- Limite d'élasticité du métal de base.
L'influence des caractéristiques mécaniques du métal de base a été considérée dans le cas des aciers E24, E355 et A70 étudiés en épaisseur 10 mm.

La vitesse de fissuration de la ZAC est toujours inférieure à celle du métal de base. L'écart entre ces vitesses de fissuration varie en fonction de ΔK. Pour quantifier cette évolution, nous avons calculé le rapport des vitesses de fissuration de la ZAC et du MB pour ΔK égal à 20 et 40 MPa$\sqrt{m}$, et le rapport des niveaux de m obtenus respectivement dans la ZAC et le métal de base.
Les résultats de ces calculs sont rassemblés dans le tableau 4.
Tableau 4

Nuance de l'acier	R_e (MPa)	$(da/dN)_{MB}/(da/dN)_{ZAC}$		m_{ZAC}/m_{MB}
		ΔK (MPa$\sqrt{m}$) 20	40	
E24	280	1,6	1,2	1,09
E355	395	1,9	1,3	1,14
A70	515	3,1	1,7	1,46

Pour un même niveau ΔK, l'écart entre les vitesses augmente avec la limite d'élasticité du métal de base : pour ΔK = 20 MPa$\sqrt{m}$, le rapport $(da/dN)_{MB}/(da/dN)_{ZAC}$ passe de 1,6 pour l'acier E24 à 3,1 pour l'acier A70.

Cet écart tend à diminuer aux plus fortes valeurs de ΔK : dans tous les cas, les résultats dans le métal de base et la ZAC se superposent pour ΔK élevé.

De même, le rapport m_{ZAC}/m_{MB} augmente sensiblement avec la limite d'élasticité du métal : il croît de 1,09 à 1,46 quand R_e passe de 280 à 515 MPa.

- Epaisseur de la tôle
L'acier E36-Z a été étudié en 2 épaisseurs (20 et 40 mm). Les résultats présentent (figure 4) un effet significatif de l'épaisseur sur la vitesse de fissuration dans la ZAC. La réduction très importante des vitesses de fissuration dans le cas de l'épaisseur 40 mm est due à la présence de contraintes résiduelles de compression à coeur de l'éprouvette [7]. La loi de PARIS est mal vérifiéée, les valeurs de m et C que l'on peut cependant estimer ne suivent pas la relation trouvée entre m et log C .

- Rapport de charge ($R_s = \sigma_{min}/\sigma_{max}$)
Dans le cas de l'acier E36-Z soudé en 40mm d'épaisseur, deux niveaux de R_s ont été étudiés (0,1 et 0,7). La figure 5 montre que, pour R_s = 0,1 les écarts entre les vitesses de fissuration sont grands entre le métal de base et la ZAC ; pour ΔK = 20 MPa $\sqrt{m}$ le rapport $(da/dN)_{MB}/(da/dN)_{ZAC}$ est supérieur à 30.

Par contre pour R_S = 0,7 les différences sont sensiblement plus faibles ; m_{ZAC}/m_{MB} passe de 2 à 1,2 quand R_S passe de 0,1 à 0,7.

- Traitement thermique de détensionnement.

Comme le présente la figure 9, dans le cas de joints en acier E36-Z (épaisseur 40 mm), la loi de vitesse de fissuration de la ZAC, après traitement de détensionnement, est comparable à celle du métal de base.

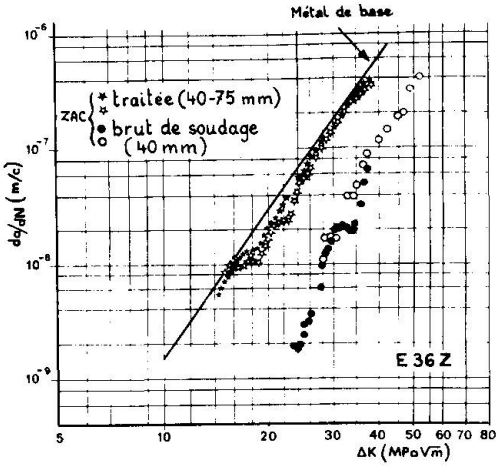

Figure 9 Effet d'un traitement de détensionnement

4.4. Phénomènes de fermeture à la pointe de la fissure

Au cours d'un essai en traction repétée la plastification cyclique peut conduire à une fermeture à la point de la fissure. On peut analyser les résultats en considérant que l'endommagement se fait quand la fissure est ouverte cette partie du cycle étant caractérisée par ΔK_{eff}.

La figure 10 présente une application de ce concept dans le cas de la fissuration dans la ZAC d'un joint en acier E36-Z. Les résultats pour R_S = 0,1 exprimés en fonction de ΔK_{eff}, se superposent à ceux obtenus sur le métal de base pour R_S = 0,7, valeur pour laquelle la fissure est complètement ouverte. Ce même concept a été utilisé pour rendre compte de l'effet de R_S sur la vitesse de fissuration du métal de base [8].

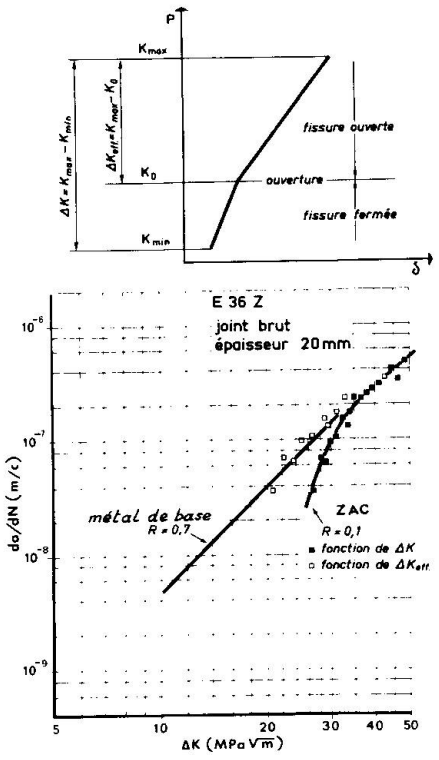

Figure 10 Vitesse de fissuration en fonction de ΔK_{eff}

En fait, quelles que soient les conditions de sollicitation (niveau R_S , présence de contraintes résiduelles de soudage) on obtient une courbe unique si l'on ne s'intéresse qu'à la portion du cycle pendant laquelle la fissure est complètement ouverte.

L'ensemble des résultats présentés s'explique donc par l'évolution des contraintes résiduelles existant à la pointe de la fissure.

Ces observations permettent aussi d'expliquer les résultats souvent contradictoires obtenus dans la littérature, en prenant en compte le niveau et le signe des contraintes résiduelles résultant de la procédure de soudage et du mode de prélèvement des éprouvettes. Enfin on peut en déduire que l'augmentation des capacités d'écrouissage cyclique d'un acier (croissance de n') par une analyse chimique ou des traitements thermomécaniques adaptés doit conduire à des caractéristiques de résistance à la fissuration plus élevées.

5 - CONCLUSIONS

- Pour des tôles de faible épaisseurs (< 20 mm), la vitesse de fissuration, par fatigue, $da/dN = C\ (\Delta K)^m$, dans la zone affectée par la chaleur, est légèrement inférieure à celle du métal de base, quand $\Delta K < 30$ MPa $\sqrt{m}$.
- On trouve, dans ce cas, une relation linéaire entre m et logC, correspondant à la fissuration dans le métal de base ou dans la zone affectée par la chaleur.
- L'écart s'accentue quand on fait croître l'épaisseur ou la limite d'élasticité de la tôle. Les résultats ne vérifient plus les relations précédentes.
- L'application de R_S élevés ($\geq 0,7$) ou l'application d'un traitement de détensionnement conduit à des lois de fissuration voisines de celle du métal de base.
- L'ensemble des résultats expérimentaux s'interprète par les phénomènes de fermeture de la fissure dus aux contraintes locales monotones (résultant du soudage ou de l'application d'une contrainte statique) ou cycliques (conséquence de la plastification à la pointe de la fissure).
- D'un autre côté, on peut augmenter considérablement la résistance à la fatigue des assemblages soudés par divers procédés post-soudage qui agissent sur la phase d'amorçage et dont l'efficacité croît avec la limite d'élasticité de la tôle. [9].

REFERENCES

1. KITAGAWA (H), MISUMI (M),. An estimation of effective stress intensity factors by a crack model considering the mean stress.
   1st Jap. Nat. Symposium on Fracture Mechanics Jap. Soc. Mech. Eng. Juin 1981, pp. 710-717.

2. BAUS (A), CHARBONNIER (J.C.), LIEURADE (H.P.), MARANDET (B), ROESCH (L), SANZ (G). Etude par la mécanique de la rupture de la ténacité, de la fissuration par fatigue et de la fissuration par corrosion sous contrainte d'aciers à très haute résistance.
   Mém. Scient. Rev. Mét. Décembre 1975, pp. 891-935.

3. GURNEY (T.R.). An analysis of some fatigue crack propagation data of steels subjected to pulsating tension loading.
   Welding Research International. Vol. 9, n° 4, pp. 45-58.

4. REGNIER (L), TRUCHON (M). Travaux non publiés.

5. LIEURADE (H.P.). Thèse d'Etat. Metz 1978.

6. BAUS (A), LIEURADE (H.P.), MICHAUT (B), TRUCHON (M). Relation entre les paramètres de fissuration et les caractéristiques cycliques d'une gamme étendue d'aciers.
   4ème Conf. Int. sur "la Résistance des Métaux et Alliages". Nancy 1976.

7. TRUCHON (M), LIEURADE (H.P.), PUTOT (C). A study of fatigue crack propagation in E36 steel welded joints.
   Conf. Int. "L'acier dans les Structures Marines". Paris Octobre 1981.

8. BENOIT (D), LIEURADE (H.P.), MILLE (P), PLUVINAGE (G). Phénomène de fermeture à la pointe d'une fissure de fatigue dans le cas des aciers.
   Revue de Métallurgie Juillet-Août 1980, pp. 773-783.

9. LIEURADE (H.P.). La résistance à la fatigue des assemblages soudés.
   Métaux Corrosion Industrie, n° 586, Juin 1974, pp. 1-24.

Design Fatigue Life of Welded Cruciform Joints

Calcul de la durée de vie des assemblages soudés en croix

Lebensdauerberechnung von geschweissten Kreuzverbindungen

N. RECHO
Dr. Ingénieur
C.T.I.C.M.
Puteaux, France

J. BROZZETTI
Directeur, Dép. des Recherches
C.T.I.C.M.
Puteaux, France

SUMMARY
The paper presents an attempt to identify a simple relationship between the phenomena describing the propagation of a plane crack subjected to constant amplitude loading (Paris law type). Experimental fatigue results for welded cruciform joints plotted on a classical log N-log Sr scale are used. The objective is to determine the coefficients of the Paris law through the use of global S-N curves, and to establish a simple method, based on fracture mechanics models of fatigue, for the evaluation of the design fatigue life of cruciform welded joints.

RESUME
Cet article se propose d'identifier une relation phénoménologique qui décrit la propagation d'une fissure plane sous cycles d'amplitude constante (du type loi de Paris) aux résultats d'essais globaux obtenus sur des assemblages soudés cruciformes, dont les efforts sont transmis par les cordons de soudures, et tracés sous la forme classique des courbes S-N. L'objectif est double: d'une part, déterminer les coefficients de la loi de Paris à partir de cette seule information globale, d'autre part, d'établir une méthode simple de vérification de la durée de vie de ces assemblages basée sur les concepts de la mécanique de la rupture.

ZUSAMMENFASSUNG
In diesem Beitrag wird der Versuch unternommen, ein phänomenologisches Verhalten, das die Rissfortpflanzung unter konstanter Schwingbreite beschreibt (entsprechend der Paris-Gleichung) mit den Gesamtversuchsergebnissen geschweisster Kreuzverbindungen, welche durch Wöhlerkurven dargestellt sind, zu identifizieren. Es werden zwei Ziele verfolgt: Einerseits die Beiwerte der Paris-Gleichung aus diesen Gesamtergebnissen zu bestimmen und andererseits eine einfache, auf der Bruchmechanik gründende, Näherungsmethode für die Lebensdauer von ermüdungsbeanspruchten Kreuzverbindungen auszuarbeiten.

1. INTRODUCTION

From a code specifications stand point, the design life of welded joints is checked on the basis of S_r-N Curves |1|, |2|, |3|, which relate, for given classified details, the stress variation S_r (stress range) against the number of cycles N. This relation, known as the WOHLER line, is written as :

$$N = A\, S_r^b$$

A and b are two constants which are determined on an experimental basis. These coefficients depend in reality of many factors, whose influence are still not well established. This explains, the reason why fatigue test results show very wide dispersion. Figure 1, which gathers a set of S-N lines of various test series of specimens which belong to the same statistical population referred as load carrying welds of cruciform welded joints - type K4 in the conventional classification - shows the evidence for this statement.

The purpose of this paper is twofold : one is to show how the coefficients of the PARIS law, which is a fracture mechanic model of fatigue, may be deducted from global information as given by a S_r-N line, the other is to derive simplified formulae which gives the fatigue life with a reasonable good agreement for the type of welded joint considered. An example will illustrate the validity of this approximate formulation.

(fig.1)

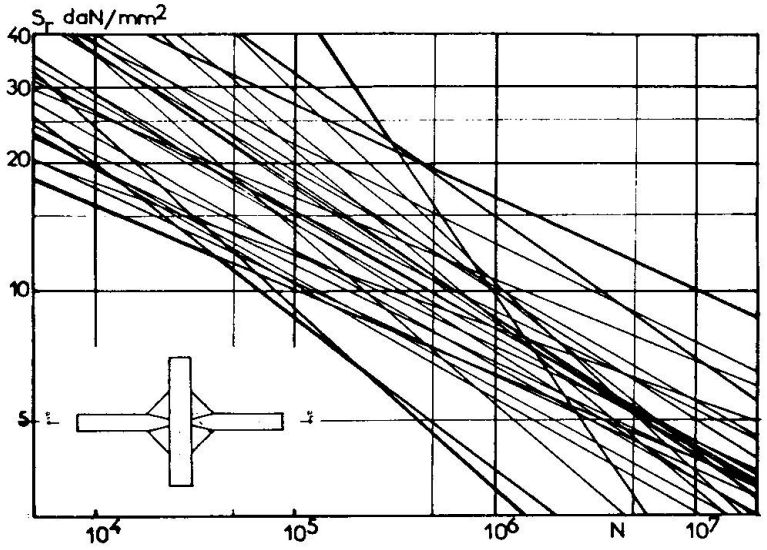

2. EVALUATION OF THE COEFFICIENTS OF PARIS LAW IN TERMS OF THE S-N RESULTS

2.1 Presentation of the joint geometry

Several reasons have motivated the choice of a cruciform welded joint in which the applied load is transmitted through fillet welds (with or without lack of penetration) (fig. 2) to validate the underlined approach :

a) this type of welded detail shows two crack initiation mecanisms, one at the root of weld which results from the design of the weldment, i.e., partial penetration welds , the other at the toe of the weld due to local stress concentration or defects.

b) the fatigue life for such detail is mainly determined by the crack growth period (for which the PARIS law is applicable).

c) and finally, for this type of welded joint, a sufficient amount of data exists in the literature, to enable us to study statistically the influence of various design variables (geometry, material, welding methods...).

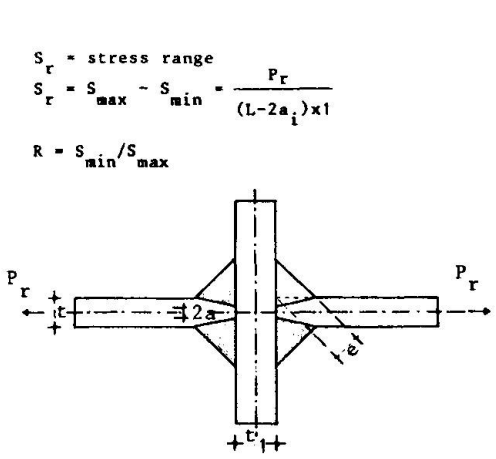

load-carrying welded cruciform joint

(fig. 2)

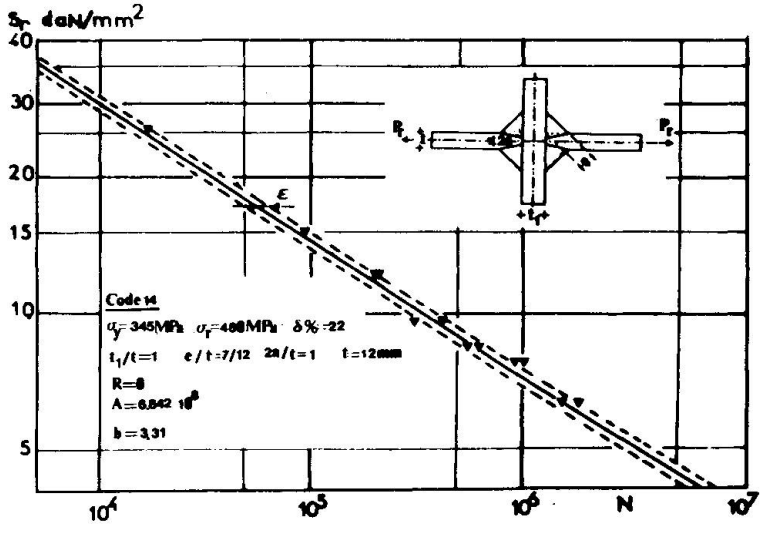

(fig.3)

2.2 Calculation of the life duration on the basis of fracture mechanics analysis

In fracture mechanics models of fatigue, the initiation period is normally neglected. The crack growth from existing defects in welded joints is assumed to follow the PARIS law (the threshold value is disregarded) :

$$da/dN = D(\Delta K)^n \qquad (1)$$

da/dN : is the crack growth propagation from crack size a.
ΔK : is the amplitude of the stress intensity factor
D and n : are two constants which depends on the material

When applying a crack propagation law, one must know the crack size from which this law is applicable. For load carrying welds (as in cruciform joints) where a lack of penetration is present, the size of the lack of penetration (2a in fig.2) is a good estimate of the initial crack size. But for a crack which originates at the toe of the weld (in case of full penetration welds) a crack size must be assessed [4]. As well, the parameters of the PARIS law D and n must to be known. The determination of these constants presents some difficulties, since the crack propagates generally in the HAZ, and this needs special fracture mechanic specimens which reproduce the HAZ of the welded zone to determine the D and n constants. To overcome this difficulty, we have used an engineering approach which consists in identifying the PARIS law with S-N lines in order to evaluate an average value of D and n (this will be explained in § 2.3).

According to the definitions given in figure 2, the life duration (or number of cycles to rupture) for crack initiating at the root may be derived from equation (1) :

$$N = \frac{P_r^n}{D} \int_{a_i}^{a_f} \frac{da}{(\Delta K)^n} P_r^{-n} \qquad (2)$$

In this law the stress intensity factor (ΔK) may be written as :

$$\Delta K = S_r . K_t . \sqrt{\pi a} . f(a) . f(p) \qquad (3)$$

K_t is the stress concentration factor (S.C.F.) $\Delta\sigma/S_r$, $\Delta\sigma$ is the variation of the principal maximum stress at the notch. The evolution of the S.C.F. in terms of

the crack length may be approximated by the following relation :

$$K_t = K_o + K\left(\frac{12}{t}\right)^{\alpha} a^{\alpha} \qquad (4)$$

and the geometrical correction factor f(a) which depends on the geometry of the cruciform joint, and on the size of the propagating crack may be approximated by the following relation

$$f(a) = f_o + F\left(\frac{12}{t}\right)^{\beta} a^{\beta} \qquad (5)$$

In both relations, (4) and (5) t is in mm, and K_o, K, f_o and F have been calculated by F.E.M. [5]. In relation (3), f(p) is the correction for the existing plastic zone, which may be evaluated from [5] :

$$f(p) = \left\{1 - \frac{1}{2} f(a_i) \frac{1}{(1-R)^2} \frac{k_t S_r^2}{\sigma_e}\right\}^{-1/2} \qquad (6)$$

It has been observed that the value of f(p) which is, in most case, close to 1 does not have a significant effect on the life duration.

Taking into account (4) and (5), (2) becomes

$$N = \frac{1}{D \cdot f^n(p)} \int_{a_i}^{a_f} \frac{da}{\left\{\left(\frac{\sqrt{\pi a}}{L-2a}\right)\left(k_o + K\left(\frac{12}{t}\right)^{\alpha} a^{\alpha}\right)\left(f_o + F\left(\frac{12}{t}\right)^{\beta} a^{\beta}\right)\right\}^n} P_r^{-n} \qquad (7)$$

Knowing the coefficients D and n of the PARIS law, the relation (7) allows us to evaluate the number of cycles to failure.

2.3 Evaluation of D and n through an identification procedure

A classical representation of fatigue test results is represented on figure 3, each point defined by the couple of values (S_{ri}, N_i) indicates a test result. Because of the significant dispersion which exists in the experimental results, a statistical treatment of the data is required to estimate the fitting curve. Generally the data are plotted on a log-log scale, and a simple linear regression is used to evaluate the unknown parameters (log A, b) through a minimization procedure of the sum of squares errors ε_i :

$$\log N = \log A + b \log S_r + \varepsilon_i \qquad (8)$$

The results of such statistical treatment on a large series of test results, performed on the same type of welded cruciform joints was already shown in figure 1. With the help of the definition stated in figure 2, equation (8) is written as :

$$N = \left\{A/(L-2a_i)^b\right\} \cdot P_r^{\,b} \qquad (9)$$

By equating the relations (7) and (9), the coefficients of PARIS law may be evaluated as :

$$n = -b$$

$$D = \frac{(L-2a_i)^b}{A \cdot f^n(p)} \int_{a_i}^{a_f} \frac{da}{\left\{\left(\frac{\sqrt{\pi a}}{L-2a}\right)\left(k_o + K\left(\frac{12}{t}\right)^{\alpha} a^{\alpha}\right)\left(f_o + F\left(\frac{12}{t}\right)^{\beta} a^{\beta}\right)\right\}^n} \qquad (10)$$

In the previous relation, the values of b, A are obtained through statistical analysis, L and a_i are experimental values, and k_o, K, f_o, F, α and β are numerical values (see § 2.2).

2.4 Results of the statistical analysis

Through the procedure that has been explained above, a set of D, and n coefficients where evaluated. Several variances analysis were performed in order to assess the significance of influencing parameters on D and n values. Results of these variance studies are summarized hereafter [5] :

- the material properties of steel (yield point, max stress, percent elongation) do not have any influence.
- the R ratio, has a slight influence which appears only when $R > 0$, (this conclusion is not surprising because the specimens are small).
- there exists a linear relation between log D and n, which does not seem to depend on the grade of steel, but on the type of failure mechanism (root or toe initiation). For welded load carrying cruciform joints the relation is the following.

$$D = \frac{2,52}{(67)^n} 10^{-5} \quad \text{(units : daN, mm)} \qquad (11)$$

Figure 4 gives a comparison of test results and proposals from various published sources with the relation given by equation (11). The use of this equation reduces to a great extent the scatter in fatigue data.

(fig. 4)

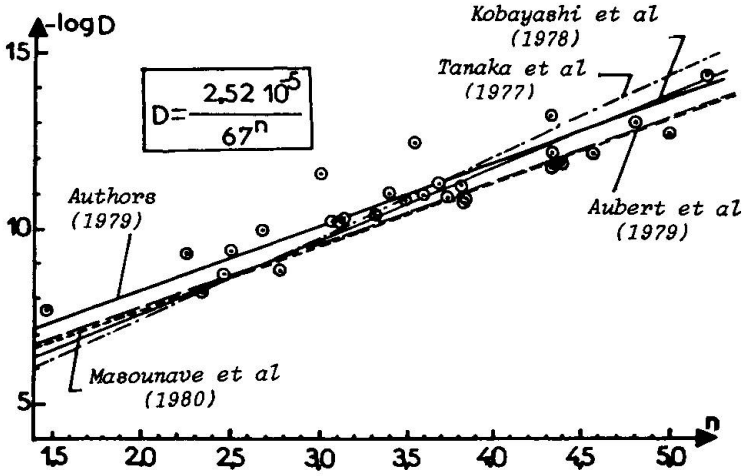

3. A SIMPLIFIED FORMULAE BASED ON FRACTURE MECHANIC CONCEPTS TO EVALUATE THE LIFE DURATION OF LOAD CARRYING WELDED CRUCIFORM JOINTS.

3.1 Derivation of a simplified formulae

For design purposes, the evaluation of the life duration through the direct use

of the equation (7) may be too cumbersome. For an engineering approach, there is still a need for simplied formulae, which do not have the handicap in the classical approach which, for a given detail, defines "probabilistic" safe S-N lines from test results with a wide scatter. The WOHLER line concept fails in determining the influence of purely determistic design variables, like geometry and failure mechanism for example.

We have determined for load carrying fillet welded cruciform joints that mean life may be predicted with a reasonable agreement according to the following expression

$$N = \frac{1}{D}.\bar{I} \cdot P_r^{-n} \qquad (12)$$

in which :

a) $\bar{I}$ = is a factor which depends on the geometry, and n. and is given by the empirical relation : $\bar{I} = (t/12)^{(n/2 + 1)} I$,(13), with $I = \exp(a_1 + a_2 n)$ (14)

Constants a_1 and a_2 are functions of the non dimensional geometrical characteristics of the welded joints (fig.2) t/t_1, e/t and 2a/t which are determined from the charts of figures 5 and 6.

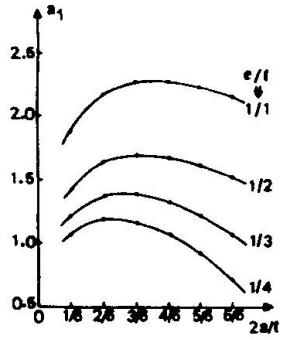

(fig. 5)

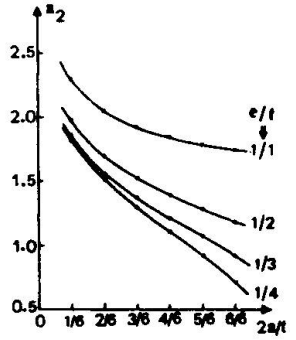

(fig. 6)

b) D is dependent on n according to relation (11)

c) the exponant n may be chosen as the mean value of the slopes of the experimental S-N lines for the sample. It has been found through statistical analysis of data provided from the literature that, for small specimens the mean value of n is 3.6 and the standard deviation is 0.8. The frequency diagram of the n values is given in figure 7 along with the associated Gaussian distribution.

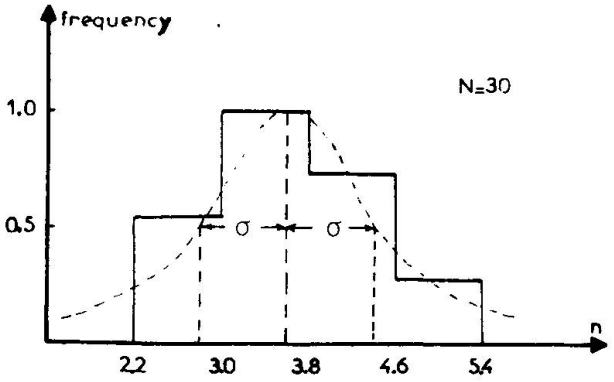

(fig. 7)

d) Numerical example. As an example let us evaluate the S-N lines of the load carrying welds of two cruciform joints, whose geometries are defined in table I.

Table I

Ref	t mm	1 mm	t/t_1	e/t	2a/t	Crack initiations
1	25	19	1	0,54	1	weld root
2	25	22	1	0,62	1	weld root

- Joint 1 :
from charts 1 and 2 of figures 5 and 6
for 2a/t = 1 $a_1 = 1{,}58$
e/t = 0,54 $a_2 = 1{,}23$
then equation (14) gives $I = \exp(1.58 + 1.23 \times 3.6) = 401$
and the number of cycles equ. 12 :

$$N = \frac{(67)^{3.6}}{2.52 \times 10^{-5}} \left(\frac{25}{12}\right)^{\frac{3.6}{2}+1} \times 401 \times P_r^{-3.6} = 4.65\ 10^{14} P_r^{-n}$$

Pr can be expressed in term of the stress range σr

$$P_r = t \times 1 \times \sigma_r = 25\sigma_r$$

then :

$$N = 4.432 \times 10^9\ \sigma_r^{-3.6}$$

- Joint 2 :
we have from figures 5 and 6

$$a_1 = 1.68 \quad , \quad a_2 = 1.32$$

and finally :

$$N = 6.60\ 10^9\ \sigma_r^{-3.6}$$

Figure 8 gives a comparison between test results and the previous calculated above S-N lines from the simplified equation 14.

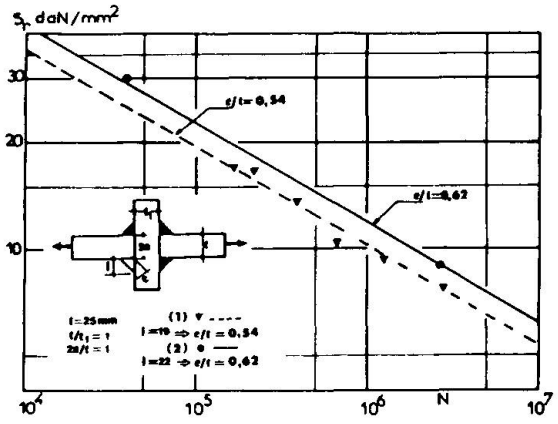

(fig. 8)

4. CONCLUSIONS

The principal outcome of the simplified approach for the evaluation of the fatigue life of welded joints, based on fracture mechanic concepts as presented here, is the possibility of taking into account variables which are ignored by the classical WOHLER line type of approach and which may influence the fatigue life. These

variables are the geometry of the joint (thickness sizes...) and the failure mechanisms.

An identical study (not reported here) |5| has been made to evaluate the fatigue life of cruciform welded joint with non load-carrying welds. In those type of joints (refered in the literature as type K2) the crack occurs at the weld toe, partly due to stress concentration, partly due to surface defects. In such a case the applicability of fracture mechanics is bounded by the knowledge of the initial crack size. This initial crack size may be assessed through a probabilistic criterium or by assuring a good calibration of the fatigue life test results and fatigue life as evaluated by the method developped in paragraph 2. We have found |4| that the initial crack size at the weld toe may be taken as :

a_i = 0,02 - 0,03 mm for a submerged are process
a_i = 0,015 - 0,02 mm for TIG welding
a_i = 0,01 when the automatic arc welds have been treated by shot-peening.

It is thought that the fracture mechanic concept may serve to derive simplified rules for evaluating fatigue life of welded joints which could improve present fatigue codes mainly based on the definition of classified S-N lines.

REFERENCES

1. IIW Design Recommendation for cyclic loaded welded steel structures
IIW, JWG - XIII-XV-44-80

2. CECM. Cimmittee T6, "FATIGUE" Recommendations for the Fatigue Design of Structures, 1981.

3. BS5400, Steel, Concrete and Composite bridges
Part 10, Code of practice for fatigue, 1980.

4. Recho N., Brozzetti J., Prévision par un modèle simplifié de la durée de vie d'un assemblage en croix soudé , Construction Métallique, n° 3, 1981.

5. Recho N., Comportement à la fatigue de l'assemblage en croix soudé à l'aide de la mécanique de la rupture, thèse de Docteur Ingénieur, Université Paris VI, Septembre 1980.

Note : 1 daN/mm^2 = 10 N/mm^2 = 10 MPa

Effect of Root Gap on the Fatigue Strength of Welded Joints

Effet du vide à la racine des joints soudés sur leur résistance à la fatigue

Einfluss des Zwischenraums an der Wurzel von Schweissverbindungen auf ihre Ermüdungsfestigkeit

G. SVED
The University of Adelaide
Adelaide, Australia

M.F. YEO
The University of Adelaide
Adelaide, Australia

D.S. BROOKS
The University of Adelaide
Adelaide, Australia

SUMMARY
The influence of root gaps on the static and fatigue strength of load bearing fillet welded members has been investigated using a finite element analysis, by strain gauging of large scale physical models, by testing of prototype models spark machined from solid plate, and by conducting static and low-cycle fatigue tests on real specimens. In the root gap range of 0 to 3 mm a defined reduction of fatigue strength with increasing gap was not revealed.

RESUME
L'influence du vide existant entre les pièces assemblées par cordon d'angle sur la résistance statique et à la fatigue d'éléments de construction soudés a été étudiée au moyen d'un calcul par éléments finis, au moyen de mesures de déformation par jauges d'extensométrie sur des modèles physiques à grande échelle, au moyen d'essais sur éprouvettes usinées tirées de la masse et érodées artificiellement, ainsi qu'au moyen d'essais statiques et de fatigue sous charge cyclique de pièces réelles. Pour des vides variant entre 0 et 3 mm, aucune réduction significative de la résistance à la fatigue n'a été constatée avec l'augmentation de l'écartement entre les pièces.

ZUSAMMENFASSUNG
Für geschweisste Kehlnahtverbindungen wurde der Einfluss des Spiels zwischen den Werkstücken auf die statische Festigkeit und den Ermüdungswiderstand untersucht. Dies erfolgte unter Anwendung eines Finite Element-Programmes sowie mit Hilfe von Deformationsmessungen an grossmassstäblichen Modellen und mit Versuchen an Prüflingen, die mittels Funkenerosion aus dem Grundmaterial hergestellt wurden. Zusätzlich erfolgten Versuche unter statischer und zyklischer Belastung an wirklichen Verbindungen. Für den Spielbereich von 0 bis 3 mm wurde keine bedeutende Abminderung der Ermüdungsfestigkeit mit zunehmendem Zwischenraum festgestellt.

INTRODUCTION

The cost of eliminating the gap in a weldment, as between the flange and the web of a built up I beam, can be very great. If - as our results so far indicate - a gap as big as one quarter of the nominal size of a fillet weld has no significant effect on the strength of the weldment, considerable savings can be effected in the preparation of welded joints.

In a previous study I.Tsuji and K. Ogawa (Ref.1) investigated "The effect of root gaps on the low cycle fatigue strength of cruciform welded joints". They investigated experimentally the effect of a gap varying from 0 to 3mm, and by finite elements found the stresses, using homogeneous material properties and a 1mm gap, with sloping end.

There are two effects that can alter considerably the results of a finite element analysis: the geometry of the weld, with the shape of the end of the root gap having a significant influence and metallurgical variations within the weld metal and in the heat affected zones.

To clarify the effect of these factors and of the assumption of plane stresses, it was decided to proceed with the investigation along five lines:

- Completing finite element calculations for differently shaped root gap ends and with due consideration to the variation of the mechanical properties in the weld metal and the heat affected zone.
- Manufacturing two models each 6 times full scale, machined from 10mm steel plate, one with 1mm and one with 11mm root gap. These models were strain gauged and tested statically. The results of these tests will be reported separately.
- Constructing prototype size models, with slots machined by spark erosion from solid plate, to allow geometrical effects to be investigated separately from any interfering metallurgical effects.
- Carrying out low cycle fatigue tests on conventional welded specimens.
- Cutting specimens of varying thickness (4,8,16,32,64mm) from adjoining parts of a long cruciform section weldment and fatigue testing these specimens with forces proportional to their thickness.

Visual inspection indicated that the shape of the end of the root gap was curved in some cases, straight in others. The curved end could be convex or concave, while the straight end could include an angle that varied through 90^{o}, i.e. between 45^{o} either side of the load axis.

The variation of the mechanical properties was investigated by taking hardness traverses across the weldments; these indicated the hardness varied by as much as 50 per cent within the area where yielding was expected.

The specimens used - calculation of stresses

The basic specimen used is shown in Figure 1. Each of the welded specimens was sliced from a 1 metre long weldment that had a tapered gap. A semi automatic gas shielded (CO_2) process was used - typically for an 8mm weld the weld parameters were 325A, 28V, with a welding speed of 255mm/min for zero gap. One leg length was kept constant, equal to the nominal size of the weld (6 or 8mm); the length of the other gap was increased to compensate for the gap.(See Figure 2). The welding speed was decreased with increasing gap - in a typical case the average speed was 225mm/min for a 1 metre long weldment.

The variable weld geometry had some effect on the calculated stresses.

Resolving the force acting on one weld ($P/_2$) into components normal and parallel to the minimum throat (for notation, refer to Figure 2) gives

$$\sigma_n = \frac{F_n}{\ell t} = \frac{P}{2} \cdot \frac{b}{d} \cdot \frac{1}{\ell t} \quad ; \quad \tau = \frac{F_t}{\ell t} = \frac{P}{2} \cdot \frac{t}{d} \cdot \frac{1}{\ell t} = \frac{P}{2d\ell}$$

The von Mises yield criterion is

$$\sigma_{eff} = (\sigma_n^2 + 3\tau^2)^{\frac{1}{2}} = \frac{P}{2d\ell}\left[\left(\frac{b}{\ell}\right)^2 + 3\right]^{\frac{1}{2}}$$

which reduces to

$$\sigma_{eff} = \frac{P}{2d\ell}\left[\left(\frac{d+\ell}{d}\right)^2+3\right]^{\frac{1}{2}} = \frac{P}{d\ell}\left[1 + \frac{\ell}{2d} + \left(\frac{\ell}{2d}\right)^2\right]^{\frac{1}{2}} \simeq \frac{P}{d\ell}\left(1 + \frac{\ell}{4d}\right) \ldots . \quad (1)$$

The last approximation introduces an error of less than 7% even for $\ell/d = \frac{1}{4}$ -an error which is small compared with all other approximations involved. In addition, an error on the safe side is caused by the throat thickness being considerably larger than the nominal one in most cases due to the weld penetration into the gap.

The stresses quoted in this report are generally the nominal stresses, calculated from equation (1) setting ℓ=o. However, equation (1) can be used to explain partially the relatively small effect of a root gap - the other explanation being the improved stress-flow (reduced stress concentration factor) associated with the smaller re-entrant angle at the toe of the weld.

Finite element analysis

Only the part shaded in Figure 1 was modelled by finite elements. A typical mesh layout is shown in Figure 3. The boundary conditions assumed were roller supports at nodes along edges AJ and JHGF, to account for symmetry, free nodes along BA and uniform axial displacement due to axial loading for all nodes along edge FE.

A strain hardening material was assumed; the stress-strain curve was approximated by four straight lines (Figure 4). The first, passing through the origin and terminating at a point M, had a slope of E=200 000 MPa; M corresponded to the initial yield point. The yield stress, σ_y, had five different values (σ_y = 250,270,310,350,390 MPa),to be used in different zones, established by the previously mentioned hardness traverse of the weld and of the heat affected zone. The second straight line, MN, terminated at a stress of (σ_y+ 5) MPa and a strain of 1.5%: the third straight line, NP, had a slope of 5000 MPa and terminated at a stress of $2\sigma_y$, while the last part, PR, terminated at a stress of σult = ($2\sigma_y$ + 5) MPa and a strain of 15%. At points where the stresses were multiaxial, the same relationships were assumed to hold between "effective stress" and "effective strain" increments; these were defined as the octahedral shearing stress and the octahedral shearing strain respectively.

The elastic-plastic analysis followed the "initial stress" approach.(Ref.2). Conventional shape functions were used for the 8 noded curved quadrilateral isoparametric elements employed; the material property matrix corresponded to the current value of effective strain. All integrals were evaluated by 3 x 3 Gaussian quadrature.

As a first step, the elastic stiffnesses were used to evaluate the elastic stress distribution corresponding to an arbitrary value of the (equal) displacement of the nodes along FE. These displacements and the corresponding strains and stresses were scaled to cause yield at the relatively highest stressed point taking into account different zones had different yield strengths. The analysis

was continued by applying equal increments of displacements in steps of 0.01mm to all nodes along FE. Using the previously established stiffness matrix, an extrapolated set of values was calculated for all increments in nodal displacements, nodal forces, stresses and strains. For all elements, for which the effective stress value exceeded the yield strength, an updated stiffness matrix was calculated, using the current material property matrix to conform with the stress-strain incremental values. The problem was re-solved, using the updated stiffness matrix; if the differences between the extrapolated and the re-calculated values exceeded a pre-selected convergence criterion, the process was repeated iteratively until the "residual nodal forces" fell below a convergence value. Usually five iterations were sufficient to allow applying the next increment.

Geometrical non-linearities caused by the relatively large displacements can be allowed for by adding the displacements to the nodal coordinates and re-calculating the element characteristics for the altered geometry.

The calculations were terminated when the effective strain reached the "failure" value of 15% at any one point.

Extensive use was made of graphical output facilities to avoid the collection of excessive amount of data that would be hard to scan and to interpret. In the elastic range the principal stresses were plotted by the computer at the central Gauss point of every element. In the elastic-plastic range an x was printed at every Gauss point that reached the plastic range (point M on the stress-strain curve); This was changed to a + when the effective strain reached 1.5% (point N) and to a <> when the effective stress reached $2\sigma_y$(point P). A typical output is shown in Figure 3.

Five different profiles were analysed with a 3mm gap, using slopes for the end of the gap that varied from approximately 30^0 to 55^0 with the load axis, both in the"positive" and "negative" directions. In addition square gap ends with 3,2, 1 and 0mm opening were analysed. For the zero gap nodes on the two sides of the gap (initially coincident) were allowed to move independently.

Typical calculated load-extension graphs are shown in Figure 5; the letters M, N,P, and R correspond to the previously described points on the stress-strain graph.

Conclusions from the finite element analysis

- First yielding, which was reached at approximately the same load for all gap and configuration, was always at the root of the gap (point A on Figure 3),but it was followed very closely by yielding at the toe (point B) and after a few increments of elongation at points C and D.
- After approximately 10 increments there was a continuous yielded zone between points A and B; this zone was quite extensive by the 17th step.
- The maximum load reached was 49kN±6kN, except for the square end 3mm gap (37.7kN).
- Six calculations reached "failure" after 45±7 elongation increments; exceptions were two square ended gaps (for 3mm 30 steps, for 1mm 32 steps) and one with end sloping at 30^0 (87 steps).

Fatigue tests on spark eroded specimens

Seven fatigue specimens, machined from 6mm plate to the outline shown in Figure 1, had spark eroded slots to investigate geometrical effects, free from metallurgical changes introduced by the welding process. The "weld profiles"

corresponded to a 6mm fillet weld. The fatigue tests were carried out in an Instron servo-controlled machine, under load control, at a rate of 2-3Hz. The results are summarized in Table 1.

TABLE 1.

Fatigue tests on spark eroded specimens-6mm plate, 6mm weld profile			
Specimen	Load range(kN)	Cycles to failure	Shape of end of gap
1	0.8 - 10	42720	Semi-circular
2	0.8 - 10	45110	Semi-circular
3	0.8 - 10	53290	Quarter circle
4	0.8 - 10	60580	45° slope
5	0.8 - 12	15600	Square-0.5mm gap
6	0.8 - 12	15170	Square-0.75mm gap
7	0.8 - 12	11160	Square-1.25mm gap

Specimens 1-4 had extensometers fitted across the gap. For the first two no increase in the extensometer readings were noted in the first 20 000 cycles; for specimens 3 and 4 the readings were constant until 30 000 cycles were applied.

In the second series square ended slots were spark eroded in blanks machined from 8mm plate. Results are shown in Table 2.

TABLE 2.

Fatigue cracks in specimens with rectangular spark eroded slots;8mm plate, 6mm weld profile. Load range 0.8-12kN, except for specimen No.8			
Specimen	Gap (mm)	Cycles to failure	Remarks
8	2.15	256 000 29 400	0.8 - 10kN 0.8 - 12kN 3 cracks
9	2.15	36 200	3 cracks
10	2.15	35 160	4 cracks
11	1.5	22 200	
12	1.35	22 400	
13	1.3	13 520	1 crack

Tests on large scale models

Two large scale models (6 times full size) were machined from 10mm mild steel plate. One model had a 1mm wide gap, the other a 11mm gap, both with square ends. These models were tested statically, after extensive strain gauging. Results will be reported elsewhere.

Fatigue tests on welded specimens

Test specimens were cut from 1 metre long weldments to avoid end effects. These were made with tapering gaps; the actual gap in any one specimen was measured with feeler gauges.

The first weldment had a significant gap on one side of the cross bar only; all specimens failed at the gap. The results are shown in Table 3.

TABLE 3.

Fatigue life of welded specimens-8mm thick - 8mm nominal weld. Load range 0.8kN - 28kN.			
Specimen	Gap(mm)	Cycles to failure	Fatigue cracks
14	0.45	44 300	2 at end of gap, 1 at toe
15	0.5	84 740	2 at end of gap, 1 at toe
16	0.6	43 210	2 at end of gap
17	0.7	25 900	2 at end of gap
18	0.85	65 620	2 at end of gap, 1 at toe
19	0.9	59 880	2 at end of gap, 1 at toe

The results for the specimens cut from the second weldment are shown in Table 4. In this case there were significant (although different) gaps on the two sides of the cross bar. The gap that failed is indicated by underscoring.

TABLE 4.

Fatigue life of welded specimens - 8mm thick - 8mm nominal weld Load range 0.8kN - 28kN.			
Specimen	Gap(mm)	Cycles to failure	Fatigue cracks
20	.02/.6	29 300	1 at end of gap
21	.05/1.5	33 420	Fracture across throat
22	.5/2.15	72 080	2 at end of gap, 1 at toe
23	.7/1.15	57 520	2 at end of gap, 1 at toe
24	1.0/1.3	78 810	2 at end of gap
25	1.2/2.4	73 550	2 at end of gap

In the third series a weldment with tapering gaps was sliced into 20 test pieces. These formed 4 series, each comprising 5 specimens, cut from adjoining parts of the weldment, with thicknesses of 4,8,16,32 and 64mm, to investigate the effect of triaxiality in long welds. The results of these tests are shown in Table 5.

TABLE 5. TEST RESULTS

Size Load(kN)	4mm 10.5	8mm 21	16mm 42	32mm 84	64mm 168	Average
Series A	1.1 1.8 2R 296050	1.2 1.9 2R 293600	1.2 2R 2.1 R 267750	1.1 2R 2.0 262280	1.3 2.3 2R 292423	282420 ±14360
B	0.9 2R T 1.35 171480	0.8 1.4 R 201580	0.8 1.5 2R 175500	0.7 2R 1.5 230725	0.9 R 1.6 227300	201315 ±24890
C	-	0.2 2R 1.1 122850	0.4 2R 1.0 T 129760	0 2R 0.95 187130	0.6 R 1.25 184260	156000 ±29810
D	0 0.2 2R 152050	0 0.15 2R 138930	0 0.15 2R 208625	0 0.1 2R 145270	0.1 2R 0.8 144010	157780 ±25765
Average	206000 ±63800	189240 ±67050	195400 ±50280	206350 ±44220	212000 ±55000	

{see over}

In Table 5, the entries show the following information:
(1) Size of gaps on test piece
(2) Gap size on the side at which failure occurred is indicated by underlining
(3) Mode of failure: R - root failure; 2R - root failure at both ends of the gap; T - toe failure
(4) Cycles to failure
(5) Averages and standard deviations, for both specimen sizes and for series.

CONCLUSIONS

- Results so far are restricted to relatively high stress, low fatigue life conditions.
- Neither the finite element calculations, nor the low cycle fatigue tests showed a significant reduction of strength with increasing gap size in the range investigated.
- The finite element calculations indicated that the stress levels at the toe of the weld were slightly lower than the stresses at the end of the root gap.
- The fatigue tests indicated that in many cases cracks could be seen to propogate from the end of the gap and from the toe of the weld before the specimen fractured.
- The tests on the specimens spark-eroded from the solid showed that the geometry of the gap-end had a considerable effect on the fatigue life of the specimen.
- The length of the weld (the thickness of the specimen) had no significant effect on the fatigue strength of the weld.

ACKNOWLEDGEMENTS

The research was supported by a grant from the Australian Welding Research Association; the welded specimens were provided by Johns Perry - Perry Engineering Division, Adelaide, South Australia.

REFERENCES

- I. TSUJI and K. OGAWA, "The Effect of Root Gaps on Low Cycle Fatigue Strength of Cruciform Welded Joints", Trans. of the Japan Welding Soc., vol. 7, April 1976.
- O.C.ZIENKIEWICZ,"The Finite Element Method" McGraw Hill 1977.

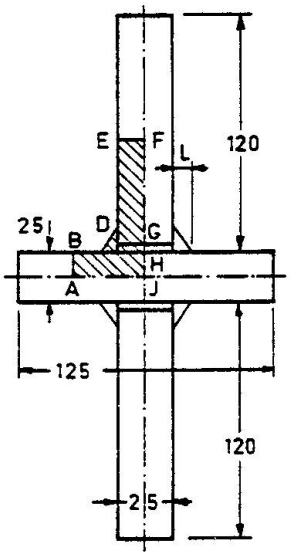

FIGURE 1. TEST SPECIMEN

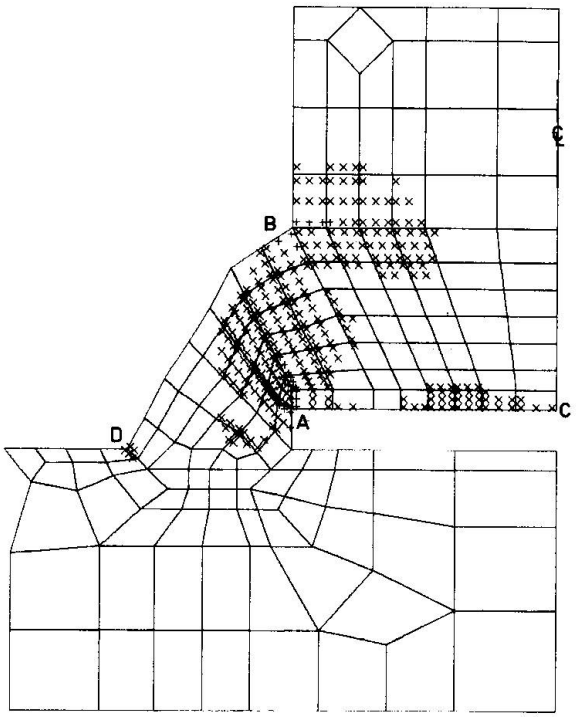

FIGURE 3. MESH ARRANGEMENT AND YIELD PATTERN

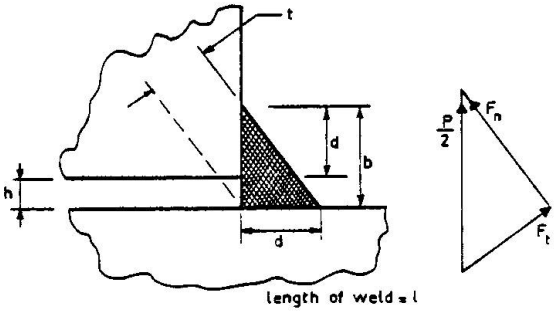

FIGURE 2. WELD GEOMETRY

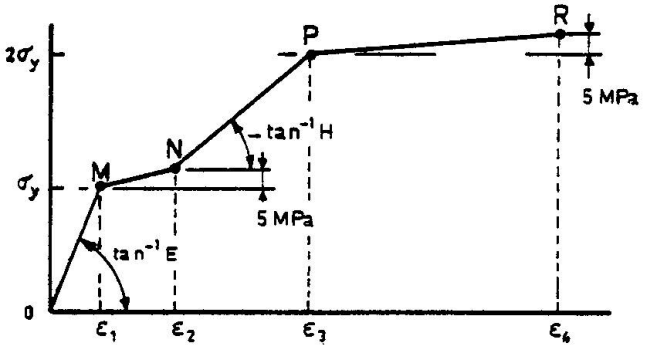

FIGURE 4. IDEALIZED STRESS_STRAIN RELATIONSHIP

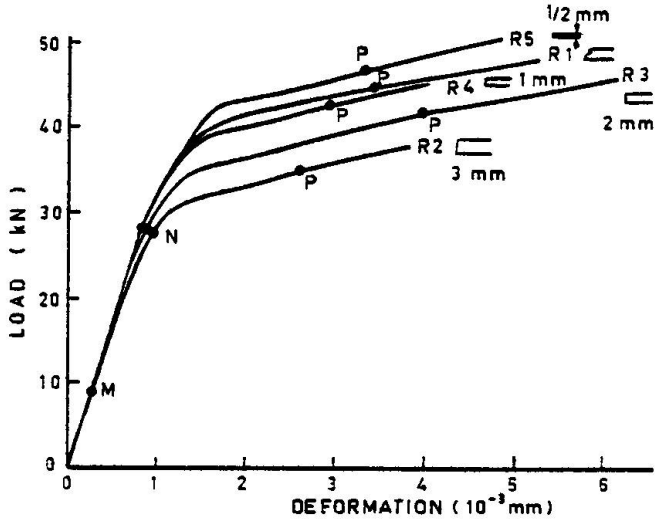

FIGURE 5. LOAD_ELONGATION CURVES OBTAINED FROM COMPUTED RESULTS

Critical Size of Fillet Welds in High Strength Steel Joints

Taille critique des cordons d'angle dans les joints en acier à haute résistance

Kritische Grösse von Kehlnähten bei Verbindungen aus hochfestem Stahl

WILLY CHAPEAU
Chargé de Cours
Université de Liège
Liège, Belgium

ANDRÉ PLUMIER
Maître de Conférences
Université de Liège
Liège, Belgium

SUMMARY

Joints built up with fillet welds and submitted to fatigue can fail either by plate fracture or by weld fracture. The first mode gives higher fatigue resistance. It takes place with welds bigger than a "critical size". Tests on high strength steels indicate that, for longitudinal welds, the statical calculation is always safe, while for transverse welds, the initial size is found to be higher than for mild steel.

RESUME

Les joints soudés par cordons d'angle sollicités en fatigue peuvent se rompre soit dans les plats assemblés, soit dans les cordons de soudure. Le premier mode donne des résistances plus élevées. Il est obtenu pour des dimensions de cordon supérieures à une "taille critique". Dans les aciers à haute limite élastique, le calcul statique du cordon donne des dimensions supérieures à cette taille critique, pour les joints longitudinaux; dans les joints transversaux, la taille critique est trouvée plus élevée que pour les aciers doux.

ZUSAMMENFASSUNG

Ermüdungsbeanspruchte Kehlnahtstösse brechen entweder im Grundmaterial oder im Schweissgut. Der Bruch im Grundmaterial ergibt eine höhere Ermüdungsfestigkeit und erfolgt ab einer bestimmten kritischen Grösse der Schweissnaht. Bei hochfesten Stählen ergibt die statische Bemessung Längsnähte, die die kritische Grösse übertreffen und somit auf der sicheren Seite liegen. Für Quernähte bei Normalstahl werden grössere kritische Abmessungen gefunden.

1. INTRODUCTION

Joints built up with fillet welds loaded by fatigue can fail either by weld fracture ot by plate fracture. Fig. 1 and 2. The latter mode gives higher fatigue resistances, so that it is interesting to know where the frontier is between the two modes. To this frontier corresponds a "critical" size of welds. Several works [1][2][3][4] tackles this problem for relatively mild steel. We complete these works by a study on high strength steels, with a yield stress of about 700 N/mm^2 .

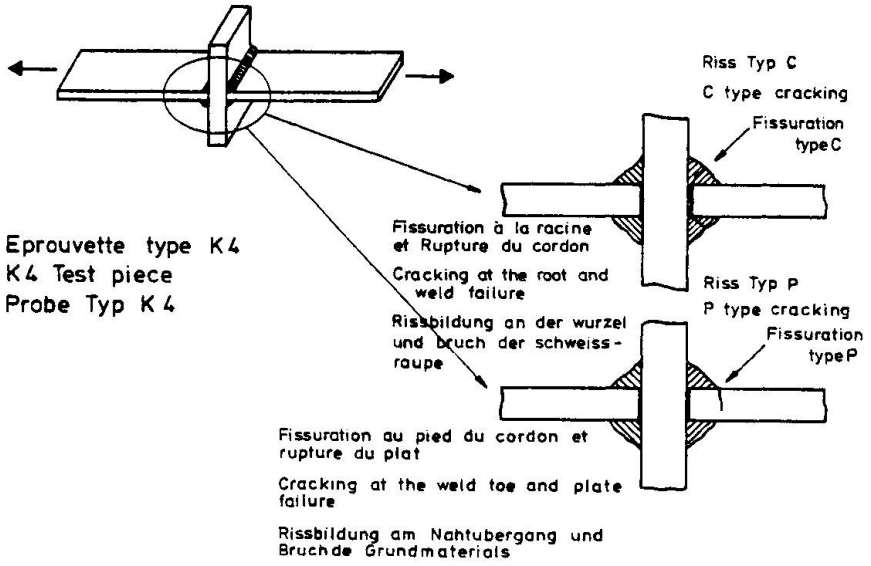

Figure 1

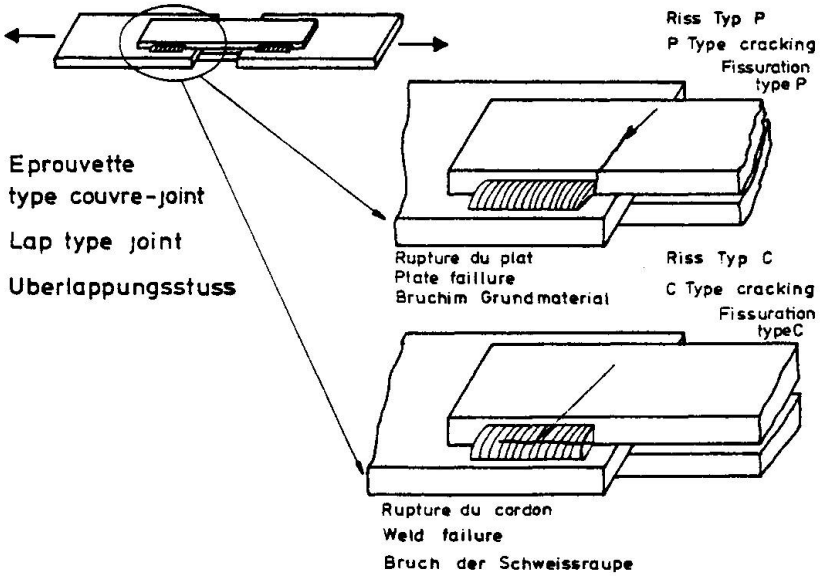

Figure 2.

2. DESCRIPTION OF TEST PIECES AND TESTING PROCEDURE.

For transverse welds the only parameter of the study is the thickness a of the weld. The general dimensions of the test pieces are defined on Fig. 3. The dimensions "a" are defined on the basis of a previous work [2]. If we refer to

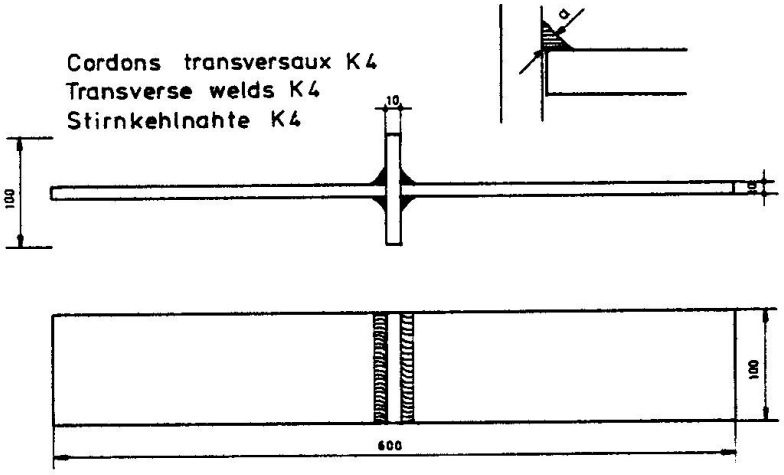

Figure 3

fig. 4, we have, for V = 0,9 T, a_{crit} = 6,4 mm.

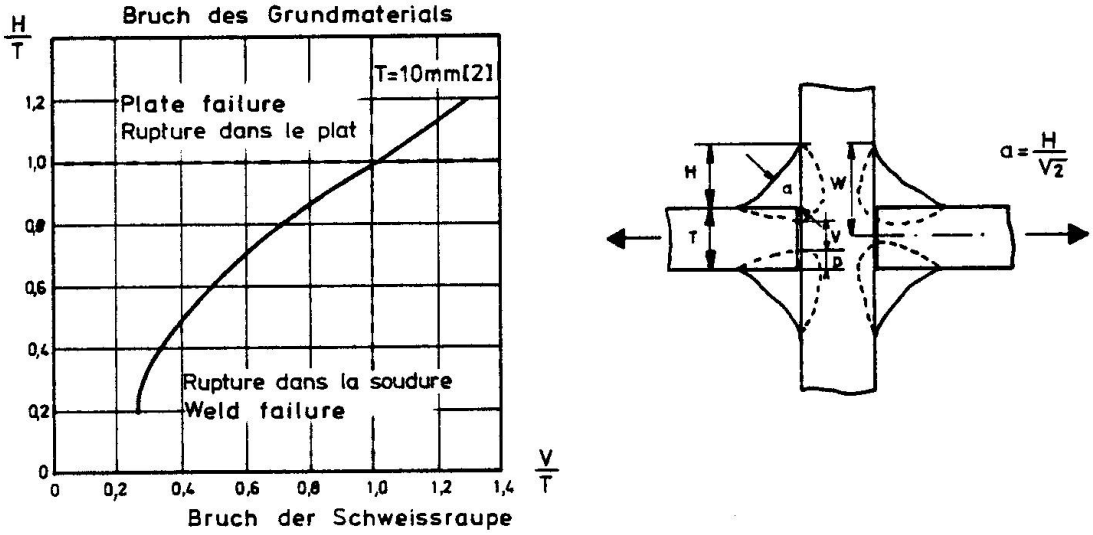

Figure 4

For our test pieces, a ranges from 5 to 12 mm. As a comparison, the necessary size for equal resistance of the joint ant the assembled plates, under static loads, is a = 7,5 mm.

No existing literature was found for defining the critical size of longitudinal fillet weld. We used the following procedure : a first serie having the critical size defined above is welded and tested. The dimensions of the next series are defined on the basis of the results of the first serie.

The fatigue tests are constant amplitude tests, with S_{max} of about 300 N/mm^2, $R = \frac{S_{min}}{S_{max}}$ of about 0,6 and a frequency of 4 Hz.

3. RESULTS OF TEST ON TRANSVERSE WELDS.

Test results are presented on fig. 5. It can be seen that there is a continuous increase of fatigue resistance with the size of welds and no discontinuity when the failure mode changes. The critical size is found of about 10 to 12 mm, which is significantly higher than 7,5 mm.

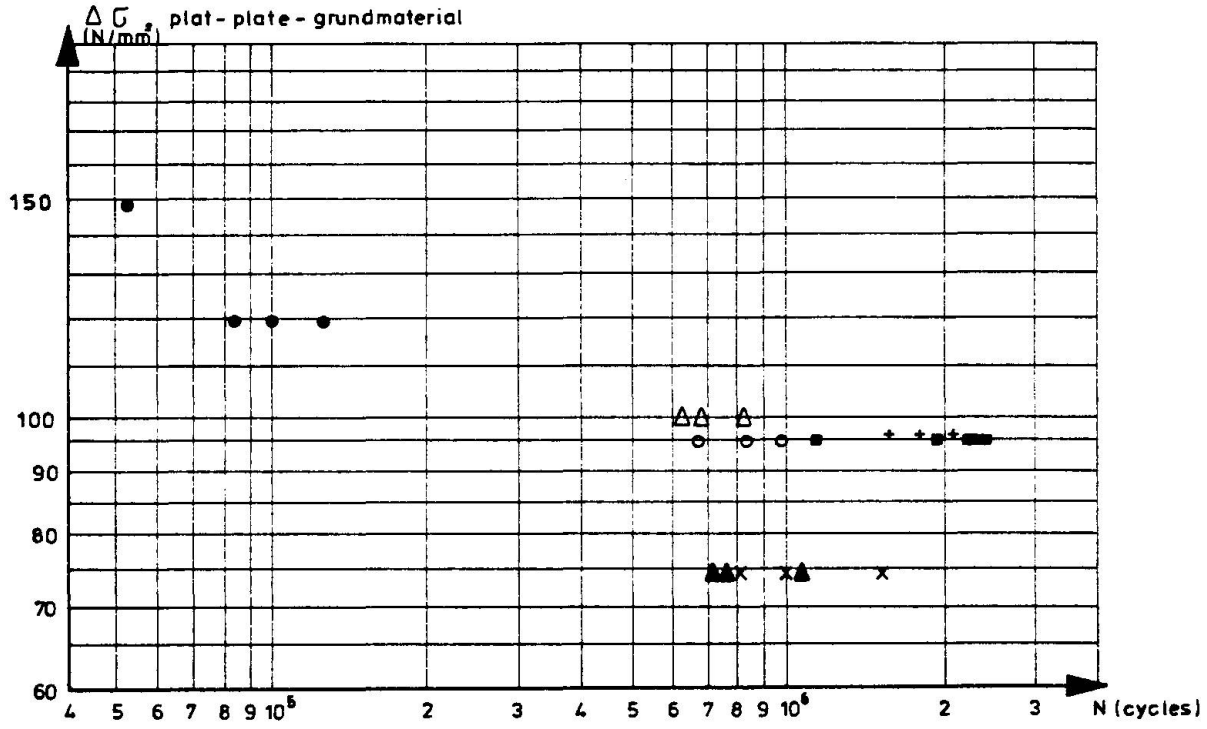

Fig. 5.

Eprouvette type k4 - AE 700
K4 type joint - Fe E 700
Kreuzstoss K4 - Stahl F_e E 700

	a (mm)
●	5
▲	5,5
X	6
Δ	7
o	8
+	10
■	12

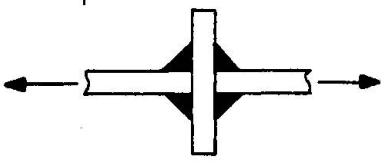

Weld failures cannot be characterized by the only stress in the plate, because it is also dependent on the size of the internal. "defect" defined by $\frac{V}{2H + T}$ (see Fig. 6). We present the test results in a diagramm taking V H and T into account on Figure 6. A significant difference of about 40 % is confirmed. A comparaison with test results from the literature

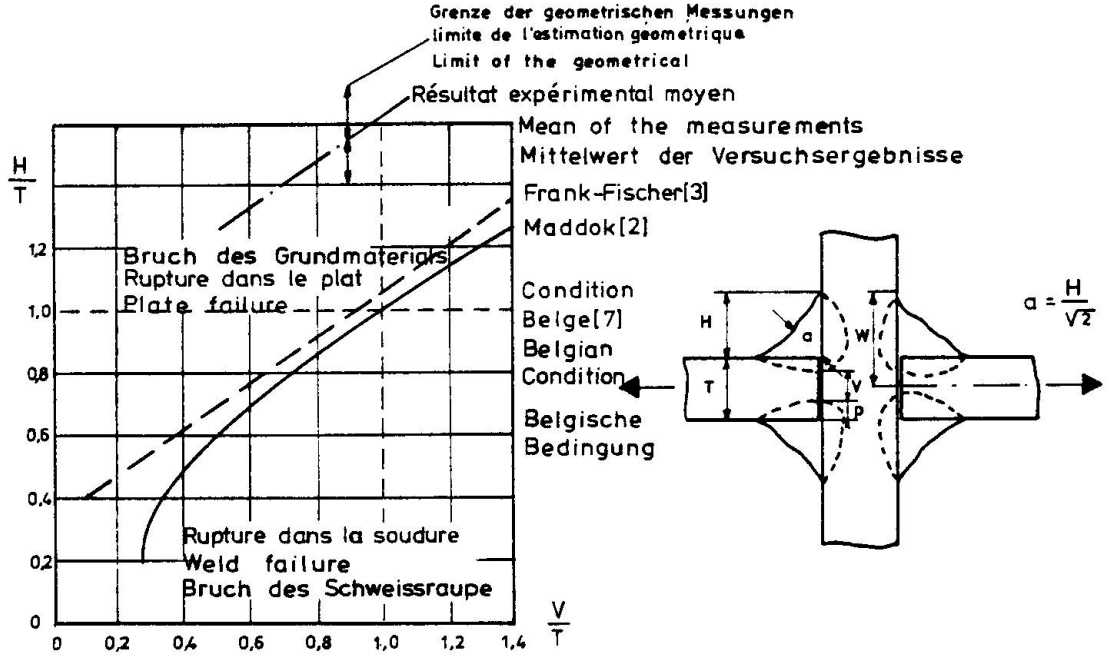

Figure 6.

shows that it is mainly caused by the relatively low fatigue resistance in the weld failure case. One explanation for those low results could be the high mean stress applied, though 250 N/mm^2 is not so high for a high strength steel.

However, as a result of the continuous rise in fatigue resistance with the weld size, independantly of the failure mode, the lack of security generated by a classical computation of the weld size is relatively minor for welds having an "a" greater than 1,2 time the critical size.

4. RESULTS OF TESTS ON LONGITUDINAL WELDS.

Test results are presented on Fig. 7.

It can be seen that there is no real discontinuity when shifting from one failure mode to the other ; the fatigue resistance increases with the weld size when a weld failure is observed, but it is found quite independant of the weld size, when there is a lap failure.

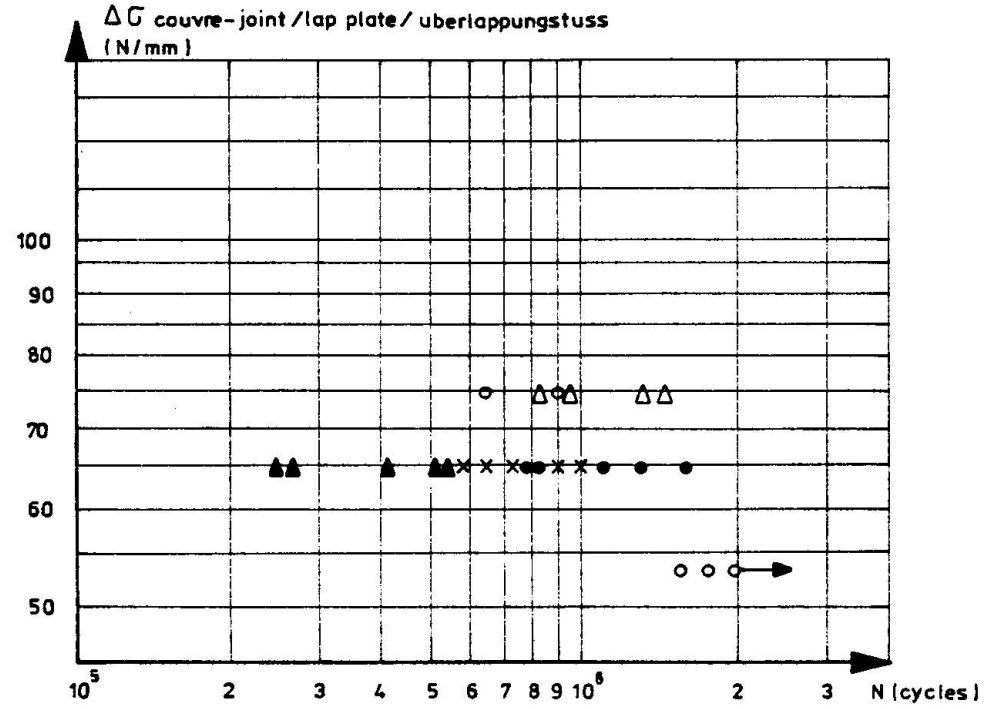

Eprouvette type couvre - joint

lap plate joint

Uberlappungstuss

	a mm	l mm	S mm²
▲	5	30	150
X	5	40	200
●	5	50	250
o	6	50	300
Δ	7	50	350

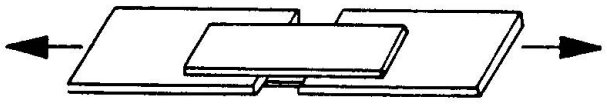

Figure 7.

As explained above, the critical size of welds is found by a step procedure. The critical area of one weld is found equal to approximately 200 mm^2 while if we design the joint for the equal resistance of the lap plates and the welds, the necessary dimension is found equal to 433 mm^2.

It is concluded that, for longitudinal loaded fillet welds in high strength steel joints, the static design ensures a plate failure under fatigue loads so that, for high strength steel joints, the critical size of longitudinal welds

has no importance in the computation.

5. ACKNOLEDGMENTS.

We acknoledge the European community for Steel and Coal and the Belgian Research Center for Constructional Steelwork (CRIF) for sponsoring the research summarized here above.

6. REFERENCES.

|1| OUSHIDA - NISHIOKA - A study of fatigue strength of fillet welded joints - Schweisstechnik (Berlin) 16 (4) - 1966.

|2| S.J. MADDOX - Assessing the significance of flaws in welds subject to fatigue - The welding journal - Welding Research supplement pp 401 - 409.

|3| K.H. FRANCK - J.W. FISHER - Fatigue strength of fillet welded cruciform joints. ASCE. Structural Division - 1979 -

|4| T.R. GURNEY - Fatigue of welded structures - pp 85 - 92. Cambridge - University Press 1968.

|5| HAIBACH - DE BACK - LIEURADE - OLIVIER - RINALDI - SIMON - Fatigue investigation of typical welded joints in steel Fe E 460 as compared to Fe E 355. Publication EUR 6340 EN.

|6| GURNEY - MADDOX - A re-analysis of fatigue - data for welded joints in steel - Document E/44/72 - A welding Institute Publication.

|7| R. BAUS - W. CHAPEAU - Application du soudage aux constructions Edition Eyrolles - 1980 - Ed. Sciences et lettres - 1977.

Leere Seite
Blank page
Page vide

Local Strain Range and Fatigue Crack Initiation Life

Variation de l'allongement local et durée de vie jusqu'à l'initiation d'une fissure de fatigue

Lokale zyklische Dehnungsdifferenz und Lebensdauer bis zur Bildung eines Ermüdungsrisses

X. ZHENG
Professor
Northwestern Polytechnical University
Xi'an, China

SUMMARY
Approximate expressions are developed for the notch tip cyclic strain range in a metallic element under stress ratios, R = 0 and R = −1. Fatigue crack initiation life is then investigated with particular emphasis on the effect of stress ratio R and relationship to the metal's tensile properties. A generalised formula is derived and compared with test results in the literature.

RESUME
Des formules approchées sont développées pour le calcul de la variation de l'allongement local à l'extrémité de l'entaille située dans un élément métallique, ceci pour des rapports de contrainte R = 0 et R = −1. La durée de vie jusqu'à l'initiation d'une fissure de fatigue est ensuite déterminée en considérant plus particulièrement l'influence du rapport de contrainte R et celle des propriétés du métal à la traction. Une expression généralisée est développée puis comparée aux résultats d'essais tirés de la litérature.

ZUSAMMENFASSUNG
Eine Näherungsbeziehung zur Bestimmung der lokalen zyklischen Dehnungsdifferenz im Scheitelpunkt einer Kerbe in einem Metallprüfkörper wird vorgeschlagen, dies für Spannungsverhältnisse von R = 0 und R = −1. Die Lebensdauer bis zur Bildung eines Ermüdungsrisses wird untersucht und zwar unter besonderer Berücksichtigung des Einflusses des Spannungsverhältnisses R und der Zugeigenschaften des Metalles. Eine allgemeine Beziehung wird hergeleitet und mit Versuchsresultaten aus der Literatur verglichen.

1. INTRODUCTION

In the past decade much work has been devoted to predicting fatigue crack initiation life (FCIL) in notched elements. Of this, very little has considered the effect of stress ratio [1] [2] or the relationship to metallic tensile properties [3] [4].

Approximate formulae are developed from Neuber's rule [5] and Hollomon's equation [6] to give the notch tip cyclic local strain range which governs the prediction of FCIL. Then with the accepted local stress-strain concept for predicting FCIL [7] [8] an approximate expression of FCIL is derived. Examples are given for the prediction of FCIL in steels from their tensile properties.

2. CYCLIC LOCAL STRAIN RANGE IN NOTCHED METALLIC ELEMENTS

2.1. Basic equations

Although the nominal stress is below yield and the element as a whole elastic, plastic deformation may occur at the notch root from stress concentration. As a basis for calculating the notch tip local strain Neuber's rule [5] [7] [8] gives :

$$K_t^2 = K_\sigma K_\varepsilon = (\sigma/S)\ (\varepsilon/e) \ , \qquad (1)$$

with : K_t (theoretical stress concentration factor), K_σ (stress concentration factor), K_ε (strain concentration factor), σ and ε (notch tip local stress and strain), S and e (nominal stress and strain in the net section). Using Hooke's law and E as Young's modulus we have :

$$e = S/E \ . \qquad (2)$$

Then from eqs. (1) and (2) we obtain :

$$\sigma\, \varepsilon = (K_t\, S)^2/E \ . \qquad (3)$$

From Hollomon's equation [6] for stress-strain behaviour in the elasto-plastic state :

$$\sigma = K\, \varepsilon_p^n \ , \qquad (4)$$

with : n (strain-hardening exponent), K (strength coefficient) and ε_p (plastic component of the local strain).

From eq. (4) K may be approximated by :

$$K = \sigma_f/\varepsilon_f^n \ , \qquad (5)$$

with : σ_f (fracture strength), ε_f (fracture ductility).

The total local strain ε is the sum of the elastic and plastic components :

$$\varepsilon = \varepsilon_e + \varepsilon_p \ , \qquad (6)$$

obtaining the elastic component ε_e from Hooke's law and eq. (4) thus :

$$\varepsilon_e = \sigma/E = K\, \varepsilon_p^n/E \ . \qquad (7)$$

Subsituting eqs. (4), (6) and (7) into (3) also gives the total local strain as :

$$\epsilon = \left[1 - \frac{\epsilon_e}{\epsilon}\right]^{\frac{-n}{1+n}} \left[\frac{1}{E\,K}\,(K_t\,S)^2\right]^{\frac{1}{1+n}} , \qquad (8)$$

or, altenatively, the plastic component ϵ_p as :

$$\epsilon_p = \left[1 + \frac{K}{E}\,\epsilon_p^{n-1}\right]^{\frac{-1}{1+n}} \left[\frac{1}{E\,K}\,(K_t\,S)^2\right]^{\frac{1}{1+n}} . \qquad (9)$$

Given S and K_t eq. (9) may be solved by iteration. The elastic component may be found from eq. (1) and hence the total local stain.

If a macrocrack initiates at notch root when ϵ_p reaches the value of ϵ_f and, for structural steel, we assume $\epsilon_f \geq 0.40$ and $\sigma_f \simeq 0.01\ E$, then, after rearranging eq. (9), the first term becomes :

$$\left(1 + \frac{K}{E}\,\epsilon_p^{n-1}\right)^{0.5} = \left(1 + \frac{\sigma_f}{E\,\epsilon_f}\right)^{0.5} \simeq 1.0 ,$$

and we have the criterion for macrocrack initiation as :

$$K_t\,S = \sqrt{E\,\sigma_f\,\epsilon_f} . \qquad (10)$$

Using these basic equations, and the argument of Barsom et al [9] that strain in the notch root plastic zone is governed by the surrounding elastic zone displacements, the variation of local strain with nominal stress may be analysed.

2.2. Pulsating stress cycles (R = 0)

The variation of the local strain with nominal stress is shown in the first quadrant of figure 1. On loading, the local strain increases to ϵ_B, along the line OAB as the nominal stress increases to S_B. Phase OA is elastic, and AB plastic with point A the elastic limit. In the plastic phase, the local strain is calculated using eqs. (9) and (7).

On unloading, the nominal stress returns to zero. The displacement of the elastic zone surrounding the notch root also reduces to zero. Thus, the local strain at the notch tip is forced to return to zero along line BCO, phase BC being elastic recovery, and CO the "forced plastic recovery".

From the above model and eq. (8), the cyclic local strain range may be expressed as :

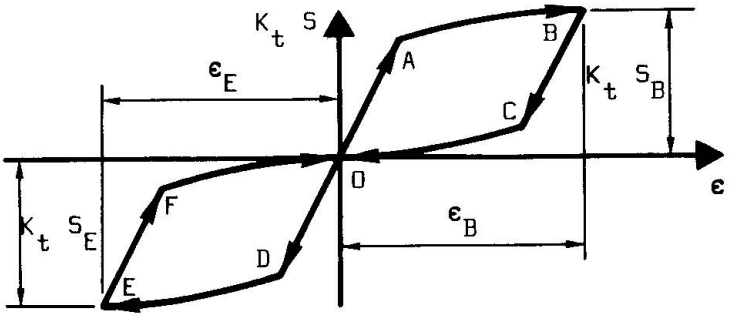

Figure 1 :
Variation of the local strain at the notch tip with the nominal stress.

$$\Delta\epsilon = \left[1 - \frac{\Delta\epsilon_e}{\Delta\epsilon}\right]^{\frac{-n}{1+n}} \left[\frac{1}{E\,K}\,(K_t\,\Delta S)^2\right]^{\frac{1}{1+n}}, \qquad (11a)$$

where $\Delta S = S_B = S_{max}$ represents the applied nominal stress range.

2.3. Full stress reversal (R = - 1)

From Figure 1 and based on the same argument, the cyclic local strain range becomes :

$$\Delta\epsilon = 2\left[1 - \frac{\Delta\epsilon_e}{\Delta\epsilon}\right]^{\frac{-n}{1+n}} \left[\frac{1}{E\,K}\,(K_t\,\frac{\Delta S}{2})^2\right]^{\frac{1}{1+n}}, \qquad (11b)$$

where $\Delta S = 2\,S_B = 2\,S_{max}$ is again the applied nominal stress range.

Test results for notched cylindrical specimens in [10] are shown in figure 2 with calculated values from eq. (11). As may be seen from figure 2, good agreement exists between the calculated curves and the experimental results. As the notch tip would be in biaxial tension a combined stress concentration factor from [11] was used for K_t. The use of tensile instead of cyclic properties in the calculation of cyclic local strain range is acceptable as, according to Barsom et al [9], the cyclic strain hardening/softening has a negligible effect on local strain range. This fact has been experimentally verified by Kremple [10].

In investigating the effect of stress ratio it can be shown that eqs. (11a) and (11b) can be rewritten as :

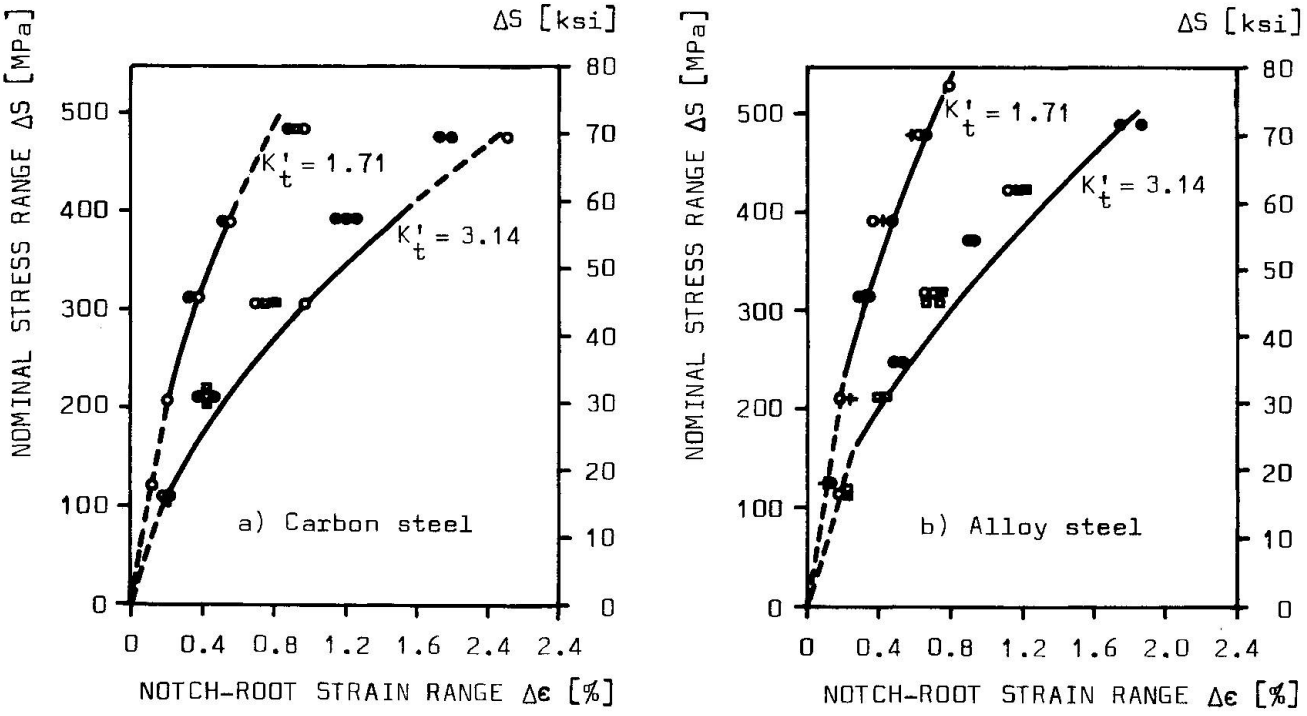

Figure 2 : Calculated local strain range (eq. 11b) and test results [10] of notched cylindrical specimens. a) Carbon steel ($E = 2.06 \cdot 10^5$ MPa, $K = 694.2$ MPa, $n = 0.199$) b) Alloy steel ($E = 2.06 \cdot 10^5$ MPa, $K = 838.3$ MPa, $n = 0.193$)

$$\Delta\epsilon = 2^{\frac{-n}{1+n}} 2 \left[1 - \frac{\Delta\epsilon_e}{\Delta\epsilon}\right]^{\frac{-n}{1+n}} \left[\frac{1}{E K} \left(\sqrt{\frac{1}{2 (1 - R)}} K_t \Delta S\right)^2\right]^{\frac{1}{1+n}} \quad \text{for } R = 0. \qquad (12a)$$

$$\Delta\epsilon = 2 \left[1 - \frac{\Delta\epsilon_e}{\Delta\epsilon}\right]^{\frac{-n}{1+n}} \left[\frac{1}{E K} \left(\sqrt{\frac{1}{2 (1 - R)}} K_t \Delta S\right)^2\right]^{\frac{1}{1+n}} \quad \text{for } R = -1. \qquad (12b)$$

Although the cyclic local strain range is still not given by a unique formula it becomes more a function of the parameter $\sqrt{1/2 (1 - R)}\ K_t \Delta S$ as n becomes smaller, thus showing the significance of stress ratio.

3. EFFECT OF STRESS RATIO ON THE FATIGUE CRACK INITIATION LIFE

Crack initiation may be assumed to occur due to the fracture of a hypothetical, uniaxial fatigue element located at the notch root in figure 3. The fatigue life of a similar smooth test specimen can thus indicate the FCIL of a notched element if the "fatigue element" encounters the same stress-strain history.

Figure 3 :

Plastic zone and hypothetical, uniaxial fatigue element at notch root.

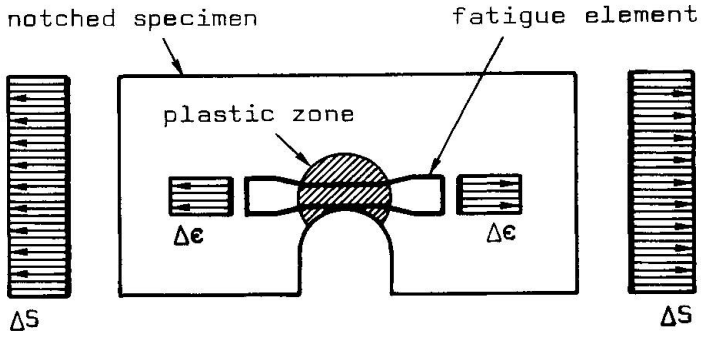

From [12] the fatigue life of a smooth specimen can be expressed as follows :

$$\frac{\Delta\epsilon_p}{2} = \epsilon_f' (2 N_f)^c , \qquad (13)$$

where $\Delta\epsilon_p$ is the plastic component of the cyclic strain range, c the fatigue ductility exponent and ϵ_f' the fatigue ductility coefficient. According to [12], this latter may be approximately set equal to ϵ_f.

Also, in low-cycle fatigue behaviour, the plastic component of cyclic strain range may be considered approximately equal to the total local strain range, i e, $\Delta\epsilon_p \simeq \Delta\epsilon$, and $(1 - \Delta\epsilon_e/\Delta\epsilon)^{-n/(1+n)} \simeq 1$.

Thus substituting eqs. (12) and (5) into eq. (13) and replacing N_f the fatigue life of the "fatigue element", with N_i, the FCIL of the notched element, we have the following expressions of FCIL :

$$2 N_i = 2^{-0.5n \cdot k_p} C_p \left[\sqrt{\frac{1}{2 (1 - R)}} K_t \Delta S\right]^{k_p} \quad \text{for } R = 0, \qquad (14a)$$

$$2 N_i = C_p \left[\sqrt{\frac{1}{2 (1 - R)}} K_t \Delta S\right]^{k_p} \quad \text{for } R = -1, \qquad (14b)$$

where : $k_p = 2/c\,(1 + n)$, (15)

$$C_p = \sqrt{E\,\sigma_f\,\epsilon_f} \,. \quad (16)$$

As may be seen from eq. (14b), if the product of $K_t\,\Delta S/2$ reaches the value of $\sqrt{E\,\sigma_f\,\epsilon_f}$, the first cycle of loading will already create crack initiation (see eq. 10), hence $N_i = 1$. Therefore, the constant value of 2, on the left hand side of eqs. (14), should be omitted. In doing so, the predicted values of C_p will correspond better to the experimentally determined data [3] [4].

Similarly the constant 2 exp $(-0.5n \cdot k_p)$ in eq. (14a) tends to unity as n becomes small, as in structural metals, so that an approximate, but unique, expression for FCIL is :

$$N_i = C_p \left[\sqrt{\frac{1}{2\,(1 - R)}}\, K_t\, \Delta S\right]^{k_p} \,. \quad (17)$$

After logarithmic transformation equation (17) will be represented as a straight line of $\log \left[\sqrt{1/2\,(1 - R)}\, K_t\, \Delta S\right]$ against $\log N_i$. Figure 4 shows the least square fit to test data in [13] for stress ratios varying between 0.05 and 0.45. Regression analysis yields the following constants : $C_p = 2.87 \cdot 10^{17}$ and $k_p = -4.89$; the correlation coefficient is $r = -0.951$ and the standard deviation $s = 0.084$. As may be seen eq. (17) represents well the test data.

Fatigue crack initiation may also be described using fracture mechanics parameters [14]. Dowling [15] pointed out that, in some cases, the following relationship exists :

$$K_t\, \Delta S = \frac{2}{\sqrt{\pi}}\, \frac{\Delta K_I}{\sqrt{\rho}} \,, \quad (18)$$

where K_I is the fracture mechanics stress intensity factor and ρ the notch root radius.

Substituting eq. (18) into eq. (17), we find :

$$N_i = C'_p \left[\sqrt{\frac{1}{2\,(1 - R)}}\, \frac{\Delta K_I}{\sqrt{\rho}}\right]^{k_p} \,, \quad (19)$$

Figure 4 :

Regression analysis of test results of FCIL at various values of stress ratio (Al-alloy 2024-T3 [13]).

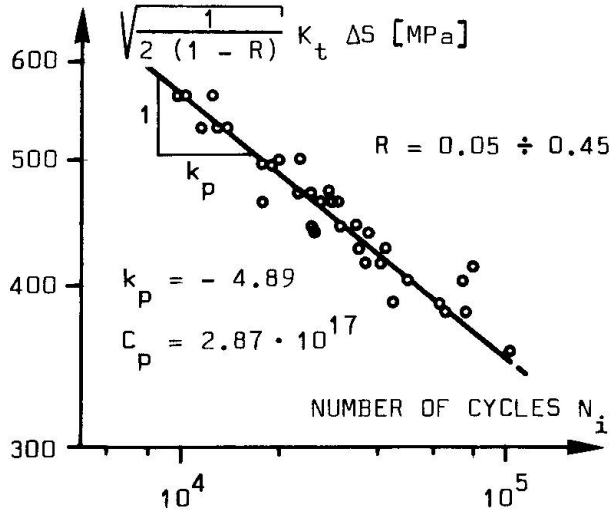

$$\text{where} : C'_p = \left[0.5 \sqrt{\pi E \sigma_f \epsilon_f}\right]^{-k_p} . \quad (20)$$

Therefore, FCIL can also be expressed as a power function of $\Delta K_I/\sqrt{\rho}$ which has been experimentally verified by different authors [3] [4] [16] [17] [20].

4. PREDICTION OF FCIL IN STEEL

The main difficulty in the prediction of FCIL lies in the evaluation of the exponent k_p (eq. 15). Once this is known, the coefficient C_p or C'_p (eqs. 16 or 20) may be calculated and subsequently introduced into eqs. (17) and (19) to yield the fatigue crack initiation life N_i.

4.1. Basic equations

To compute the exponent k_p, the values of c and n are needed. Manson [1] gives an experimental formula for c, using basic tensile properties :

$$c = 0.52 - \frac{1}{4} \log \epsilon_f + \frac{1}{3} \log \left[1 - 82 \left(\frac{\sigma_u}{E}\right) \left(\frac{\sigma_f}{\sigma_u}\right)^{0.179}\right] . \quad (21)$$

From Hollomon's equation, n may be approximated as :

$$n = \log (\sigma_f/\sigma_{ys}) / \log (500\ \epsilon_f) . \quad (22)$$

The true fracture values of σ_f and ϵ_f are given in [18] as :

$$\sigma_f = \sigma_u (1 + RA) , \quad (23)$$

$$\epsilon_f = - \ln (1 - RA) . \quad (24)$$

Here, σ_u is the ultimate stress, σ_y the yield stress, and RA the reduction in area at fracture in the tension test.

4.2. Notched specimens

Calculated values of the exponent k_p and the coefficient C_p of C'_p of three steels are listed in table 1. As shown in figure 5, the resulting curves of FCIL agree

Table 1 : Examples of tensile properties [20] [21] [22] and predicted values of k_p, C_p and C'_p for three steels.

MATERIAL		σ_u [MPa]	σ_{ys} [MPa]	RA [%]	k_p eq. (15)	C_p (modified) eq. (16)	C'_p (modified) eq. (20)
Cast steel	[21]	619	423	48.0	- 3.41	$1.70 \cdot 10^{14}$	
High-strength steel	[20]	1161	1053	52.6	- 3.13		$3.23 \cdot 10^{13}$
Fe 510	[22]	530	350	60.0*	- 3.19	$2.79 \cdot 10^{13}$	

* estimated value

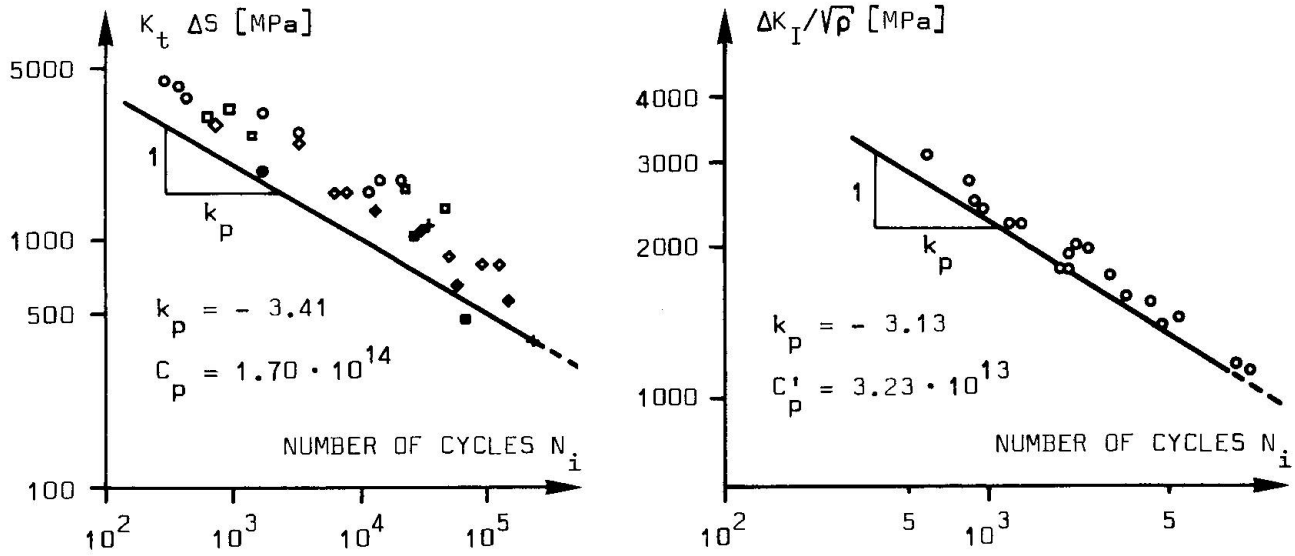

a) Cast steel, R = 0.1 [16]. b) High-strength steel, R = 0 [20].

Figure 5 : Comparison of the predicted curves for the fatigue crack initiation life N_i with test results.

well with the experimental results [15] [20] although they give, to some extent, shorter lives. It should be noted that the values of C_p and C'_p in table 1 although calculated from eqs. (16) and (20) were further modified by a multiplication factor $[\sqrt{1/2\ (1 - R)}]^{k_p}$. This is necessary when the stress ratio is the same value for all test.

These comparisons indicate a link between FCIL and tensile properties although additional work is necessary to give a more accurate correlation between them and k_p since the FCIL is sensitive to a number of other factors, in particular, the surface condition of the notch root [16] [18].

4.3. Welded elements

Yamada and Hirt [23] give the fatigue life of gusset specimens similar to the specification of Stress Category D in AASHTO [24]. Using the values in Table 1 for Fe 510 base plate material and an average stress ratio of 0.158, eq. (17) gives :

$$N_i = 2.79 \cdot 10^{13} (K_t \Delta S)^{-3.19} . \qquad (25)$$

Stress measurements on similar welded elements [25] show stress concentration factors at the crack initiation location largely in excess of 2 so that FCIL of gusset specimen becomes, for example $K_t = 3.0$:

$$N_i = 8.39 \cdot 10^{11} \Delta S^{-3.19} , \qquad (26)$$

where ΔS is the nominal stress range defined as $\Delta\sigma$ in [23].

The total fatigue life of the gusset specimens, made of Fe 510 and other structural steels, along with calculated FCIL from eq. (26) are shown in figure 6. It may be seen that the ratio of FCIL to the total fatigue life, N_i / N_f, is about

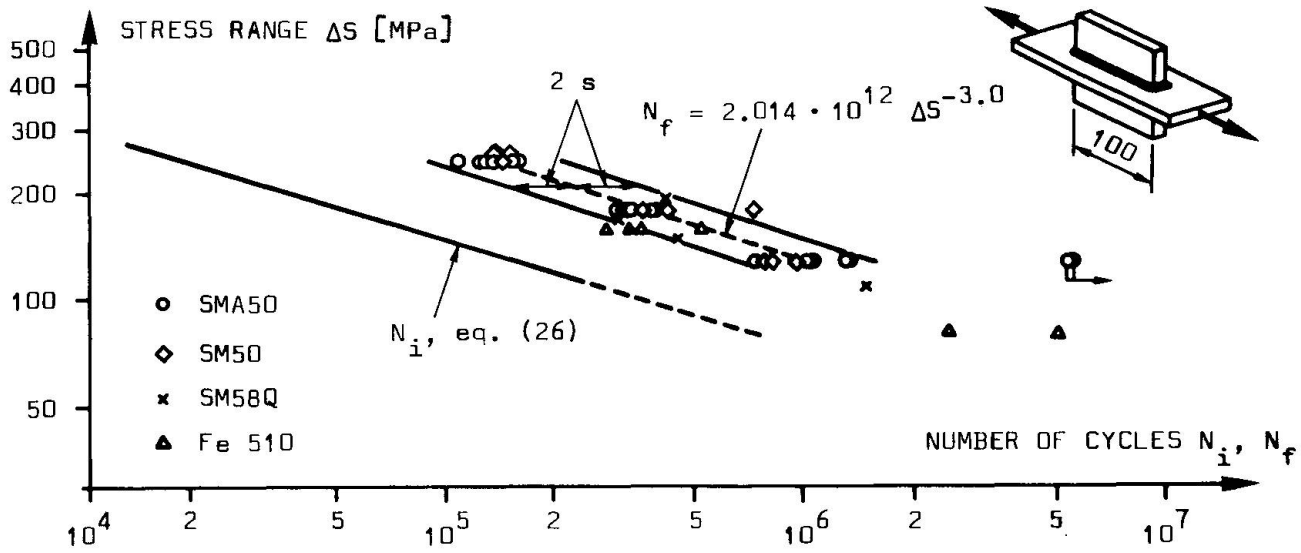

Figure 6 : Predicted FCIL and total fatigue life of gusset specimen [23].

0.16 at ΔS = 150 MPa. This agrees well with that given in [23], where the number of cycles to initiate and propagate a crack to 0.2 mm depth is considered as FCIL.

5. CONCLUSIONS

Based on the analysis developed and the comparison with test results, the following summarizing remarks may be made :

1.- Approximate formulae are derived to calculate the cyclic local strain range at the notch tip of a notched element for stress ratios of R = 0, and - 1.

2.- A generalized approximate expression for FCIL is given to indicate the effect of stress ratio on FCIL.

3.- It is possible to predict the FCIL of structural steel based on their tensile properties.

ACKNOWLEDGEMENTS

I am very grateful to Prof. J.-C. Badoux and Prof. M.A. Hirt for their support and help in my work at the Institute for Steel Construction of the federal Institute of Technology in Lausanne, Switzerland. In particular, I would like to thank Prof. M.A. Hirt for his friendly encouragement and instructive discussion throughout my stay. Appreciation is also expressed to Messrs. B. Kerridge, M. Gottier and M. Fiaux for their help in preparing this paper.

REFERENCES

[1] MOWKRAY, D.E. and McCONNELEE, J.E., ASTM STP 519, 1973, pp. 151-169.

[2] NAKAZAWA, H. et al, Bull. JSME., Vol. 12, No. 53, 1969, pp. 958-965.

[3] ZHENG Xiulin, Fatigue Crack Initiation Life of Metals (to be published in China).

[4] YOUSSEFI, K., Fatigue Crack Initiation and Propagation in Steels Exposed to Inert and Corrosive Environments, University of California, Diss. Abstr. Int., Mar. 1979, 29(9), p. 193.

[5] NEUBER, H., Trans. ASME, Dec. 1961, pp. 544-560.

[6] KLEEMOLA, H.J. and NIEMINEN, M.A., Met. Trans., Vol. 5, 1974, pp. 1863-1866.

[7] STANDNICK, S.T. and MORROW, JoDean, ASTM STP 515, 1972, pp. 229-252.

[8] YANG Qingxiong, Local Stress-Strain Method for Predicting the Fatigue Life (to be published in China).

[9] ROLFE, S.T. and BARSOM, J.M., Fracture and Fatigue Control in Structures, Prentice-Hall, Engelwood Cliffs, 1977, pp. 208-230.

[10] KREMPLE, E., Notched High-Strain Fatigue Behavior of Three Low-Strength Structural Steels, GEAP Rep. 5714, Jan. 1969, GEAP Rep. 5637, June 1968.

[11] PETERSON, R.E., Stress Concentration Design Factors, John Wiley, New York, 1962.

[12] GROSSKREUTZ, J.C., Met. Trans., Vol. 3A, 1972, pp. 1255-1262.

[13] LIU, H.W., J. Basic Eng., Trans. ASME, Mar. 1961, pp. 23-31.

[14] FROMAN, R.G., Eng. Fract. Mech., Vol. 4, 1972, pp. 333-345.

[15] DOWLING, N.E., ASTM STP 677, 1979, pp. 247-273.

[16] BARNBY, J.T., DINSDALE, K., and HOLDER, R., Fatigue Crack Initiation, Conference on the Mechanics and Physics of Fracture, Cambridge, England, 1975, Paper 26.

[17] BARNBY, J.T. and DINSDALE, K. Mater. Sci. Eng., Vol. 26, 1976, pp. 245-250.

[18] MANSON, S.S., Thermal Stress and Low-Cycle Fatigue, McGraw-Hill, New York, 1966, p. 160.

[19] ZHENG Xiulin, On Fatigue Crack Initiation Life, JIXIEQIANGDU, No. 10, 1980, pp. 54-69 (in Chinese).

[20] ZHENG Xiulin and ZHANG Jiangou (unpublished work).

[21] SMITHELLS, Collin J., Metal Reference Book, Vol. III, 4th edition, London, Butterworths, 1976.

[22] HIRT, M.A. and KUMMER, E., (unpublished data).

[23] YAMADA, K., and HIRT, M.A., Fatigue Crack Propagation from Fillet Weld Toes, Ecole polytechnique fédérale de Lausanne, ICOM 075, 1980.

[24] "Standard Specifications for Highway Bridges", American Association of State Highway and Transportation Officials, Washington, 1977.

[25] HIRT, M.A. and KUMMER, E., VDI-Berichte, Nr. 313, 1978.

Fatigue Crack Propagation and Reliability of Structural Elements

Propagation des fissures de fatigue et fiabilité des éléments de construction

Ermüdungsrissausbreitung und Betriebszuverlässigkeit von Konstruktionsteilen

D.D. CIOCLOV
Dr. -Ing., Director
Institute of Welding and Metal Testing
Timişoara, Romania

SUMMARY
Reliability theory and fracture mechanics principles were combined to indicate the time-dependent failure rate and survival probability of structural elements subjected to random loading. The analysis is illustrated for random loading of the Gaussian, stationary, narrow-band form.

RESUME
La théorie de la fiabilité et les principes de la mécanique de la rupture sont considérés conjointement, en mettant en évidence la dépendance de la vitesse de défaillance en fonction du temps et la probabilité de survivance des éléments de construction soumis à des charges aléatoires. L'analyse est illustrée pour une charge aléatoire du type Gaussien stationnaire à bande étroite.

ZUSAMMENFASSUNG
Die Zuverlässigkeitstheorie und die Methoden der Bruchmechanik wurden angewendet, um die zeitabhängige Ausfallsrate sowie die Überlebenswahrscheinlichkeit von Bauteilen unter variablen Lasten zu bestimmen. Die Betrachtungen werden für einen stationären Gauss'schen Schmalband-Belastungsprozess veranschaulicht.

1. INTRODUCTION

The materials fatigue damage occurs in two stages : a) the damage nucleation, a process which develops at microstructural levels ending with fatigue cracks initiation, b) crack propagation until the overall load carrying capacity is lost. The nucleation stage can be extended over 80 - 90 % of the fatigue life, in the case of smooth elements loaded in neutral environment, or can be suppressed in the presence of accute stress concentrators, preexistent defects or corrosive environment.In welded metallic structures stress concentrators arise from particular joint configuration while defects such as undercuts, lack of penetration or even cracks can be induced during the welding process. Undere these circumstance the damage nucleation period is short and the reliability of a structural element or of the whole structure is governed by the random interaction of the load, defects size and the material respose to the fatigue crack propagation.

In the following a procedure will be presented, in order to estimate the reliability of metallic elements containing accute defects which propagate under random loadings.

2. RELIABILITY ANALYSIS

In a metallic element which contains a crack of semilength a (figure 1), the descrease of residual strength R_r as against the number of loading cycles is expressed ba the general relationship :

$$\frac{dR_r}{dn} = \frac{dR_r}{da}\cdot\frac{da}{dn} \qquad (1)$$

The residual strength R_r of an element containing a fatigue crack can be evaluated by resorting to the basic relationships of fracture mechanics :

$$R_r = \frac{K_{Ic}}{\sqrt{J I \beta a}} \qquad (2)$$

where K_{IC} is the fracture toughness (under plain strain conditions) of the material and β is a correction for the finite dimensions of the element [1], [2] . The rate of fatigue crack propagation da/dn can be evaluated by a Paris type relationship [3] :

$$\frac{da}{dn} = C(\sigma_a \sqrt{\pi \beta a})^k \qquad (3)$$

where σ_a is the uniform stress amplitude applied sufficiently re-

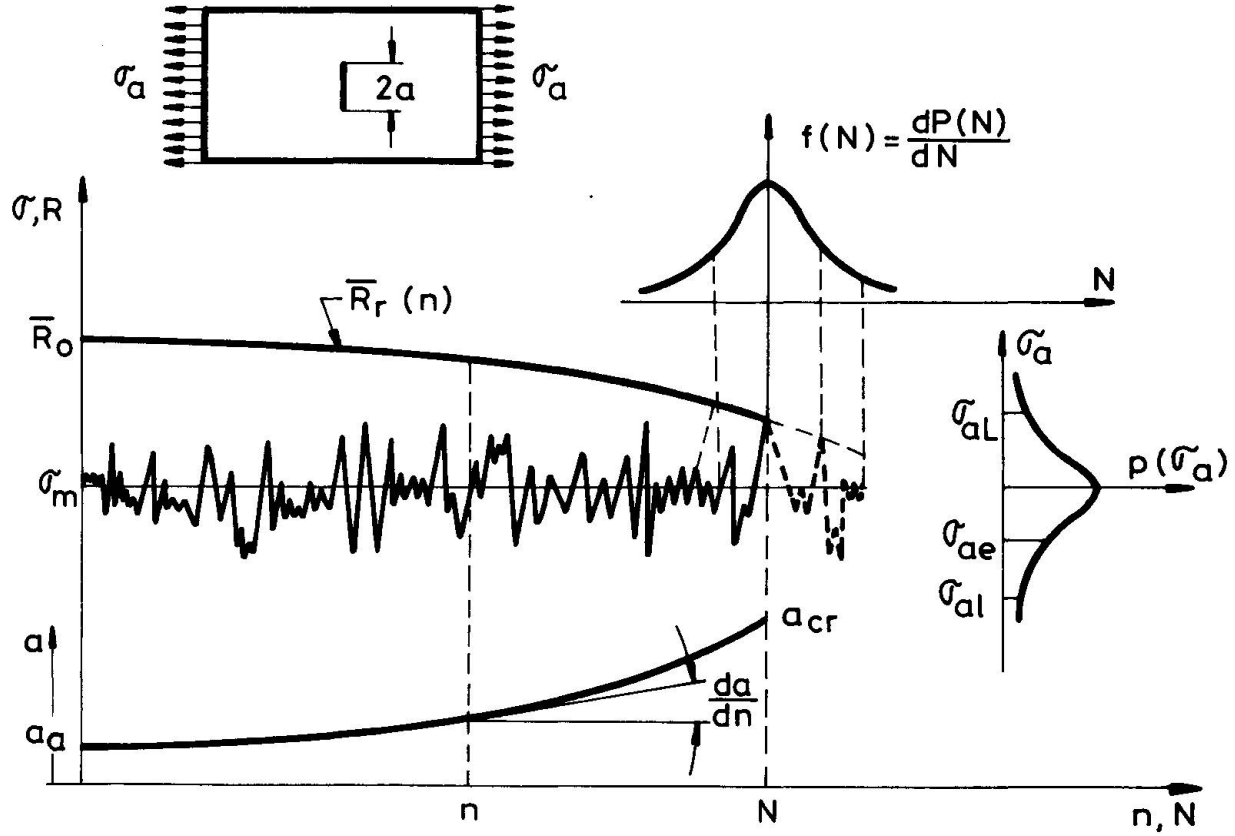

Figure 1.

moted from the crack tip region (figure 1) ; C and k are material constants.

If the random loading is stationary and centred arround the mean stress σ_m with the probability density $p(\sigma_a)$ defined on the domain $(\sigma_{al}; \sigma_{aL})$ as is illustrated in figure 1 , then the mean rate of crack propagation $\overline{da/dn}$ derived by a mean type operation in the relationship (3) is:

$$\overline{\frac{da}{dn}} = \frac{C}{\Lambda_0}(\sqrt{J\beta a})^k \int_{\sigma_{ae}}^{\sigma_{aL}} \sigma_a^k p(\sigma_a)d\sigma_a \qquad (4)$$

where σ_{ae} is the inferior threshold limit of the stress amplitude under which the fatigue cracks do not propagates any more 1

If $\sigma_{ae} < \sigma_{al}$, then in eq. (4) the inferior limit of integration is σ_{al}, while if $\sigma_{ae} > \sigma_{al}$ the correction for the load distribution truncation must be introduced :

$$\Lambda_0 = \int_{\sigma_{ae}}^{\sigma_{aL}} p(\sigma_a)d\sigma_a \qquad (5)$$

Taking the derivative in the relationship (2) one results from the conjunction with the relationship (1) and (4) the rate of the mean residual strength decreasing as against the applied loading cycles :

$$\overline{\frac{dR_r}{dn}} = -\frac{1}{2}\cdot\frac{\overline{J}\beta C(K_c)^{k-2}}{\Lambda_0 \overline{R}_r^{k-3}} \int_{\sigma_{ae}}^{\sigma_{aL}} \sigma_a^k p(\sigma_a)d\sigma_a \qquad (6)$$

By integrating in this equation and considering the relationship (2) for the initial undamaged state of the element with the mean strength $\overline{R}_0$ and a preexisting crack of semi-length a_0 (i.e. $\overline{R}_0 = K_{IC}/\sqrt{J\beta a_0}$) one results the mean residual strength R_r after n - loading cycles :

$$\overline{R}_r = \overline{R}_0\left[1 - n(\frac{k}{2}-1)\frac{\overline{J}\beta C}{\Lambda_0}(\frac{K_{IC}}{\overline{R}_0})^{k-2}\int_{\sigma_{ae}}^{\sigma_{aL}} \sigma_a^k p(\sigma_a)d\sigma_a\right]^{1/(k-2)} \qquad (7)$$

In this stage of analysis it is pertinent to outline that the mean residual strength after n-loading cycles can be computed as function of :

- the characteristic parameters of the loading distribution $p(\sigma_a), \sigma_{al}; \sigma_{aL}$;
- the parameters associated with the material strength to fatigue crack propagation : k , C and σ_{ae} ;
- a geometric parameter β which depends on the shape and dimensions of the metallic element;

- initial mean static strength $\bar{R}_0$ and fracture toughness K_{IC} .

It is to be remarked in the eq. (7) that the ratio $(K_{IC}/\bar{R}_0)^2 = \bar{J}\beta a_0$ is proportional with the initial crack length.

When the application of K_{IC} concept is not appropriate due to crack - tip plasticity effects one can resort to the critical crack opening displacement (COD) concept [1] for making explicite the residual static strength.

Knowing the expression of the residual strength $\bar{R}_0$ as function of applied loading cycles one can determine the failure risk $\lambda(N)$, or the probability of failure in the (N+1) cycle if the involved metallic element has survived N cycles. This probability is determined by the condition that the maximum loading σ_{max} (i.e. $\sigma_{max} = \sigma_a + \sigma_m$) applied in the N-th cycle be grater than the residual strength under singular loading [4] :

$$\lambda(N) = \text{Prob.}(\sigma_{max} > \bar{R}_r) = \int_{\bar{R}_r = \sigma_m}^{\sigma_{aL}} p(\sigma_a)\, d\sigma_a \qquad (8)$$

In the reliability theory one defines the reliability function Q(N) which quantifies for an element or a structure the cumula - tive probability for attaining (survival) an endurance of N cycles. The complementary function $P(N) = 1 - Q(N)$ defines the cumulative probability that fracture occurs at a certain endurance N. The following relationship between these functions exists [4],[5]:

$$Q(N) = 1 - P(N) = \exp\left[-\int_0^N \lambda(N)\, dN \right] \qquad (9)$$

From eqs. (8) and (9) one can estimate the reliability parame - ters of a structural element which instantaneous residual strength (eq.7) is governed by the fatigue crack propagation under random loadings.

If the loading pattern (applied in a region remote from the crack influence) is defined by the probability density of loading maxima $p(\sigma_{max})$ then eq.(7) remains valid in its functional

form, but with the particularization $\sigma_a \rightarrow \sigma_{max}$ and appropriate experimental constants C and k.

3. THE CASE OF NORMAL NARROW - BAND RANDOM LOADING

As an exemplification, at the application of the general theory the case of a normal or Gaussian narrow - band random stationary loading with a zero mean will be considered. For such a loading case the loading maxima repartition coincides with amplitudes repartition, being of the Rayleigh type [6] :

$$p(\sigma_a)=\frac{\sigma_a}{d_\sigma^2}\exp(-\frac{\sigma_a^2}{2d_\sigma^2}) \qquad (10)$$

which in conjunction with the relationship (7) one determines the expression of the mean residual stress $\bar{R}_r$ after n-loading cycles :

$$\bar{R}_r=\bar{R}_0(1-A_n)^{1/(k-2)} \qquad (11)$$

where :

$$A=(\frac{k}{2}-1)\sqrt{\pi}\beta C(\sqrt{2}\,d_\sigma)^k\;\frac{\Gamma(\frac{\sigma_{aL}^2}{2d_\sigma^2};1+\frac{k}{2})-\Gamma(\frac{\sigma_{ae}^2}{2d_\sigma^2};1+\frac{k}{2})}{1-\exp(-\sigma_{aL}^2/2d_\sigma^2)}\,(\frac{K_{IC}}{\bar{R}_0})^{k-2} \qquad (12)$$

Since the Rayleigh distribution was truncated at the superior limit σ_{aL}, the fracture cannot occur as long as the residual strength $\bar{R}_r$ was not decreased by the fatigue damage down to the superior limit of the loading distribution σ_{aL}, when the corresponding number of cycles n^* are :

$$n^*=\frac{1}{A}\left[1-(\frac{\sigma_{aL}}{\bar{R}_0})^{k-2}\right] \qquad (13)$$

The failure risk is zero for $0\leqslant n\leqslant n^*$ and increases for $n>n^*$ according to the relationship (8) which yields :

$$\lambda(N)=\left\{\exp\left[-\frac{\sigma_{aL}^2}{2d_\sigma^2}(\frac{1-A_n}{1-A_{n^*}})^{\frac{2}{k-2}}\right]-\exp(-\frac{\sigma_{aL}^2}{2d_\sigma^2})\right\}\left[1-\exp(-\frac{\sigma_{aL}^2}{2d_\sigma^2})\right] \qquad (14)$$

Now, the reliability function Q(N) and the cumulative probability P that the fatigue crack propagation till to the complete frac - ture be accomplished in N loading cycles results from the conjunc tion of eq.(9) and (14).

$$P(N)=1-\exp\left\{\frac{(N-n^*)\exp\left(-\frac{\sigma_{aL}^2}{2d_\sigma^2}\right)+\frac{k-2}{2}\frac{1-An^*}{A}\left(\frac{2d_\sigma^2}{\sigma_{aL}^2}\right)^{\frac{k-2}{2}}\left\{\Gamma\left[\frac{\sigma_{aL}^2}{2d_\sigma^2}\left(\frac{1-AN}{1-An^*}\right)^{\frac{2}{k-2}};\right.\right.\right.\longrightarrow$$

$$\left.\left.\left.\longrightarrow\frac{\frac{k}{2}-1\right]-\Gamma\left(\frac{\sigma_{aL}^2}{2d_\sigma^2};\frac{k}{2}-1\right)\right\}}{1-\exp\left(-\frac{\sigma_{aL}^2}{2d_\sigma^2}\right)}\right\} \qquad (15)$$

In the relationships (12) and (15) $\Gamma(t,\nu)$ is the incomplete Gam- ma function whose integral expression is :

$$\Gamma(t,\nu)=\int_0^t t^{\nu-1}\,e^{-t}\,dt \qquad (16)$$

In figure 2 it is illustrated the cumulative failure probability P(N) as against the number of cycles $(N-n^*)$ for a 50 class steel element with $\bar{R}_o \doteq 55$ dN/mm^2 $K_{IC}/\bar{R}_0=10$; $\beta=1$ and $\sigma_{ae}=0$. The fa -

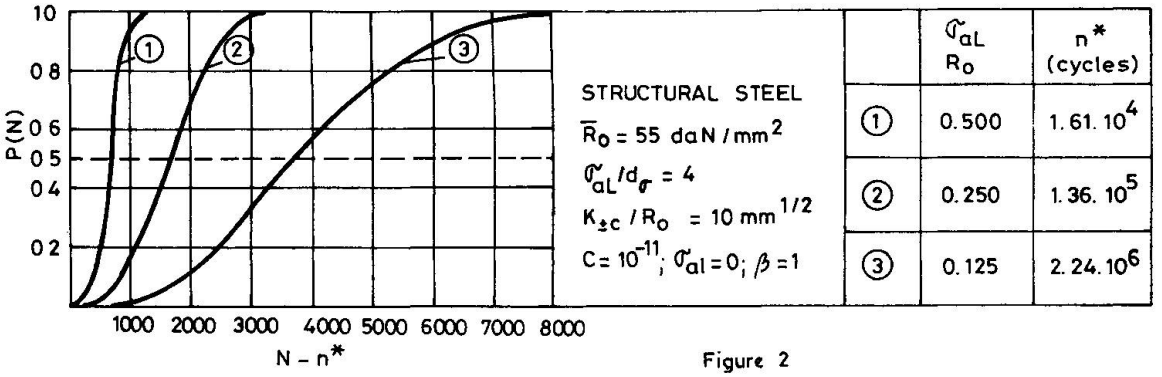

	σ_{aL} / R_o	n* (cycles)
①	0.500	$1.61.10^4$
②	0.250	$1.36.10^5$
③	0.125	$2.24.10^6$

Figure 2

tigue crack propagation parameters k=4 and $C=10^{-11}$ are typical for this type of steel [1] . The considered random loading is of Ray- leigh type with $\sigma_{aL}/d_\sigma=4$, the different pattern of loading in- tensity being specified by the ratio $\sigma_{aL}/\bar{R}_0=0{,}125;\ 0{,}250;\ 0{,}500$.
It is to be remarked from figure 2 that the statistical variabi- lity increases as the random loading intensity decreases.

The proposed analysis is pertinent for the reliability evalua - tion of a structural element in which a fatigue crack is propa-

gating. By applying the theorems of probability composition [4] [5] one can further estimate the overall reliability of a structure with elements arrangend in series (static determinate) parallel (redundant) or a combination of both pattern.

REFERENCES

1. CIOCLOV, D.D. : Mecanica ruperii materialelor. Ed.Academiei R.S. România,1977
2. SIH, G.C. : Handbook of Stress - Intensity Factors. Lehigh University Bethlehem Penn., 1973
3. PARIS, P.C., GOMEZ, M.P., ANDERSON, W.E. : The Trend in Engineering , V.31, p.9, 1961
4. CIOCLOV, D.D. : Rezistenţă şi fiabilitate la solicitări variabile. Ed.Facla, Timişoara, 1975
5. BAZOWSKI,J. : Fiabilité. Theorie et pratique de la sûreté de fonctionement. Ed.Dunod, Paris, 1966
6. BENDAT, J.S. : Principles and Application of Random Noise Theory. John Wiley, New York, 1958

Prediction of High Cycle Fatigue under Multiaxial Stress Conditions

Détermination de la résistance à la fatigue sous état de contraintes multiaxiales

Bestimmung der Ermüdungsfestigkeit bei mehraxialen Spannungszuständen

JOHN O. NØKLEBY
Dr. Ing.
Det Norske Veritas
Oslo, Norway

SUMMARY
Four criteria for prediction of high cycle fatigue under multiaxial stress conditions are described, i.e. the octahedral stress criterion, the shear stress criterion, the internal friction criterion and the shear stress intensity criterion. From comparison between predictions and experimental results from the literature it is found that the two latter criteria give the best predictions.

RESUME
Quatres critères pour la détermination de la résistance à la fatigue sous conditions de contraintes multiaxiales sont décrits, c'est-à-dire le critère de contrainte octahèdral, le critère de contrainte de cisaillement, le critère de friction interne et le critère d'intensité de contrainte de cisaillement. La comparaison entre les résultats calculés et expérimentaux, tirés de la littérature, montre que les deux derniers critères donnent de meilleures prédictions.

ZUSAMMENFASSUNG
Es werden vier Berechnungskriterien für die Bestimmung der Ermüdungsfestigkeit bei mehraxialen Spannungszuständen beschrieben. Es sind dies die Kriterien der Oktaederspannung, der Schubspannung, der inneren Reibung und das Kriterium der Schubspannungsintensität. Ein Vergleich von Berechnung und Versuchsergebnissen aus der Literatur zeigt, dass mit den letzteren zwei Kriterien die besten Vorhersagen erzielt werden können.

1. INTRODUCTION

By means of modern fatigue analysis, for example by the finite element method, the stress state in any point of a component may be determined. In the general case, it will be given in terms of the stress matrix

$$T = \begin{bmatrix} \sigma_x & \tau_{xy} & \tau_{xz} \\ \tau_{xy} & \sigma_y & \tau_{yz} \\ \tau_{xz} & \tau_{yz} & \sigma_z \end{bmatrix} \qquad (1)$$

In the case of fatigue loading, each of the six independent components of the matrix may in principle vary arbitrarily. Fatigue data available to the designer, however, are usually given in terms of SN curves measured with test specimens having uniaxial stress. The designer then needs some criterion for converting the multiaxial load variation to some equivalent, one dimensional stress variation, before the fatigue evaluation can be performed.
In the following, four criteria for such conversion are described and evaluated. It is assumed that all the stress components vary sinusoidally and with the same frequency, i.e.

$$\begin{aligned} \sigma_x &= \sigma_{xs} + \sigma_{xa} \cdot \sin(\omega t - \phi_x) \\ \sigma_y &= \sigma_{ys} + \sigma_{ya} \cdot \sin(\omega t - \phi_y) \\ \sigma_z &= \sigma_{zs} + \sigma_{za} \cdot \sin(\omega t - \phi_z) \\ \tau_{xy} &= \tau_{xyz} + \tau_{xya} \cdot \sin(\omega t - \phi_{xy}) \\ \tau_{xz} &= \tau_{xzs} + \tau_{xza} \cdot \sin(\omega t - \phi_{xz}) \\ \tau_{yz} &= \tau_{yzs} + \tau_{yza} \cdot \sin(\omega t - \phi_{yz}) \end{aligned} \qquad (2)$$

2. METHODS

2.1 The octahedral stress criterion

With this criterion, the variation of the shear stress in the octahedral plane is analysed.
In this plane, the shear stress is expressed as a vector with length proportional to the von Mises equivalent stress. If the stress components vary proportionally (in phase), the direction of the vector is fixed throughout the cycle, whereas the lenght of the vector varies. Hence a line segment in the plane defines the points that have been coverered by the vector during the cycle. The length of this segment is defined as the octahedral shear stress range. The equivalent stress variation is defined to be proportional to the octahedral shear stress range. With proportional loading, therefore, the octahedral stress criterion is identical to the von Mises criterion.
In the case of non proportional loading, the direction of the vector changes with time. During the cycle, the end point of the vector describes a closed curve in the plane. In this case, the octahedral shear stress range is defined as the greatest distance obtainable between two points of this curve.

2.2 The shear stress criterion

The shear stress (or Tresca) criterion could be applied directely to fatigue analysis in cases of proportional loading. For cases of non proportional laoding, an extended version of the criterion is described in ASME's Boiler and Pressure Vessel Code. The principle there is that the greatest shear stress range obtainable in any plane in space is used as the characteristic stress parameter. The stress range in a plane is defined in the same manner as described

above for the octahedral plane. The equivalvent stress variation is defined to be proportional to this range. In the Code, a special, analytical procedure is applied to arrive at this result.

2.3 The internal friction criterion

This criterion appears as an extension of the shear stress criterion. Here, not only the shear stress range in the plane $\Delta\tau$ is considered, but also the normal stress range on the plane $\Delta\sigma$. They are combined linearly to $\Delta\tau_c$

$$\Delta\tau_c = \Delta\tau + \alpha \cdot \Delta\sigma \qquad (3)$$

The equivalent stress variation is defined to be proportional to $\Delta\tau_c$. The plane of analysis is the plane where $\Delta\tau$ is the greatest. In simple cases, this plane can be determined analytically, whereas for complicated load cycles a numerical approach offers the simplest solution.
The constant α can be found if the material's fatigue strength is known in tension as well as torsion (denoted σ_o and τ_o respectively). The ratio between them (σ_o/τ_o) is by many ivestigators regarded as a material parameter. For ductile steels, σ_o/τ_o - ratios in the range 1.45 to 1.75 have been measured. In lack of measured data, the value $\sigma_o/\tau_o = \sqrt{3}$ is recommended. This corresponds to $\alpha = 0.16$ in eq. (3).

2.4 The shear stress intensity method

This method is based on an idea put forward by Novozhilov in (2) and modified for application to fatigue by Simbürger in (3). The idea is the following: Through a point in space, an infinite number of planes can be laid. A stress state in the point is reflected as a shear stress τ_p in each of these planes. The root-mean-square value of all these shear stresses is defined as the shear stress intensity, τ_i. Regarding the planes as tangential planes to a sphere with surface A, we get

$$\tau_i = \sqrt{\int_A \tau_p^2 \cdot dA} \qquad (4)$$

It can be shown that τ_i is proportional to the von Mises equivalent stress. For fatigue evaluation, the shear stress in a plane τ_p is exchanged by the shear stress range in the plane, $\Delta\tau_p$. Hence a $\Delta\tau_i$ is determined, and the equivalent stress variation is defined to be proportional to $\Delta\tau_i$. In cases of proportional loading, thus, this criterion is identical to the von Mises criterion and hence to the octahedral stress criterion.
Various modified versions of this criterion have appeared in recent german literature. Most of them are mentioned in (3). Generally, they are devised in order to reduce the calculational work (of solving eq. 4 numerically) and to include the σ_o/τ_o - ratio as a material parameter. In most cases, the validity of these versions is restricted to loadcases of two dimensional stress states.

3. RESULTS

The predictions of the above 4 methods have been compared to 224 fatigue tests with multiaxial loading reported in the literature. All these tests were performed with smooth, steel specimens. The deviation between predictions and measurements is denoted "ERROR" and is measured in per cent. Positive "ERROR" means predictions on the conservative side.
The results are shown in figs. 1-4. It is seen that the internal friction criterion and the shear stress intensity criterion are the best ones.

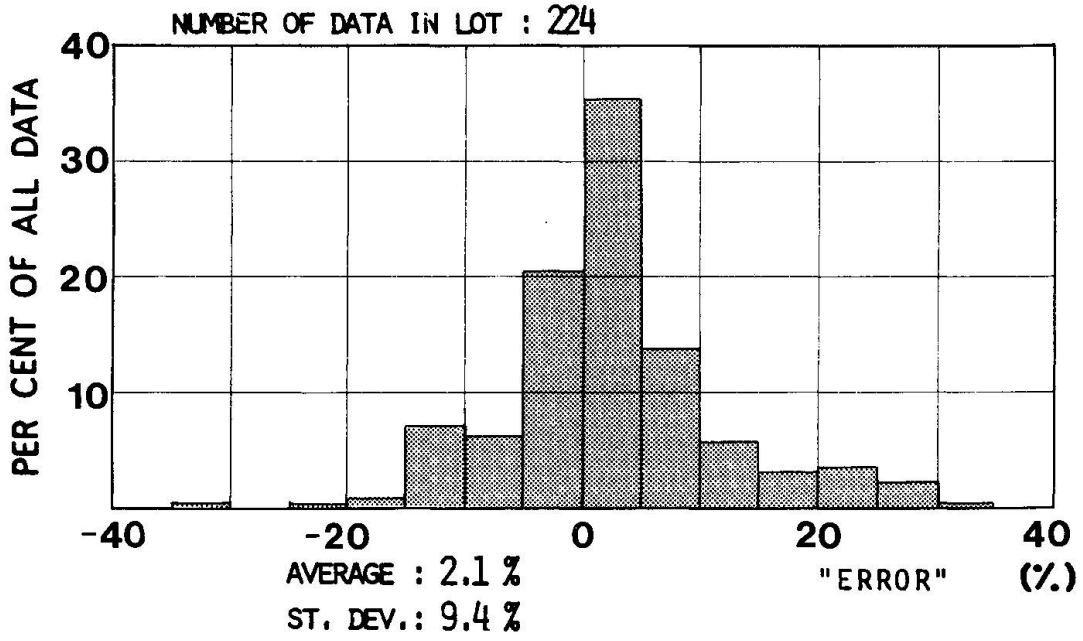

Fig. 1 Distribution of "ERROR" for octahedral stress criterion

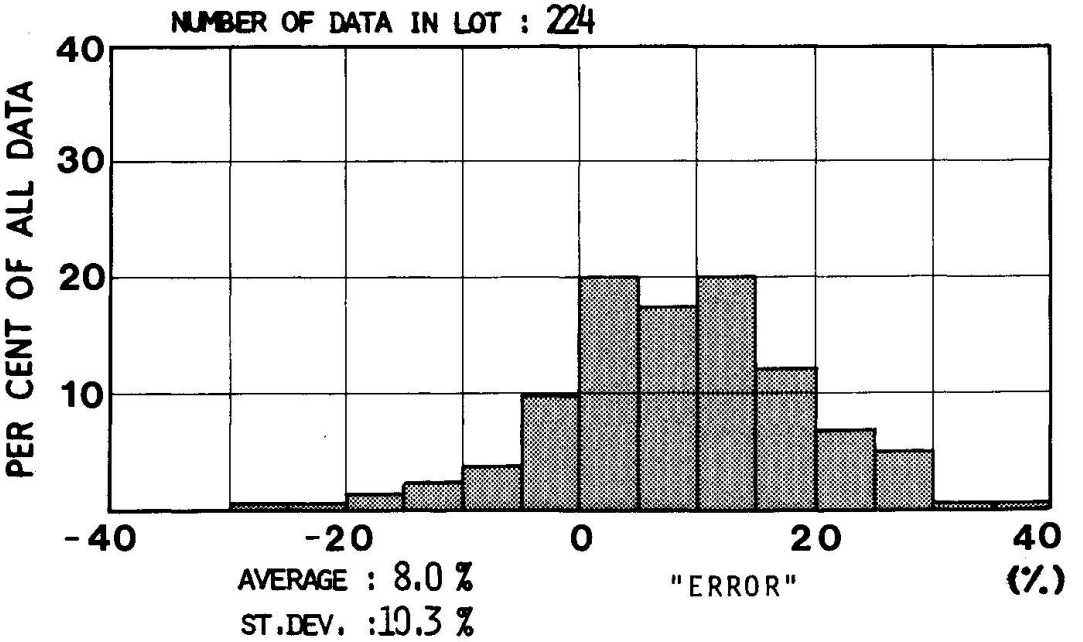

Fig. 2 Distribution of "ERROR" for the shear stress criterion.

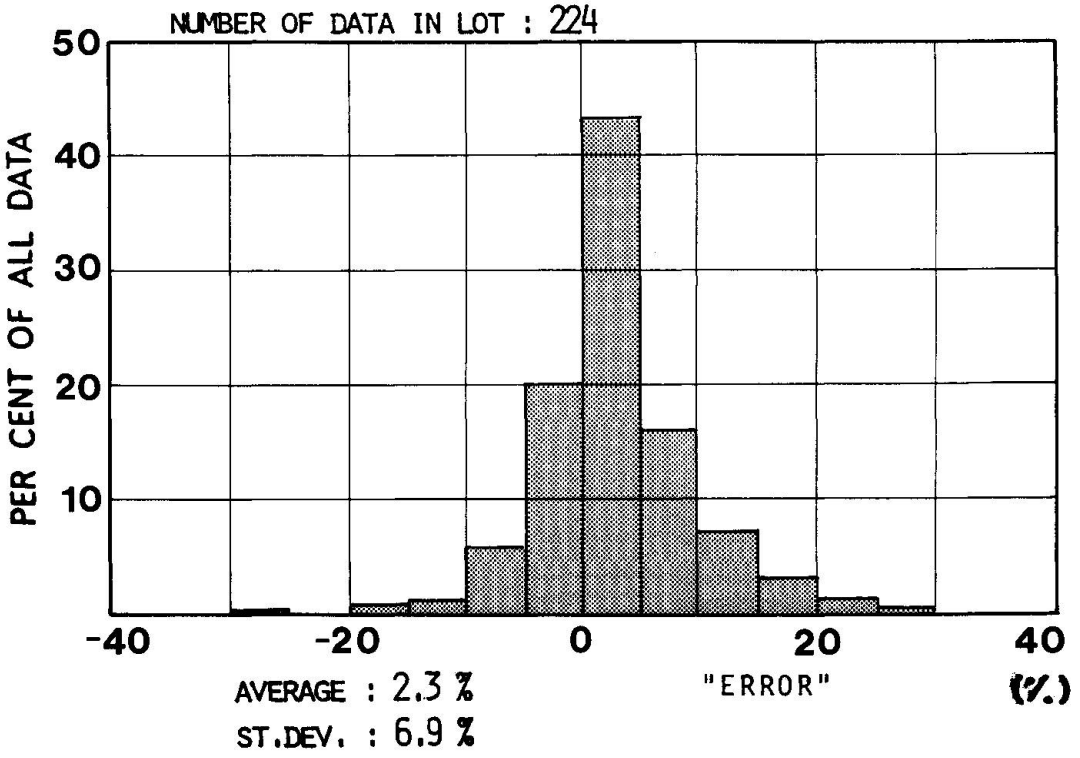

Fig. 3 Distribution of "ERROR" for internal friction criterion.

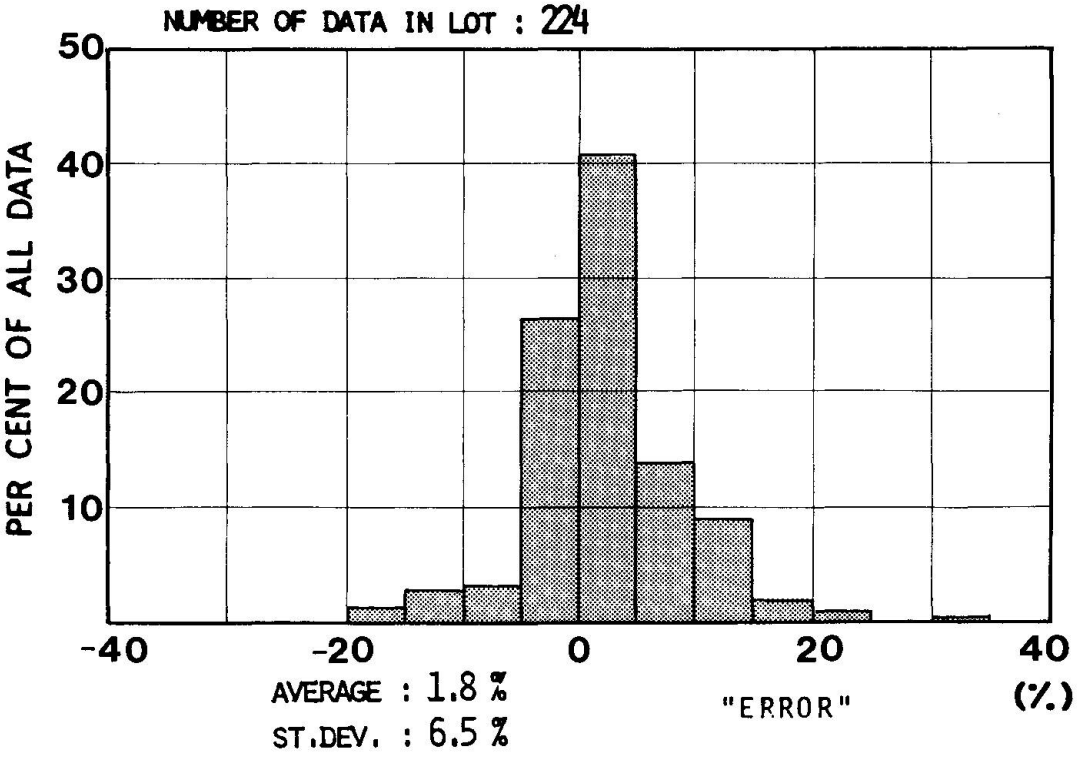

Fig. 4 Distribution of "ERROR" for shear stress intensity predictions

4. THE σ_o/τ_o RATIO

Based on the experimental data, the improvement in predictions obtained from including the σ_o/τ_o - ratio as a material parameter was investigated. This was done by performing the comparison between experimental and predictional results for two versions of the internal friction criterion, one with variable α and one with the fixed value $\alpha = 0.16$. The two approaches gave surprisingly small differences in the overall results, and it was concluded that the effort of measuring the fatigue strength in torsion is justified only in special cases of multiaxial fatigue evaluation.

5. MEAN STRESS EFFECT

In 70 of the experimental results, a static stress was included in the loading. This gave a proper background for evaluating criteria for equivalvent static stress under multiaxial stress conditions.
Two criteria are dominating in the literature here, namely the Sines criterion defining the first stress invariant ($\sigma_x + \sigma_y + \sigma_z$) as the equivalent static stress, and the von Mises criterion. The results clearly show that the latter gives best correlation between predictions and measurements.

6. REFERENCES

1 Nøkleby: Fatigue under multiaxial stress conditions
MD 81001, Div. of Machine Elements,The Norwegian Inst. of Technology, Trondheim, Norway.

2 Novozhilov: Theory of Elasticity
Pergamon Press, London, 1961

3 Simbürger:Festigkeitsverhalten Zäher Werkstoffe bei einer mehrachsigen, phasenverschobenen Schwingbeanspruchung mit körperfesten und veränderlichen Hauptspannungsrichtungen.
LBF-Bericht FB 121, 1975
Laboratorium für Betriebsfestigkeit, Darmstadt, Germany

Determination of Fatigue Life of Bicyclic Loaded Metal Structures

Détermination de la durée de vie de structures métalliques soumises à des charges alternées bicycliques

Bestimmung der Lebensdauer von Metallkonstruktionen, die durch Doppelfrequenzbelastung beansprucht werden

V.I. TRUFIAKOV
Professor
E.O. Paton Electric Welding Institute
Kiev, USSR

V.S. KOVALCHUK
Dr. Ing.
E.O. Paton Electric Welding Institute
Kiev, USSR

SUMMARY
It was established that at a fixed frequency ratio a linear dependence is observed between the amplitude ratio of two-frequency cycle and the decimal logarithm of fatigue life ratio. It is invariant to the variation of the main factors determining the fatigue strength of materials and joints. The given relationship permits to determine the fatigue life at bicyclic loading from Wöhler curves. Determination procedure is given.

RESUME
Il a été établi que, pour un rapport fixé des fréquences bicycliques, on peut observer une relation linéaire entre le rapport des amplitudes et le logarithme décimal du rapport des durées de vie. Cette relation est indépendante de la variation des principaux paramètres caractérisant la résistance à la fatigue des matériaux et des assemblages. La relation proposée permet de déterminer à partir des courbes de Wöhler la durée de vie sous un chargement bicyclique. On donne le processus de cette détermination.

ZUSAMMENFASSUNG
Es hat sich gezeigt, dass bei konstantem Verhältnis der zwei Frequenzen ein linearer Zusammenhang zwischen dem Spannungsamplitudenverhältnis und dem dekadischen Logarithmus des Lebensdauerverhältnisses besteht. Dieser Zusammenhang ist invariant zu den Grundfaktoren, die die Dauerfestigkeit der Werkstoffe und Verbindungen bestimmen. Diese Gesetzmässigkeit erlaubt es, die Lebensdauer bei der Doppelfrequenzbelastung mit den Wöhlerkurven zu bestimmen. Das Verfahren dazu wird angegeben.

Bicyclic loading (Fig.1), at which smaller value but higher-frequency components generated by all kinds of vibrations are superimposed on the main low-frequency cycles, is characteristic not only of aircraft, ships, reactor bodies, gas-turbine engines, but also of bridges [1], crane girders [2], mast-aerial constructions [3] and other structures (Fig.2). The data in the Table permit to judge frequency-amplitude ratios of loading components typical for the elements of these structures.

The detrimental effect of vibrations is usually not taken into account when calculating the cyclic fatigue life of structures or it is only taken into account by increasing the amplitude of the main alternating loading by a value corresponding to the high-cyclic component. However, as shown by the research, the results of which have been generalized in the previously compiled reviews and separate publications [4,5,6,9, et al.] the fatigue strength under bicyclic loading decreases to a greater extent, than at one-cyclic loading with a maximum amplitude $\sigma_{a.s}$, equal to the total value of the amplitudes of both cyclic components ($\sigma_{a.l}$ and $\sigma_{a.h}$). Here, the fatigue life variation can be affected not only by the amplitude ratio $\sigma_{a.h}/\sigma_{a.l}$ (Fig.3), but also by the frequency ratio f_h/f_l [7,8]. With the increase of f_h/f_l, the fatigue life monotonically decreases. At the same time, in case of small frequency ratios (at bending, axial loading and twist-bending) or when the rotation frequency is higher than that of bending (at testing for rotation bending), not the decrease but the increase of fatigue life was observed in some studies under bicyclic loading (Fig.3).

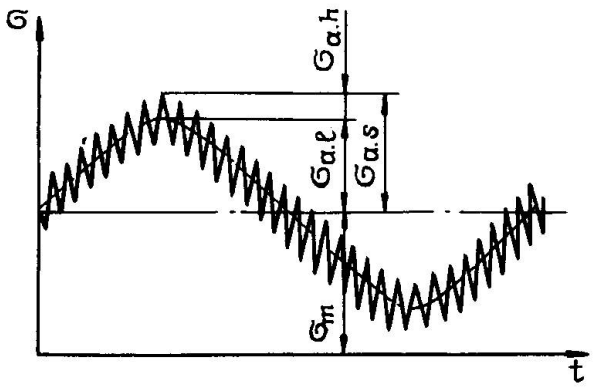

Fig.1. Bicyclic loading (scheme)

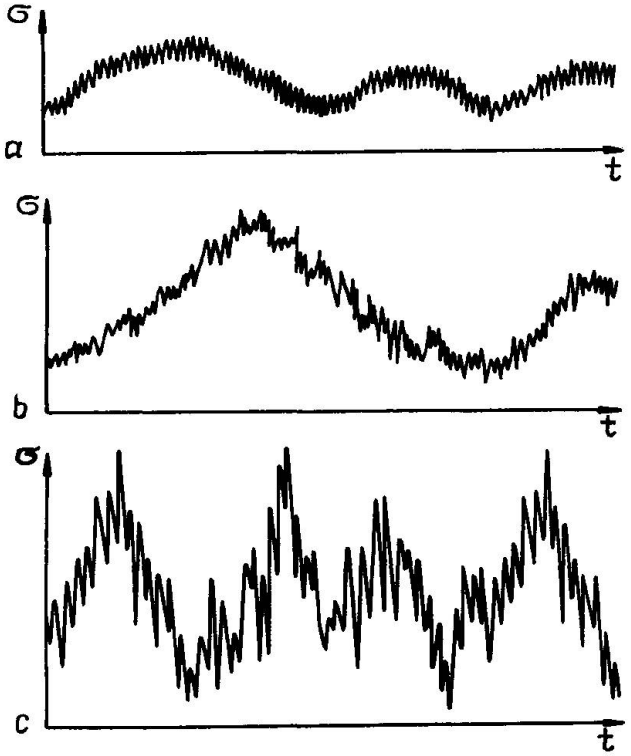

Fig.2. Change of stresses determined by oscillography: a) main beam of a bridge span l =23m; b) in a brace of a bridge lattice girder l =77m; when a train is passing at 83 km/h speed; c) in the mast guy-ropes.

It should be noted that under rotation bending conditions, the bicyclic loading is only ensured when the stress amplitude ratio is not high, and the bending frequency exceeds the rotation frequency. With the amplitude ratio increase and at excess of rotation fre-

Table. Amplitude and frequency ratios of load components

	Elements of structures and workpieces	Possible ratios of	
		amplitudes $\sigma_{a.h}/\sigma_{a.s}$	frequencies f_h/f_l
1.	Main beams and braces of railway bridge girders	0.05...0.25*	30...100*
2.	Metal structures of radio- and telemasts	0.1...0.5*	1.5...150*
3.	Crane girders	0.01...0.25	10...1000
4.	Power plant elements	0.03...0.5	100...1000
5.	Hydraulic turbines	0.1...0.5	2.5...150
6.	Spindles of blooming and rolling mills	0.01...0.5	15...30
7.	Cutting chains of coal cutters	0.1...0.5	15...20
8.	Fuselages, vane suspensions, ailerons and stabilizers of passanger planes	0.03...0.5	1.5...5000

*According to the data of measurements in several installations. It is possible that the amplitude and frequency range can be even greater for bridges and masts.

quency over the bending one, the nature of stress change noticeably differs from the bicyclic case. Here, the fatigue testing results of a different quality are obtained. Investigations of aluminium alloys at similar levels of stresses and frequency ratios showed that in case of rotation bending the superimposition of a high-frequency component increases the fatigue life, and under bending in one plane it considerably decreases. Furtheron, testing results only for axial loading and plane bending are given.

Alongside the experimental evaluation, various authors have made suggestions also for fatigue life calculation under bicyclic loading. They are based on linear cumulative damage hypothesis [3,10, et al.], the hypothesis of spectral summation [11], energy concepts [8], and empirical relationships [6,12,13, et al]. These suggestions mostly referred to specific workpieces, loading conditions and materials. Thus, evidently, their validity, as shown by the comparison of calculated values and experimental data of other authors, is preserved in certain rather narrow ranges of amplitude and frequency ratio variations [14] It is to be noted here that, apparently, Miner's hypothesis

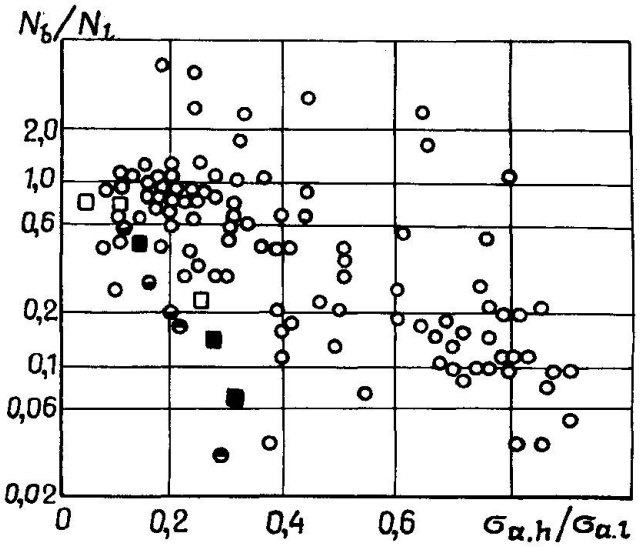

Fig.3.The effect of amplitude ratio on fatigue life change at bicyclic loading. o - [5], □ - [9], ■ - [6], ● - [4], ◒ - [4].

cannot be used to describe the fatigue damage accumulation. Possibly, it may lead to satisfactory results only in low-cycle region at relatively low f_h/f_l and for conditions not associated with significant temporal processes [15]. The unacceptability of Miner's hypothesis in multicycle area is demonstrated, in particular, by data in the work [16]. Specimen testing at bicyclic loading and at onecyclic loading with an equal value of maximum stresses showed that at bicyclic loading the fatigue life is noticeably decreased even when the average stress value is equal to the maximum average value of low cyclic component (Fig.5).

The suggestions made do not permit to conclude that at present a new quite well-based procedure for bicyclic loading fatigue life evaluation is being established or contemplated. It should be based on the premises or relationships, expressing regular connection between the parameters of bicyclic loading and fatigue strength valid in a wide range of amplitude and frequency ratio variation. The approach to the bicyclic loading parameter selection to obtain the simplest estimation dependences has not yet been sufficiently well grounded, either. In the investigations performed the total stress $\sigma_{a.s} = \sigma_{a.l} + \sigma_{a.h}$ was used to estimate the bicyclic loading fatigue life, and the relationship was established between $\sigma_{a.h}/\sigma_{a.s}$ and $N_b/N_{l.s}$, where N_b - bicyclic loading fatigue life and $N_{l.s}$ - fatigue life corresponding to the summary amplitude $\sigma_{a.s}$. The usage of $\sigma_{a.h}/\sigma_{a.s}$ ratio excludes the possibility of obtaining a linear connection between bicyclic loading parameters and fatigue life N_b since at linear change of $\sigma_{a.l}$ and $\sigma_{a.h}$ amplitudes the ratio $\sigma_{a.h}/\sigma_{a.s}$ varies non-linearly. As will be shown later, it is also expedient to evaluate the relative fatigue life by N_b/N_l ratio, and not $N_b/N_{l.s}$ i.e. to determine the effect of high cyclic component on the decrease of initial fatigue life N_l, corresponding to loading with $\sigma_{a.l}$ amplitude and not to the conditional fatigue life $N_{l.s}$ at hypothetical amplitude $\sigma_{a.s}$.

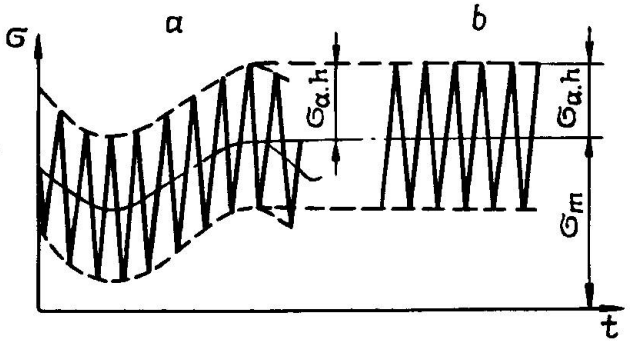

Fig.4. Loadings at pure bending compared in the work [16].

The advantages of using these ratios are shown in the investigation [14]. Fig.5. in the coordinates $\sigma_{a.h}/\sigma_{a.l}$, $lg(N_l/N_b)$ shows the results of all tests made by different authors with an average range of frequency ratio

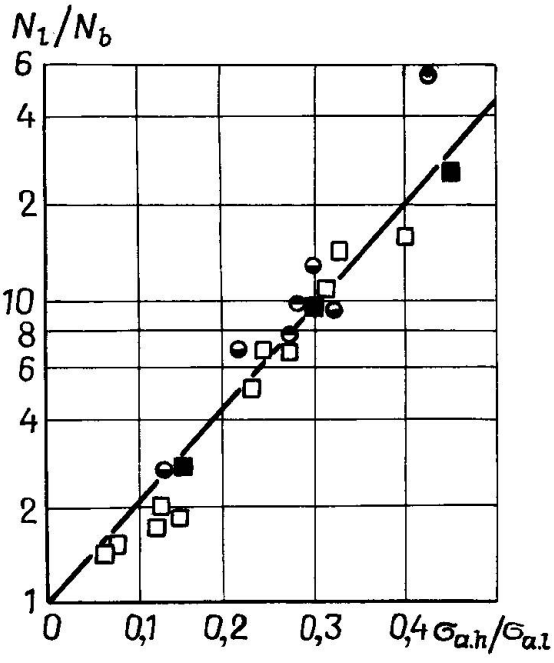

Fig.5. The generalization of testing results at two-frequency loading: □ - D16AT alloy, tension [9], ■ - D16T alloy, tension [6], ● - 0X12H steel, bending [4], ◒ - 45 steel, bending [4].

(mainly f_h/f_l =100...600), which could be converted to the given system. There is an agreement between the test results, despite the fact that the specimens differed in shape and sizes and were fabricated of different materials. In the given coordinate system a linear dependence was observed in a rather wide range between $\sigma_{a.h}/\sigma_{a.l}$ and N_l/N_b .

If we proceed from the existence of such a dependence, then the bicyclic loading frequency can be determined from the fatigue curves of onecyclic loading:

$$N_b = \frac{N_l}{\varkappa} \qquad (1)$$

where $\varkappa$ - factor dependent on $\sigma_{a.h}/\sigma_{a.l}$ amplitude ratio and f_h/f_l frequency ratio.

To confirm the invariance of $\varkappa$ factor at the change of the main factors, affecting the fatigue strength of materials and joints, and also to obtain an appropriate expression for its determination, the large-scale specimens (Fig.6) were tested at one- and bicyclic loading at various stresses - from the level slightly above the endurance limit up to the yield strength. Here, the $\sigma_{a.h}/\sigma_{a.l}$ ratio varies from 0.05 to 0.9.

155x20 mm section flat specimens (Fig.6a) were made of low-carbon steel (σ_T =300 MPa, σ_B =510 MPa) and 12X18H10T chrome-nickel steel (σ_T =350 MPa, σ_B =650 MPa). The concave recesses in the sides created in various samples a stress concentration α_σ , equal to 1.5; 2.5 and 3.5. Specimens of high-strength steel (σ_T =1070 MPa, σ_B = 1120 MPa) had a 80x18 mm section and a stress raiser in the form of a whole in the thinned part of the plate (Fig. 1,c). Taking into account a possible effect of residual stresses [17] on the fatigue strength of welded structures, the role of this factor in $\varkappa$ change was evaluated on specimens with beads (Fig.1,b), and on an actual joint (Fig.1,d). In the stress raiser zone the beads created initial residual stresses close to the base metal yield strength. The tests were performed both at axial loading and at bending. As for the low-cyclic loading, the tests were performed at a symmetrical, zero-to-tension and asymmetrical cycles (r= +0.5). To eliminate the errors associated with a possible effect of frequencies at one- and bicyclic loading, f_l frefuency in a multicycle region did not exceed 20 min^{-1} . f_h frequency was 300 min^{-1} under axial loading and 1800 min^{-1} at bending. The required ratio f_h/f_l with 10^2-5.10^3 range was ensured by varying f_l . An initial stage of crack development was used as a fatigue testing completion criterium. The testing was stopped when crack depth reached 2-3 mm. Part of the specimens were

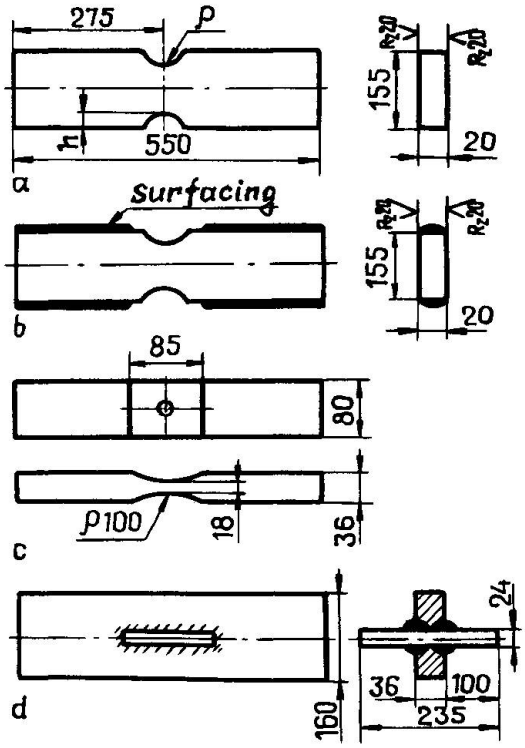

Fig.6.Specimens for testing at one- and bicyclic loading.

tested till they completely broke down.

Each factor studied significantly affected the fatigue strength of samples at one- and bicyclic loading. However, the studies performed have proved that $\varkappa$ coefficient remains invariant to the changes associated with the degree of stress concentration, residual stresses, stress ratio, type and level of loading, temperature and fatigue testing completion criterium. In this case all the relationships between $lg\,\varkappa$ and $\sigma_{a.h}/\sigma_{a.l}$ are of a stable linear type. The main dependences are shown in Fig. 7. At the same time, the change of $\varkappa$ is drastically affected by the amplitude (Fig.7) and frequency (Fig.8) ratios. With the increase of these ratios $\varkappa$ becomes considerably greater. These two factors mostly determine $\varkappa$ factor value. It is to a lesser degree that $\varkappa$ is sensitive to steel properties (Fig.8,b). With the change of frequency ratios and strength properties of material a linear relationship is maintained between $lg\,\varkappa$ and $\sigma_{a.h}/\sigma_{a.l}$

The established dependences give the following expression for determining the factor of bicyclic loading fatigue life decrease.

$$\varkappa = \left(\frac{f_h}{f_l}\right)^{\vartheta \frac{\sigma_{a.h}}{\sigma_{a.l}}} \qquad (2)$$

where ϑ - factor, reflecting the material effect. It may change within 1.3...1.8 for steels. $\varkappa$ value may also be determined according to the nomogram, given in Fig.9.

When $\varkappa$ factor in the initial equation (1) is replaced by its value (2), we obtain a final formula for bicyclic loading fatigue life determination:

$$N_b = \frac{N_l}{\varkappa} = \frac{N_l}{\left(\frac{f_h}{f_l}\right)^{\vartheta \frac{\sigma_{a.h}}{\sigma_{a.l}}}} = N_l \left(\frac{f_l}{f_b}\right)^{\vartheta \frac{\sigma_{a.h}}{\sigma_{a.l}}} \qquad (3)$$

In this formula, N_l - is the fatigue life of material, joint, element, etc., which, in the assigned conditions corresponds to low cyclic loading with $\sigma_{a.l}$ amplitude. According to formula (3) the bicyclic loading fatigue life N_b is always less than N_l. At the same time, as noted above

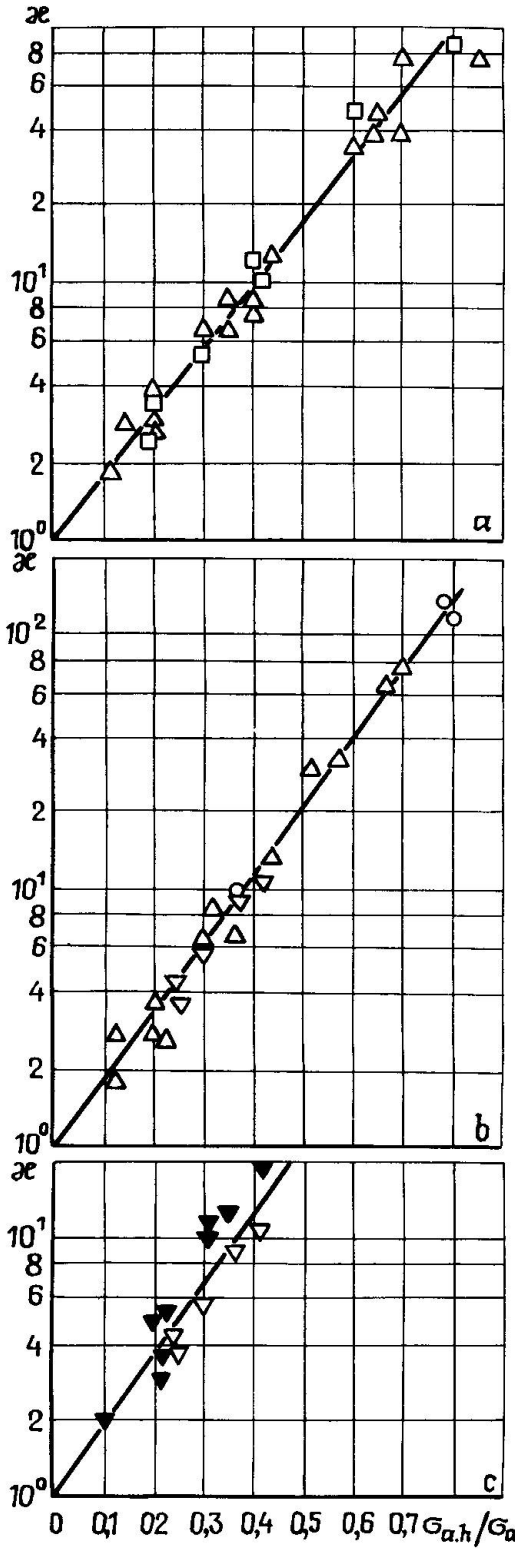

Fig.7.Coefficient $\varkappa$ invariance to the change of: a)stress concentration: □ - α_σ=1.5; △ - α_σ=2.5; △ - α_σ=3.5; b)cycle asymmetry: ○ - r=0.5; ▽ - r =0; ▽ - r =-1; c)residual stressed state: ▽ - Ω =0; ▽ - Ω = σ_T.

at small frequency ratios an increase of bicyclic loading fatigue life was observed in certain investigations. In this connection it becomes necessary to determine the boundaries of formula (3) applicability. In case of small values of f_h/f_l the change of $\sigma_{a.s}$ amplitude depends not only on $\sigma_{a.h}/\sigma_{a.l}$, but also on phase shift between the components. In a certain interval of φ phase shift, the $\sigma_{a.s}$ summary amplitude can decrease to values lower than $\sigma_{a.l}$ [14]. If we take into consideration the fact that $\sigma_{a.h}/\sigma_{a.l} < 0.3$ and the resulting load cycle form $\sigma_{a.s}$ is distorted without the appearance of additional extremums, then the increase of fatigue life in the given conditions under the effect of bicyclic loading is readily explained.

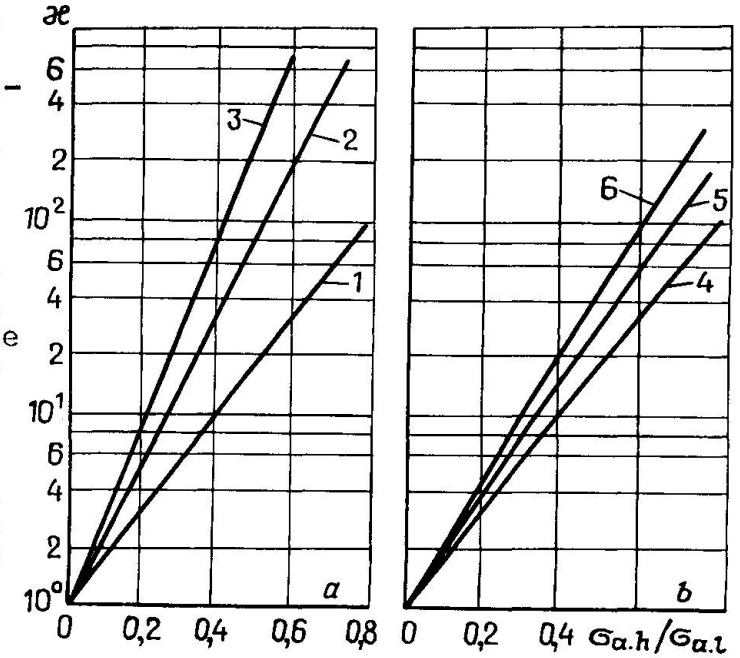

Fig.8.Relationship between æ and frequency ratio(a) and steel type(b): 1- $f_h/f_l = 10^2$; 2- $f_h/f_l = 10^3$; 3- $f_h/f_l = 5.10^3$; 4-low-carbon steel; 5-chrome-nickel steel; 6-high-strength steel.

When $\sigma_{a.h}/\sigma_{a.l} < 0.5$ the summary amplitude depending upon φ angle, can be both lower and higher than the low-frequency component amplitude. Accordingly, N_b can be increased or decreased compared to N_l. At $\sigma_{a.h}/\sigma_{a.l} > 0.5$ the summary amplitude is higher than the low-cyclic component amplitude. The fatigue life will decrease under the effect of this factor, and, possibly, due to the appearance of additional extremums.

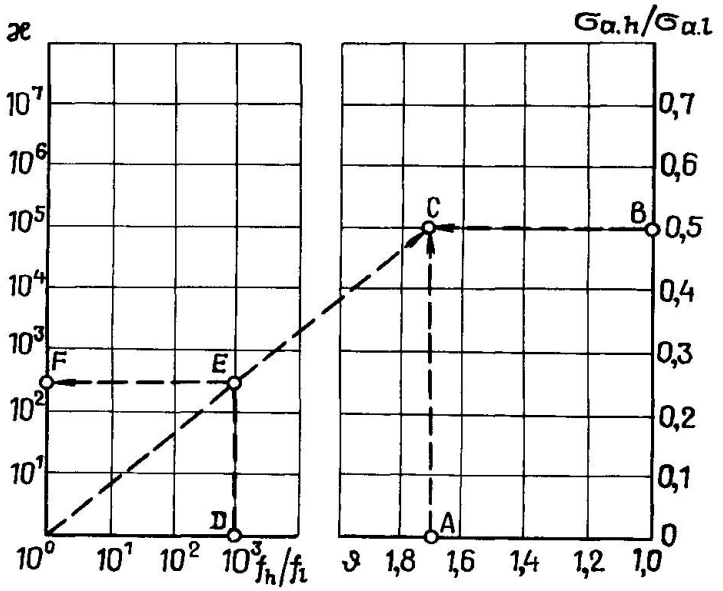

Fig.9.Nomogram for æ determination.

The situation becomes different at $f_h/f_l > 10$. Irrespective of amplitudes and initial phases of loading components $\sigma_{a.s} > \sigma_{a.l}$. The analysis performed showed that $\sigma_{a.s}$ deviation from the maximum possible value at a synphase summation of harmonic loads did not exceed 5% within the whole range of amplitude ratios. The damage accumulation is also favoured by individual stress cycles, changing with f_h frequency. In such conditions, N_b will always be much lower than N_l. Thus, at $f_h/f_l \geq 10$, the formula (3) can be used without restrictions. When $f_h/f_l < 10$, it is valid for a fixed value of phase shift, meeting maximum value of

resulting amplitude $\sigma_{a.s}$ .For other values of phase shift the formula (3) can give only under-estimated values of N_b .

The validity of formula (3) was also verified by comparing the experimental data obtained earlier by other authors with the calculated data. In most cases the ratio between calculated data and the experimental ones was close to a unit, while individual deviations lay within the scattering range of 0.75-1.5.

It appears that there is every reason to believe, that the proposed method of bicyclic loading fatigue life estimation is quite suitable for engineering calculations and can be used within a wide range of amplitude and frequency ratio change.

REFERENCES

1.SERGIEVSKY,A.:Fatigue strength of railway bridge spans in service , Transzheldorizdat, 1963.
2.GÄSSNER,E., SVENSON O.: Einfluss von Störschwingungen auf die Ermüdungsfestigkeit, Stahl und Eisen, 1965, N5.
3.GUSHCHA,O., LEBEDEV,V., ROYTSTEIN,M.:Masts with guy-ropes in service, Promyshlennoje Stroitelstvo, 1970, N4.
4.ZAITSEV,G., FARADZHOV,R.M.: Strength of steels used for hydraulic turbines, NIIinformtyazhmash, 1970.
5.BUGLOV,E., FILATOV,M., KOLIKOV,E.: Material resistance at bicyclic loading, Problemi prochnosti, 1973, N5.
6.DVORKIN,Ya.: The effect of bicyclic loading parameters on D16T alloy samples fatigue life, Zavodskaya laboratorija, 1973, N4.
7.BUGLOV,E., KOLIKOV,E., FILATOV,M.: Studies of fatigue at biharmonic loading, Problems of strength, 1970, N1.
8.ZAITSEV,G., ARONSON, A.: Fatigue strength of hydraulic turbines, Mashinostrojenije, 1975.
9.BOGDANOV,B.: Strength and fatigue life of aircraft structures, Kiev, CVF, 1965, p.124-127.
10.STARKEY,W. and MARCO,S.: Effects of complex stress-time cycles on the fatigue properties of metals, Transactions of the ASME, 1957, vol.79, N6, p.1329-1336.
11.REICHER,V. A hypothesis of spectral summation and its application to fatigue strength determination at random loads.-In:Problems of strength in structural mechanics, 1968, p.267-274.
12.AOKI,J., HATSUKO,K., NAKAMURA,H., KUNIO,T.: The study on the fatigue strength by varying the stress amplitude with the superimposed the based sinusoidal stress wave, Transactions of JSME, 1965, vol.31, N222.
13.YAMADA,T., and KITAGAWA,S.:Investigation of fatigue strength of metals under actual service loads (with two superimposed cyclic loadings), Bulletin of JSME, 1967, N38, p.245-252.
14.TRUFIAKOV,V., KOVALCHUK,V.: Change of bicyclic loading fatigue strength, In:Strength of welded joints and structures, 1974.
15.BUGLOV,E.: Low-cyclic fatigue and some properties of structural material hysteresis curve at bicyclic loading, In: Strength of materials and structures, Naukova dumka, 1975.
16.NISHIHARA,T., and YAMADA,T.: Fatigue life of metals under varying repeated stresses, Proceedings of Sixth Japan National Congress for Applied Mechanics, 1956.
17.TRUFIAKOV,V.: Welded joint fatigue, Kiev, Naukova Dumka, 1973.

Fatigue Threshold Concept Applied to Metal Structures

Concept de la limite de propagation des fissures due à la fatigue appliqué aux structures métalliques

Konzept des Grenzwertes für Ermüdungsrisswachstum angewendet auf Stahlkonstruktionen

A.F. BLOM
Research Engineer
Aeronautical Research Laboratory
Bromma, Sweden

SUMMARY
The concept of the fatigue threshold stress intensity factor as a design criterion is presented. This concept is of particular importance for structures having to sustain very many load cycles. The experimental evaluation and the influence of various parameters of this factor are examined.

RESUME
L'application du concept de la limite inférieure à la propagation des fissures par la différence du facteur d'intensité de contrainte comme critère de dimensionnement est présenté. Ce concept est d'une importance particulière pour les structures subissant de très grands nombres de cycles de charges. L'évaluation expérimentale de ce facteur et l'influence de divers paramètres sur ce facteur sont examinées.

ZUSAMMENFASSUNG
Die Anwendung des unteren Grenzwertes für das stabile Risswachstum der Spannungsintensitätsdifferenz als Dimensionierungsgrundlage wird vorgestellt. Dieses Konzept ist für Bauteile, welche sehr vielen Lastwechsel unterworfen sind, von grosser Bedeutung. Die experimentelle Bestimmung und der Einfluss verschiedener Parameter auf diesen Grenzwert wird untersucht.

1. INTRODUCTION

Traditionally, metal structures that must sustain a very large number of load cycles N have been designed from ordinary SN-curves (Wöhler-diagrams) where it for most metals appear to exist a fatigue limit $\Delta\sigma_e$, see Fig. 1. To avoid fatigue failures of such structures they have been designed so that the applied stress range S always should be below the fatigue limit.

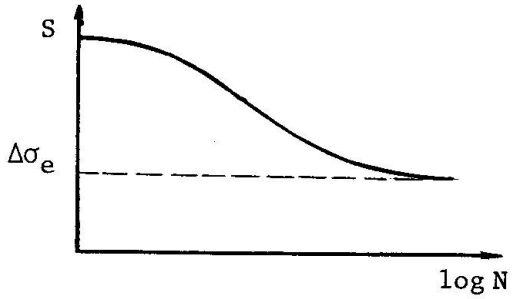

Fig. 1 SN-diagram

The experimental procedure for determining the fatigue limit of a material is very tedious and will be quite expensive if it is properly accounted for all those variables that influence the value of the fatigue limit.

This paper presents an alternative approach to the "fatigue limit" problem. This approach which is based on fracture mechanics was originally developed in the aircraft industry, but has recently come to an extensive utilization in the design also of structures such as wind turbine blades, diesel engines, steam turbines and electric generators [1].

The design concept to be discussed here is the fatigue threshold concept which simply states that for a given load there exist cracks of a certain length that will not propagate. Inversely, we can for a given crack length calculate which load magnitude that will not cause crack growth [2].

2. FRACTURE MECHANICS AND FATIGUE

Various empirical crack-growth laws have been proposed over the past decades. Most of the early expressions were of the form given in Eq. (1). However, no real success with the difficult task of correlating the crack-growth rate da/dN to applied stress, crack length etc. was obtained before 1961 when Paris [3] proposed that the stress intensity range $\Delta K = K_{max} - K_{min}$ should be incorporated in a crack propagation law as shown in Eq. (2).

$$\frac{da}{dN} = C\,\sigma^m\,a^n \qquad (1)$$

$$\frac{da}{dN} = C\,(\Delta K)^m \qquad (2)$$

Paris came to this conclusion based on the results from experiments with aluminium. He also gave the value 4 of the exponent m for his test results. Further experiments have shown that for most metals the value of m varies between 2.3 and 6.7 [4]. The very large number of experiments that have been performed since Paris proposed his power relationship clearly indicate that Eq. (2) is not entirely valid over the whole range of ΔK. This means that a log-log plot of da/dN against ΔK is not linear but sigmoidal, see Fig. 2. In this figure we can distinguish between three distinct regions. At low ΔK the fatigue crack growth rate decreases progressively faster until the threshold, ΔK_{th}, for a non-propagating crack is reached. This region is our major concern and will be further dealt with in the following chapters. Next region is composed of a straight line and constitutes the part of the curve where Eq. (2) can be utilized. A third region exists at high ΔK where the slope of the curve increases rapidly as the maximum stress intensity approaches the fracture thoughness K_c.

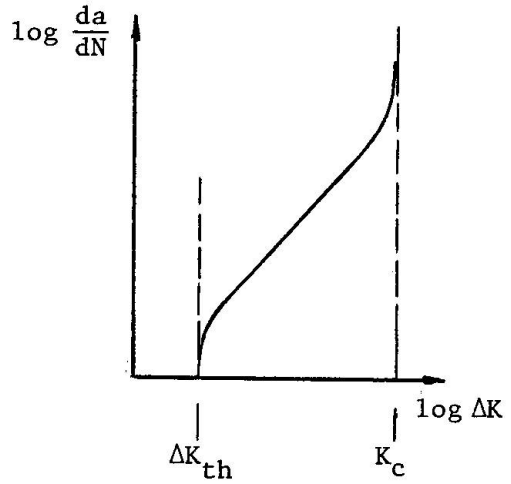

Fig. 2 Schematic shape of fatigue crack growth versus stress intensity variations.

3. THE THRESHOLD STRESS INTENSITY FACTOR ΔK_{th}

3.1 Utilization of ΔK_{th}

In the preceding chapter it was shown that the fatigue crack growth rate is a function of ΔK, the variation in stress intensity. Below a certain threshold value ΔK_{th} the fatigue crack growth rate equalizes zero as indicated in Fig. 2.

The existence of a threshold value means that specimens subjected to certain loads will not fail in fatigue if all existing flaws are smaller than a critical crack length. The reversed situation may also be of interest, when the designer knows the sizes of the cracks from measurements he will be able to calculate which stresses are allowed if fatigue should be avoided.

The utilization of threshold values is particularly important for components which are subjected to very large numbers of cycles during service, e.g. engine parts such as crankshafts.

The threshold stress intensity factor is, however, not a genuine material constant but is dependent on some parameters such as R-value, temperature and environment. The influence of these parameters and some others will be scrutinized in the next chapter. This dependence on other parameters must be born in mind when the experimental evaluation of ΔK_{th} is performed so that the right service conditions are imposed. Caution also to an uncritical adoption of results presented in the literature: how were these values measured, under which conditions and is the metallurgical composition exactly the same for the tested material as for the actual one?

Another application of the threshold value concept is when a comparable judgement about the fatigue qualities of several materials should be performed. This can be the case when, for instance, an old material should be replaced by a new one.

3.2 Some numerical values of ΔK_{th}

Some values of ΔK_{th} are given in Table 1 merely to give an indication of their magnitude and to compare various materials. Note that the threshold stress intensity factor also is meaningful for polymers. All results in Table 1 were given in [5].

Material	Conditions	R	ΔK_{th} [MPa $\sqrt{m}$]
mild steel SIS 1450-01	air	0.1	12.0
		0.5	7.1
		0.9	4.4
mild steel SIS 1450-01	salt water	0.1	7.0
		0.5	3.6
		0.9	2.5
A 533 B	base material	0.25	7.1
	— " —	0.5	5.5
	HAZ	0.25	6.8
	HAZ	0.5	5.2
Al 5083		0.1	2.0
Inconel		0.1	6.5
PVC		0.1	0.68
		0.5	0.32
		0.75	0.29

Table 1 Some threshold values ΔK_{th} for various materials [5]

3.3 Definition of the threshold value

Before going into more detailed discussions in the following chapters, let us ponder about the definition of the threshold value ΔK_{th}. From Fig. 2 it follows that the existence of ΔK_{th} requires the crack growth rate to equalize zero. This would be the case when for an infinite number of cycles no crack growth occurs. However, to perform experiments with an infinite number of cycles would be not only tedious and discouraging but also quite impractical. Therefore it is fortunate that the threshold value is associated with a fatigue crack growth rate of around one lattice spacing per cycle. This value which corresponds to about 4×10^{-7} mm per cycle is the minimum crack growth rate possible on physical grounds, [6]. However, in a corrosive environment

lower average rates could be observed, due to that the crack growth in those cases only takes place on part of the crack front during each cycle, [6].

For practical purposes it seems appropriate to utilize a crack growth rate of the magnitude 10^{-7} - 10^{-6} mm per cycle as a definition of a valid threshold value. Recently though many workers including the present author perform tests down to a maximum crack growth of 10^{-8} mm to ensure that no further crack growth occurs.

4. PARAMETERS INFLUENCING ΔK_{th}

As was previously stated the threshold value ΔK_{th} is not a genuine independent material constant but is influenced by various parameters. The forthcoming chapter will deal with some of the more prominent ones.

4.1 Crack size

Most experiments that have been performed to evaluate thresholds ΔK_{th} or fatigue crack growth data are based upon linear elastic fracture mechanics. However, in the vicinity of a very small crack the plastic zone size is not neglectable compared to the crack length and we may thus expect some peculiarities to occur if we still use the concept of stress intensity factors. Short cracks generally exhibit higher fatigue crack growth rates and lower threshold stress intensities than do longer cracks [2, 7]. There is much confusion on which crack size that should be considered short. It appears that this is dependent on the actual material as indicated in Fig. 3 [8] where ΔK_{th} is plotted versus the crack length for three different materials at R = 0. In the pertinent literature crack sizes below 0.5 mm are often referred to as short cracks [2].

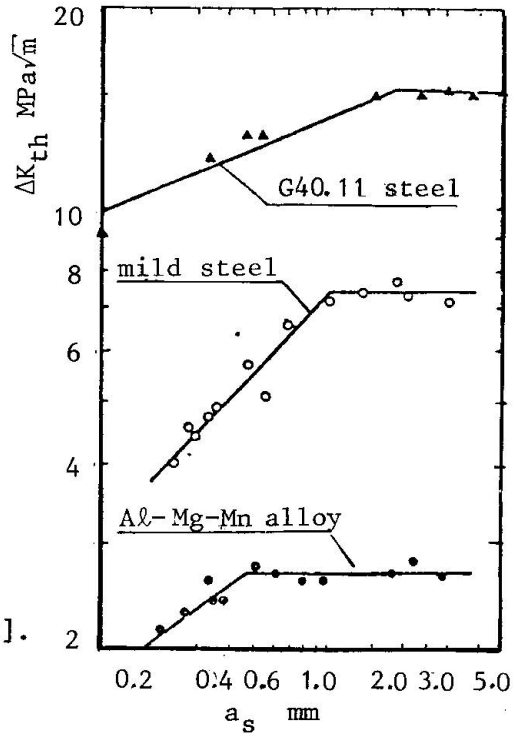

Fig. 3 Dependence of ΔK_{th} on crack length [8]

An approach to account for the behaviour of short cracks was proposed by El Haddad [9] where a constant length ℓ_o, see Eq. (3) is added to the physical crack size. The term ℓ_o which is assumed to be a material constant can be determined from the ordinary threshold stress intensity factor ΔK_{th} and fatigue limit $\Delta\sigma_e$ as

$$\ell_o = \frac{1}{\pi}\left(\frac{\Delta K_{th}}{\Delta\sigma_e}\right)^2 \qquad (3)$$

In the following we will restrict ourselves to situations with "normal" crack sizes when discussing how different parameters influence the threshold stress intensity factor.

4.2 Loading modes

Almost all performed experimental evaluations of ΔK_{th} have been restricted to pure mode I loading. Recently, however, interest has been shown in the establishment of threshold stress intensity factors also for other modes, particularly mode II and mixed-modes [10, 11]. It was found that the mode II and the mixed mode I and II thresholds for mild steel can be lower than the pure mode I threshold [10, 11]. Experimental results from [10] are shown in Fig. 4 together with a lower bound derived in [11]. It was proposed in [10] that the reason for the very low values shown in Fig. 4 might partially be due to that crack initiation

rather than crack extension was monitored. In the following only pure mode I thresholds are to be discussed. For more information on other loading modes it is referred to [2, 10 and 11].

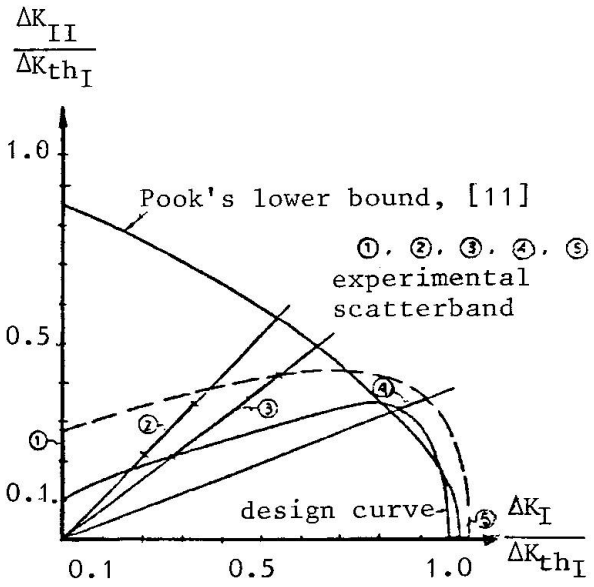

Fig. 4 Mixed mode thresholds for R = 0.1 [10]

4.3 R-dependence

It is nowadays well established that the stress ratio $R = \sigma_{min}/\sigma_{max}$ greatly influences both the fatigue crack growth and the threshold stress intensity factor. The general conclusion from studies on the effect of stress ratio R on the threshold value ΔK_{th} is that an increasing R tends to decrease the threshold value. This behaviour is confirmed for various materials by a great number of authors, e.g. [2, 12].

There is, however, some confusion about the varying influence of R on different materials and also how environmental conditions influence the R-dependence. One might ponder about why the stress ratio influences the rate of fatigue crack growth. At very high propagation rates when K_c, the fracture toughness, is approached, the influence is attributed to different fracture mechanisms such as integranular cracking, cleavage and void coalescence. In the intermediate region relatively little effect is observed. This results in a schematic curve as in Fig. 5 when the influence of R is considered. The effect of R on region I in Fig. 5 can, however, not be clarified by means of different fracture mechanisms as accounted for above for the case of very high crack propagation rates.

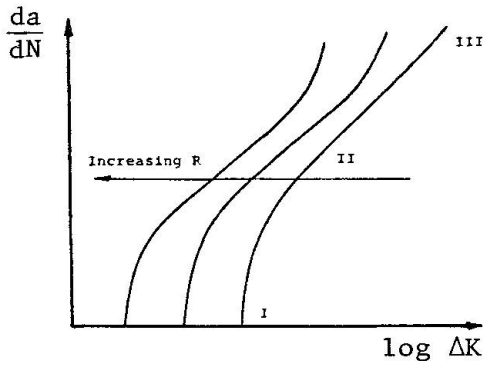

Fig. 5 R-dependence on fatigue crack-growth rate
I Threshold region
II Intermediate region
III Fracture toughness region

Some different theories have been proposed to account for R effects on the threshold value ΔK_{th}.

A crack closure concept originally proposed by Elber is often utilized. Elber [13] stated that, as a result of permanent tensile plastic deformation left in the wake of a propagating fatigue crack, the cracks are partially closed, even though loading may be tension-tension. Crack extension takes place only during those portions of the cycle where the crack is open. It follows that for a given maximum load, the crack will remain open longer during each cycle for higher values of the mean load, i.e. higher minimum loads and thus higher R-values. This will explain the trend shown in Fig. 5.

Crack closure can, however, not entirely explain the effect of R on the threshold behaviour. It is shown, e.g. in [14], that the threshold value in vacuum is independent of the stress ratio R. This independence of ΔK_{th} on R should according to [15] indicate that there is no crack closure in vacuum. Recent work, however, closely shows that crack closure indeed occurs in vacuum. In [16] it is stated that crack closure is more pronounced in vacuum than in air. Thus, it is obvious that crack closure alone cannot adequately be used to explain the effects of stress ratio R.

Several researchers, e.g. [14, 17 and 18], have proposed that the R-dependence could be explained by environmental effects. In [17] it is stated that environmental effects due to hydrogen embrittlement explains the stress-ratio effect while crack closure is assumed to be of only secondary importance. In [14] a two-component mechanism is introduced. This two-fold mechanism is proposed to take account for environmental actions such as intergranular corrosion. One of the two components involves the creation of damage ahead of the crack tip in the form of integranular facets and the other component can be viewed as a linking of these facets to the main crack by a tensile tearing process. Ritchie, [18], agrees with Beevers et al, [14] about the R-dependence beeing due primarily to environmental effects. However, he claims that the above mentioned mechanism does not correctly describe the affection by environment.

The most recent opinions [1] seem to be that both crack closure and environmental effects should be accounted for, e.g. [19, 20], when the R-dependence on ΔK_{th} is discussed.

4.4 Thickness

The threshold stress intensity factor ΔK_{th} is generally not supposed to be affected by the thickness of the test specimen. Radon [21] has, however, recently found an influence of thickness at low stress ratios. It was found that ΔK_{th} decreased with thickness for a low alloy steel. It remains to be seen whether this will be shown also for other materials.

4.5 Frequency

At threshold conditions it seems that the influence of frequency is almost negligible [2]. Slight variations in the threshold value due to influence of the frequency can, however, be found in the literature. In [15] a lowering of the threshold value with increasing frequency from 342 to 1000 Hz was found. It was suggested that this behaviour might be due to a localized heating of the crack tip. In [22] the opposite behaviour was observed, i.e. an increased threshold value with increasing frequency from 30 to 1000 Hz. It therefore seems that no general statement can be done about the influence on ΔK_{th} of the frequency. When exposure to various detrimental environments occurs the situation is entirely different. Increasing frequencies then generally yield higher threshold values due to less time for environmental interaction. This is especially noticeable at very low frequencies.

4.6 Temperature and environment

Results on the effect of temperature and environment on ΔK_{th} are unfortunately somewhat contradictory why it is difficult to draw any general conclusions. Recent work by Ritchie [20] and Stewart [23] indicate that a concept of oxide-induced crack closure satisfactorily explains the influence of environment on ΔK_{th}. It is found that ΔK_{th} often is lower in dry environment, hydrogen or air, than in moist air and water at low stress ratios. This is explained [20, 23] with corrosion/fretting debris building up at the crack tip and thus reducing the effective cyclic stress intensity range.

The effect of temperature on ΔK_{th} is quite unclear and apparently varies for different materials. As example it was found in [24] that the threshold value for a mild steel plate was lower and higher, respectively, at 200°C and 360°C that at 20°C. For weld metal [24] ΔK_{th} was similarly shown to be lower between 20°C and 200°C, but higher at 360°C, than at 20°C.

It is concluded that all experimental evaluations of ΔK_{th} should necessarily be performed in an environment and at temperatures closely simulating the operational conditions.

4.7 Microstructure

Mostly it appears that the threshold value increases with increasing grain size [19, 25-27]. This has been found for many metals such as aluminium, various steels and titanium. Some materials though, for instance copper [28], do not show any variation in ΔK_{th} with grain size changes. Metallographic observations in [25] showed that at threshold the crack often arrests at grain boundaries and inclusions which may clarify the relatively large scatter in test results for materials with coarse grain sizes and inclusions. The structure sensitivity of ΔK_{th} is primarily considered to be associated with the closure process [19, 26]. The closure level is highest in the threshold region due to changes in the transgranular crack mode from the opening mode at higher ΔK-values to a combination of shear mode and opening mode.

It has been found that the threshold stress intensity factor is a function of yield strength and Young's modulus [19, 26]. A nearly linear plot of ΔK_{th} versus the square root of $E\sigma_y$ for several metals is considered [19] to be indicative of ΔK_{th} being related to a critical crack tip opening displacement.

4.8 Amplitude

All discussions so far have been presented assuming a constant load amplitude. It is, however, well known that both single overloads and random loading greatly affect the threshold value. When a specimen is subjected to overloads a plastic zone forms at the crack tip. This plastic zone can be of sufficient magnitude to prevent further crack growth which results in that a too high threshold value is registered.

To account for the load history, Klesnil and Lukáš [29] proposed the following relationship

$$\Delta K_{th} = \Delta K_{th,0} \left(\frac{\Delta K_{Ip}}{\Delta K_{th,0}} \right)^{\alpha} \tag{4}$$

where $\Delta K_{th,0}$ is the threshold value without prior loading, ΔK_{Ip} is the just preceding stress intensity factor and α is an exponent strongly dependent on the tensile strength of the steel.

In [30] the fatigue strength of cracked mild steel plate specimens was studied. It was found that a narrow-band random loading produced significantly greater fatigue strength than did estimates based on linear summation of constant amplitude fatigue crack growth data. More accurate results were obtained when the effect of prior loading on the threshold value, utilizing Eq. (4), was accounted for.

Experiments performed on a commercial nickel-base and titanium-base alloy, [22], disclosed various interesting effects of single and multiple cycle overloads on the threshold value. It was found that the overload modified threshold value, ΔK^*_{th}, increased exponentially with the magnitude of the prior overload. Further, it was shown that the effect of relative overload on relative threshold value is independent of the stress ratio R, but that overloads produce much larger absolute magnitude increases in the threshold value at low R than at high R. Also, it was shown that the number of overloads, overload rate, cycle shape, temperature and frequency can affect the threshold value but that these variables are much less important than the magnitude of the overload.

5. EXPERIMENTAL METHODS

It is obvious from the preceding chapter that all experimental evaluations of ΔK_{th} should account for such parameters as temperature, environment, stress ratio etc. simulating the operational conditions as closely as possible. Also, in order to avoid load history interactions, the load must be decreased very carefully.

Concerning test equipment and test specimens most workers use servo-hydraulic testing machines and standardized fracture mechanics specimens such as the Center-Cracked-Tension and the Compact Tension specimen. It has recently been proposed that a modified wider Compact Tension specimen would be more suitable [5].

The conventional test method is the load shedding technique where the load is manually decreased at selected crack length intervals. This method is thoroughly investigated by Bucci and his co-workers, [31, 32], who have developed a tentative ASTM standard based on their results. Stringent requirements are proposed for the load shedding procedure to avoid load history effects. It is stated that the reduction in P_{max} for adjacent load steps must be lower than 10 per cent of the previous P_{max} and further must the crack extension within each adjustment of the maximum load be at least 0.5 mm. This method has, however, some drawbacks, such as being rather time consuming with respect both to test equipment and personell. This is due to that the crack length has to be monitored during the test and that the load must be reduced very slowly in order to eliminate any load history effects from prior overloads. Further there will be cusps on the ΔK versus time curve which are not very appealing from a physical point of view.

These disadvantages are substantially reduced when the load shedding is performed in a continous manner utilizing a computer controlled test system [33, 34]. In Ref. [33] a stress intensity gradient technique is used and in Ref. [34] a technique is described which utilizes crack opening displacement as controlling parameter. The main objection against these methods is the relatively high cost of computerized test systems and even if such systems are available they ought to be saved for more sophisticated tests such as spectrum or random fatigue testing.

A simple method to measure ΔK_{th} was proposed by Jerram and Priddle, [35]. Their method which operates automatically seems to be rather cost effective as computer control is avoided. One serious disadvantage is, however, the inability of the method to keep the load ratio, R, constant throughout the test. As it is well established that R significantly influences the threshold stress intensity ΔK_{th}, the usefulness of the method seems rather limited.

If it would be possible to combine the advantage with a control unit as in [35], with the possibility of keeping R constant throughout the test, as in [33, 34], then a quite efficient method would be available. How this is accomplished is described in [5].

6. APPLICATIONS

It is evident from many recent papers that the threshold stress intensity factor ΔK_{th} is a parameter of great technical importance. Applications were ΔK_{th} has been used include different structural components such as: boiler feed pump shafts [36], low pressure turbine rotor shafts [36], turbo generator rotor [36], nuclear reactor gas circuitry [37], pipes [38], cylinder cover of diesel engines [39], engine shafts [39], connecting rods [39] and turbine blades [40].

7 CONCLUSIONS

The fatigue threshold concept as a design criterion has been discussed. This concept which simply states that the applied stress intensity range ΔK should be below the threshold stress intensity factor ΔK_{th} is of particular importance for structures sustaining very many load cycles, i.e. where no crack growth can be allowed.

It has been discussed how the threshold stress intensity factor is experminentally evaluated. The influence of various parameters was scrutinized and it is concluded that all experiments should necessarily simulate the operational conditions as closely as possible.

8. REFERENCES

1 BÄCKLUND, J., BLOM, A.F. and BEEVERS, C.J.: Fatigue Thresholds, Proceedings from the first International Conference on Fatigue Thresholds, Stockholm. Sweden, 1-3 June 1981, Vol. 1 and 2, Engineering Materials Advisory Services Ltd., United Kingdom 1981/82.

2 BLOM, A.F.: The Threshold Stress Intensity Factor in Fatigue, Report No. LiTH-IKP-S-136, Linköping University, Institute of Technology, Dept. of Mech. Eng., 1980, Also ICAF Doc. 1180, International Committee on Aeronautical Fatigue.

3 PARIS, P.C., GOMEZ, M.P. and ANDERSON, W.E.: A Rational Analytic Theory of Fatigue, The Trend in Engineering, Vol. 13, 1961, pp. 9-14.

4 NELSON, D.V.: Review of Fatigue-Crack-Growth Prediction Methods, Experimental Mechanics, Vol. 17, 1977, pp. 41-49.

5 BLOM, A.F., BÄCKLUND, J. and JILKÉN, L.: Specimens and Test Equipment for Economical Fatigue Threshold Testing, in Ref. [1].

6 POOK, L.P.: Analysis and Application of Fatigue Crack Growth Data, Journal of Strain Analysis, Vol. 10, No. 4, 1975, pp. 242-250.

7 SCHIJVE, J.: Differences Between the Growth of Small and Large Fatigue Cracks. The Relation to Threshold K-values, in Ref. [1].

8 ROMANIV, O.N., SIMINKOVICH, V.N. and TKACH, A.N.: Near-Threshold Short Fatigue Crack Growth, in Ref. [1].

9 El HADDAD, M.H., TOPPER, T.H. and SMITH, K.N.: Prediction of Non-Propagating Cracks, Engineering Fracture Mechanics, Vol. 11, 1979, pp. 573-584.

10 BLOM, A.F., BÄCKLUND, J. and JILKÉN, L.: An Engineering Approach to Mixed Mode Thresholds, in Ref. [1].

11 POOK, L.P.: Mixed Mode Threshold Behaviour of Mild Steel, in Ref. [1].

12 PARIS, P.C. and HERMAN, L.: Twenty Years of Reflection on Questions Involving Fatigue Crack Growth, Part II - Some Observatons of Crack Closure, in Ref. [1].

13 ELBER, W.: The Significance of Crack Closure, ASTM STP 486, Damage Tolerance in Aircraft Structures, American Society for Testing and Materials, 1971, pp. 230-242.

14 COOKE, R.J., IRVING, P.E., BOOTH, G.S. and BEEVERS, C.J.: The Slow Fatigue Crack Growth and Threshold Behaviour of a Medium-Carbon Alloy Steel in Air and Vacuum, Engineering Fracture Mechanics, Vol. 7, 1975, pp. 69-77.

15 SCHMIDT, R.A. and PARIS, P.C.: Threshold for Fatigue Crack Propagation and the Effects of Load Ratio and Frequency, ASTM STP 536, Progress in Flaw Growth and Fracture, American Society for Testing and Materials, pp. 79-93.

16 LAFAIRE-FRENOT, M.C., PETIT, J. and GASC, C.: A Contribution to the Study of Fatigue Crack Closure in Vacuum, Fatigue of Engineering Materials and Structures, Vol. 1, 1979, pp. 431-438.

17 MUSUVA, J.K. and RADON, J.C.: The Effect of Stress Ratio and Frequency on Fatigue Crack Growth, Fatigue of Engineering Materials and Structures, Vol. 1, 1979, pp. 457-470.

18 RITCHIE, R.O.: Contribution on "Slow Fatigue Crack Growth and Threshold Behaviour of a Medium Carbon Steel in Air and Vacuum" by R.J. Cooke, P.E. Irving, G.S. Booth and C.J. Beevers, Engineering Fracture Mechanics, Vol. 7, 1975, pp. 187-189.

19 BEEVERS, C.J.: Some Aspects of the Influence of Microstructure and Environment on ΔK Thresholds, in Ref. [1].

20 RITCHIE, R.O.: Environmental Effects on Near-Threshold Fatigue Crack Propagation in Steels: A Re-Assessment, in Ref. [1].

21 RADON, J.C.: Fatigue Crack Growth in the Threshold Region, in Ref. [1].

22 HOPKINS, S.W., RAU, C.A., LEVERANT, G.R. and YUEN, A.: Effect of Various Programmed Overloads on the Threshold for High-Frequency Fatigue Crack Growth, ASTM STP 595, Fatigue Crack Growth Under Spectrum Loads, American Society for Testing and Materials, 1976.

23 FREEMAN, B.L., SMITH, P. and STEWART, A.T.: The Influence of Corrosion Debris on Crack Closure at Near-Threshold Fatigue Crack Growth Rates, in Ref. [1].
24 PRIDDLE, E.K.: The Threshold Stress Intensity Factor for Fatigue Crack Growth in Mild Steel Plate and Weld Metal: Some Effects of Temperature and Environment, in Ref. [1].
25 PRIDDLE, E.K.: The Influence of Grain Size on Threshold Stress Intensity for Fatigue Crack Growth in AISI 316 Stainless Steel, Scripta Metallurgica, Vol. 12, No. 1, 1978, pp. 49-56.
26 MINAKAWA, K. and McEVILY, A.J.: On Near-Threshold Fatigue Crack Growth in Steels and Aluminum Alloys, in Ref. [1].
27 GERBERICH, W.W. and MOODY, N.R.: A Review of Fatigue Fracture Topology Effects on Threshold and Growth Mechanisms, ASTM STP 675, Fatigue Mechanisms, Ed. J.T. Fong, American Society for Testing and Materials, 1979, pp. 292-341.
28 MULLNER, H., WEISS, B. and STICKLER, R.: The Effect of Microstructure on the Fatigue Threshold in Copper, in Ref. [1].
29 KLESNIL, M. and LUKÁŠ, P.: Influence of Strength and Stress History on Growth and Stabilisation of Fatigue Cracks, Engineering Fracture Mechanics, Vol. 4, 1972, pp. 77-92.
30 POOK, L.P. and GREENAN, A.F.: The Effect of Narrow-Band Random Loading on the High Cycle Fatigue Strength of Edge-Cracked Mild Steel Plates, International Journal of Fatigue, January 1979, pp. 17-22.
31 HUDAK, Jr. S.J., SAXENA, A., BUCCI, R.J. and MALCOLM, R.C.: Development of Standardized Methods of Testing and Analyzing Fatigue Crack Growth Rate Data, AFML TR-78-40, Air Force Materials Laboratory, 1978.
32 BUCCI, R.J.: Development of a Proposed Standard Practice for Near-Threshold Fatigue Crack Growth Rate Measurement, ALCOA Report No. 57-79-14, Aluminum Company of America, 1979.
33 SAXENA, A., HUDAK, Jr. S.J., DONALD, J.K. and SCHMIDT, D.W.: Computer-Controlled Decreasing Stress Intensity Technique for Low Rate Fatigue Crack Growth Testing, Journal of Testing and Evaluation, Vol. 6, No. 3, 1978, pp. 167-174.
34 KAISAND, L.R. and LeFORT, P.: Digital Computer Controlled Threshold Stress Intensity Factor Fatigue Testing, in ASTM STP 613, Use of computers in the fatigue laboratory, Eds. H. Mindlin and R.W. Landgraf, American Society for Testing and Materials, 1976, pp. 142-159.
35 JERRAM, K. and PRIDDLE, E.K.: System for Determining the Critical Range of Stress-Intensity Factor Necessary for Fatigue-Crack Propagation, Journal Mechanical Engineering Science, Vol. 15, No. 4, 1973, pp. 271-273.
36 LINDLEY, T.C. and STEWART, A.T.: Fatigue Crack Growth Threshold Applications, in Ref. [1].
37 PRIDDLE, E.K.: High Cycle Fatigue Crack Propagation Under Random and Constant Amplitude Loading, International Journal of Pressure Vessels and Piping 4, 1976, pp. 89-117.
38 MUKHERJEE, B. and VANDERGLAS, M.L.: Fatigue Threshold Stress Intensity and Life Estimation of ASTM-A106B Piping Steel, Journal of Pressure Wessel Technology, Vol. 102, 1980, pp. 294-302.
39 STENVALL, P.: The Adopting of the Threshold Philosophy - A Modern and useful Tool for Designing and Controlling, in Ref. [1]
40 WANHILL, R.J.H.: Some Case Studies and the Significance of Fatigue Thresholds, in Ref. [1].